FCTUC FACULDADE DE CIÊNCIAS
E TECNOLOGIA
UNIVERSIDADE DE COIMBRA

Wireless power transfer system for continuous charging of electric vehicles

André Pereira Mendes

September 2017

Wireless power transfer system for continuous charging of electric vehicles

Supervisor:

Prof. Dr. André Manuel dos Santos Mendes

Co-Supervisor:

Emanuel Gonçalves Marques

Jury:

Prof. Dr. Aníbal Traça de Carvalho Almeida

Prof. Dr. André Manuel dos Santos Mendes

Prof. Dr. António Paulo Mendes Breda Dias Coimbra

Dissertation submitted in partial fulfillment for the degree of Master of Science in Electrical and Computer Engineering.

September 2017

Acknowledgements

This journey has been full of challenges and difficulties, but like everything else, with hard work and perseverance anything is possible. However, to say that anything can be accomplished without help would be a ridiculous statement.

In that sense, I would first like to thank my family, in particular my parents because without their help and guidance nothing like this would have been possible. I also have to express great gratitude for my brother Miguel because of the continuous support throughout this journey and for always being a friend. Additionally, I would like to thank my sister Sofia for always being helpful and giving good advice.

The invaluable help from my supervisor Professor André Manuel dos Santos Mendes is also very important and without it, this would have been much more difficult. His vision and advice were always an assurance that the work would be moving in the right direction. I would also like to thank Emanuel Gonçalves Marques for his great advice and help in the conclusion of this thesis.

Finally, I would like to thank my closest friends and colleagues that I met while studying at University of Coimbra. Your support, encouragement and companionship allowed me to keep being motivated to finish this work.

Resumo

O veículo de combustão interna é, ainda hoje, a opção preferida na mobilidade automóvel. No entanto, com os crescentes incentivos à redução do uso dos combustíveis fósseis e a aposta em energias renováveis, levaram ao aparecimento de outros tipos de veículos. Nesse sentido, o veículo eléctrico (VE) apresenta-se como uma alternativa viável que combina alto rendimento e bom desempenho.

A energia armazenada nas baterias é necessária para o funcionamento do VE e precisa de ser carregada periódicamente. Por outro lado, o carregamento requer que o utilizador intervenha no processo, o que implica, entre outros problemas, o eventual esquecimento de efetuar o carregamento do VE. Surge então a necessidade de arranjar formas rápidas, eficientes e cómodas para o carregamento das baterias do VE.

Assim, neste trabalho é proposto um sistema de transferência de energia sem fios para carregamento de veículos eléctricos de forma dinâmica, isto é, enquanto o veículo se movimenta. Este sistema baseia-se nas leis de Ampère e Faraday e tem um funcionamento semelhante ao de um transformador, apesar de os entreferros serem bastante maiores. Por forma a transferir energia suficiente para um veículo em movimento diferentes variáveis devem ser tidas em conta. Neste trabalho dá-se especial atenção à estrutura de acoplamento, em particular às diferentes geometrias usadas tanto no primário como no secundário.

Fundamentalmente o estudo passa por uma comparação detalhada das geometrias que apresentem viabilidade para WPT em movimento, com a análise dos parâmetros que influenciam a transferência de energia, como sejam o factor de acoplamento e a indutância mútua. Estes estudos foram feitos com auxílio de um software de elementos finitos que permite a análise magnética e elétrica do sistema. As simulações foram feitas em regime estacionário e transitório, em que três diferentes tipos de movimento foram estudados referentes aos eixos x, y e z. O principal objectivo é avaliar a tolerância a desalinhamentos das estruturas consideradas bem como a influência da velocidade dos veículos na transferência de energia.

Palavras-Chave: VE, WPT, topologias, longo, segmentado

Abstract

The internal combustion vehicle is, still today, the preferred option for automobile mobility. However, the increasing incentives towards the reduction of fossil fuel consumption and the investment in renewable energies lead to the outbreak of other types of vehicles. In that sense, the electric vehicle (EV) presents itself as a viable alternative that combines high efficiency and good performance.

The battery's electric charge is necessary for the vehicle operation and needs to be charged periodically as the car moves. On the other hand, charging requires the user to intervene in the process, which implies, among other problems, the possibility to forget to charge the EV. The need arises to find quick, efficient and convenient ways to charge batteries of EVs.

Thus, in this work a dynamic wireless power transfer system (WPT) for continuous charging of electric vehicles on the road is proposed. This system is based on the laws of Ampère and Faraday and operates in a similar manner to the transformer, although with larger air gaps. In order to transfer sufficient energy to a moving vehicle several variables must be taken into account. In this work, special attention is paid to the magnetic coupling structures, in particular to the different geometries used in both the primary and secondary.

Essentially, the study involves a detailed comparison of the geometries that present feasibility for dynamic WPT, with the analysis of the parameters that influence the transfer of energy, such as coupling factor and mutual inductance. These studies were made with the aid of a finite element software that allows a magnetic and electrical analysis of the system. The simulations were done in a steady state and transient state environment, in which three different types of movement were considered along the x, y and z axis. The main goal is to evaluate the tolerance to misalignments of the chosen structures as well as the influence of vehicle speed in the energy transfer.

Keywords: EV, WPT, topologies, long, segmented

"Thoroughly conscious ignorance is the prelude to every real advance in science."

— James C. Maxwell

Contents

List of Acronyms

AC	Alternating Current
CPT	Capacitive Power Transfer
DC	Direct Current
EV	Electric Vehicle
EMF	Electromagnetic field
EMI	Electromagnetic Interference
FEA	Finite Element Analysis
FEM	Finite Element Method
ICE	Internal Combustion Engine
IPT	Inductive Power Transfer
LASER	Light Amplification by Stimulated Emission of Radiation
OLEV	On-line Electric Vehicle
OLPT	On-line Inductive Power Transfer
RAPT	Resonant Antennae Power Transfer
RMS	Root Mean Square
RPEV	Road Powered Electric Vehicle
SAE	Society of Automotive Engineers
VLF	Very Low Frequency
WPT	Wireless Power Transfer

List of Symbols

$\boldsymbol{B}$	Magnetic flux density
$\boldsymbol{H}$	Magnitude of the magnetic field
δ	Lamination thickness of the magnetic material
ℓ	Length of the coil
μ	Permeability of the material
μ_0	Vacuum magnetic permeability
ω	Angular frequency
ω_0	Resonance angular frequency
Φ	Magnetic flux
$\Re$	Reluctance of the material
A	Cross section area of the coil
C_p	Primary capacitor
C_s	Secondary capacitor
$d\boldsymbol{s}$	Surface element
$d\boldsymbol{\ell}$	Length element
e	Electromotive force
E_{transf}	Energy transfered to the secondary
f	Operating frequency
i	Instantaneous electric current
I_p	Rms value of primary current
I_s	Rms value of secondary current
k	Coupling factor
L	Self inductance
L_p	Self inductance of the primary coil
L_s	Self inductance of the secondary coil
M	Mutual inductance

M_{ps} Mutual inductance from the primary coil to the secondary coil

M_{sp} Mutual inductance from the secondary coil to the primary coil

N Number of turns

P_{avg} Average power at the load

P_f Losses due to Foucault currents

P_h Hysteresis loss

P_{out} Maximum power that the system can transfer

Q_{source} Reactive power at the primary source

Q_s Quality factor of the secondary coil

R_{load} Equivalent load resistance after rectification

R_p Resistance of the primary coil

R_s Resistance of the secondary coil

V Volume of the magnetic material

V_{inv} Inverter voltage

List of Figures

List of Tables

Chapter 1

Introduction

Interest in other ways of powering transportation systems has been growing as the use of fossil fuels is increasingly discouraged. The remarkable investment towards the use of environmentally friendly technologies has pushed forward several alternatives that have great potential to completely revolutionize the market. One of such technologies is the electric vehicle (EV), which is capable of running solely on electricity.

Similarly to the internal combustion engine (ICE) vehicles, energy can be used immediately by the traction motors or stored on-board. EVs make use of batteries that contain electric charge and need to be recharged periodically. The storage characteristics of the current batteries lack the power density to compete evenly with gasoline powered vehicles [1]. As the need to higher ranges arises, the charging times also increase, as well as the battery's total weight. Furthermore, the high initial investment cost and the limited range provided deter people from considering this option.

The physical and economic limitations are not the only bottlenecks in this technology. The current modes of EV charging use plugs and require the user to connect them manually to a mains power outlet or a dedicated charging station. This compromises the security of people and can expose them to potential safety hazards. Besides, these charging stations are exposed to the elements and external conditions which can cause some of these stations to be out of service. On a related note, the users themselves are prone to forgetfulness in charging the EV or mishandling the electrical equipment. All of these considerations have an overall negative impact in the EV's reputation, therefore the need arose to find new ways to charge an EV with ease, safety and reliability.

To overcome this, several technologies based on wireless power transfer (WPT) have been proposed and studied [2, 3]. Their main objective is to increase safety and also to make it

an automatic system independent of the user. Applications range from low power small scale level to high power transmission systems. The ability to transfer energy without wires tackles much of the inconveniences described previously.

1.1 Wireless power transfer systems

A wide range of applications have been made for WPT systems since the advent of alternating current (AC) electrical systems. It all started when, in 1891, Nikola Tesla invented his famous Tesla coil. The system had two loosely coupled circuits (primary and secondary) tuned at resonant frequency with external capacitances. Despite the existence of some spark losses, this invention was able to transfer energy with an efficiency of 85% [4]. From then on, more recent applications have benefited from this great advancement in science. This includes home appliances like electric toothbrushes and mobile phones [5, 6] or transcutaneous medical implants [7]. More recently, high power applications like the EV and other material handling systems have been studied and applied in practical environments.

Fig. 1.1 illustrates that WPT systems can be, in general, divided into two main types [8]. They are defined based on the physical phenomena of electromagnetic field propagation into near field or far field. Near field methods are used for transmission over relatively short distances and can be done with inductive coupling or capacitive coupling. Conversely, for far fields the objective is to transfer over long distances and in this case the transmission is done with beamed electromagnetic power, i.e. lasers and microwaves.

Inductive power transfer (IPT) is, like the name implies, the transfer of energy through electromagnetic induction. It follows the same operation as a loosely coupled transformer,

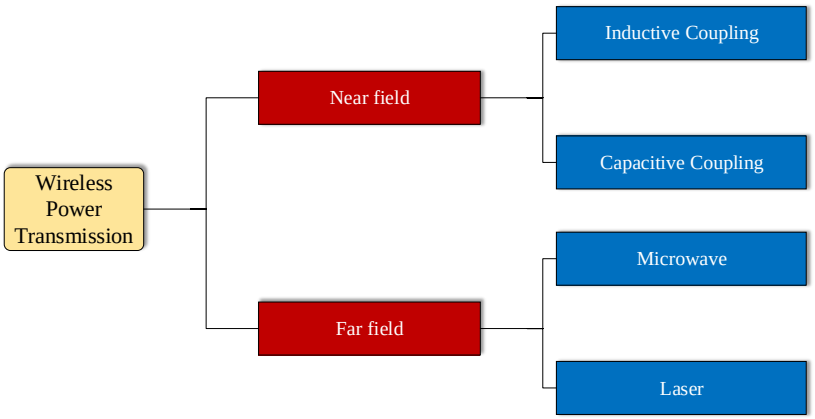

Figure 1.1: Wireless power transmission types.

thus by powering the primary of a circuit with an AC current, a time variant electromagnetic field will be created that will then induce a voltage in a secondary coil, effectively transmitting power without wires.

A particular case within IPT is the resonant inductive coupling, in which two circuits are operating at the same resonant frequency with capacitances connected to them, allowing for higher power transfer efficiency. Capacitive coupling represents the transfer of energy with electric fields and is also known as capacitive power transfer (CPT). Electrodes, such as metal plates, transfer energy between each other by the oscillation of a high-frequency electric field. The transmitter and receiver plates form a capacitor and the space in between acts as the dielectric. Unfortunately, to achieve high levels of energy transfered the electric fields must reach high intensities, which limits possible applications. The most significant advantage of CPT is its cost and size at lower power levels, thus its applications are restricted to small portable electronic devices [3].

The far field types offer great possibility of high power transfer at large frequency levels. Microwave power transmission uses two or more resonant antennae tuned to the same frequency to achieve power transfer over longer distances than the previous types. However, human exposure to radio frequency radiation can be dangerous, even more so as shielding these systems is difficult [3]. Furthermore, operating with frequencies in the MHz range with current power electronics technology is not recommended. On another note, electricity can be converted into laser beams to achieve long distance WPT. Despite offering great energy density, it can still pose some risks associated with the beam itself [8].

Knowing all these types, it is clear that the most adequate WPT type for EVs is the resonant IPT. They have the capability of providing enough power (>10 kW) to current EVs with safe, reliable and robust characteristics. Electrical isolation enables operation in wet and dusty environments. Furthermore, the galvanic isolation between the transmitter and receiver eliminates any risk of electric shock. They are also virtually maintenance free and immune to vandalism [9]. Current types of IPT systems applied to EVs are used in stationary or dynamic settings. For stationary IPT a primary coupler is placed under the ground in a specific location (e.g. parking lot or bus stop) and the vehicle simply needs to be on top of that coupler to start charging.

A road powered EV (RPEV) system is charged while moving along a road without the need to stop at a station [10]. On-line inductive power transfer (OLPT), is just a similar name to represent any system prepared to charge EVs on the move. Table 1.1 shows a comparison regarding performance, cost, size and necessary power levels for the most relevant wireless

Table 1.1: Comparison of different types of WPT systems [3].

Technology	Performance			Cost	Size	Suggested Power Level
	Efficiency	EMI	frequency			
Inductive Power Transfer (IPT)	medium	medium	10-50 kHz	medium	medium	medium/high
Capacitive Power Transfer (CPT)	low	medium	100-500 kHz	low	low	low
On-Line Inductive Power Transfer (OLPT)	medium	medium	10-50 kHz	high	high	high
Resonant Antennae Power Transfer (RAPT)	medium	medium	100 - 500 kHz	medium	medium	medium/low

power transfer techniques.

1.2 Dynamic charging of electric vehicles

During the oil crisis of the mid 1970s, interest in new ways to power vehicles along a roadway increased. The first prototypes were designed with low power levels (6 kW) and didn't show great potential to an operational system. After that, a 8 kW prototype was made at Lawrence Berkeley National Laboratory, and was also a not fully operational system [11]. In the 1990s, the PATH team at University of California, Berkeley built a proof of concept 35 passenger electric bus. They achieved an efficiency of 60% but were limited by the operating frequency [4].

As will be further clear in the next chapters, the current leading research teams in dynamic wireless power transfer are the team at Korea Advanced Institute of Science and Technology (KAIST) and the Auckland Research team at University of Auckland. Researches at KAIST have been working with on-line EVs (OLEV) since 2009 and already have some roads electrified. They focus on stretched types of primary tracks and have achieved above 70% efficiency in all their prototypes. Since the 1990s, a research team at Auckland has been focusing on WPT systems. Their studies involve stationary IPT with a single coupler. Despite that, they have been working more recently on segmented structures for RPEV that use multiple primary couplers along the road [12].

Although the dynamic charging system requires more investments on the power tracks than the stationary charging system, more cost saving can be achieved from the smaller batteries with extended battery life [14]. Table 1.2 shows the advantages and disadvantages of the RPEV technology. A successful implementation of the dynamic IPT system would improve the acceptance of electric vehicles, and solve the most critical aspects in their use [9].

Table 1.2: Advantages and disadvantages of RPEV [13].

Technology	Advantages	Disadvantages
Dynamic charging	• Improves effectiveness of space and time necessary for charging because the battery is recharged on the road during a trip. • Eliminates the range anxiety associated with EVs. • Avoids queuing at charging stations. • Enables unrestricted cruising where the infrastructure is available. • Minimizes the size and cost of the on board battery pack.	• Necessary infrastructure. • Design issues. • High investment cost. • Effects of electromagnetic field exposure.

1.3 Motivation and Objectives

From this brief introduction it is clear that wireless power transfer systems associated with continuous powering of electric vehicles can have a great benefit in the transportation systems. However, as stated in table 1.2 there is a great deal of design issues to work with, and in particular for this thesis, the design is focused on the primary track and secondary pickup. Their architecture can be very influential in the final performance of the system, namely in the power transfer levels, induced voltages, coupling factors and mutual inductances. All of these parameters will differ with the design considered. In that sense, the work done in this thesis has the following objectives:

- Investigate the WPT systems currently being studied in roadway applications.
- Understand how the on-line IPT system works and describe its components.
- Compare the different viable designs for primary and secondary structures and establish a set of designs to study.
- Build those designs with a finite element method, in order to comprehend how they work electrically and magnetically.
- Study the system in steady state and transient state for different positions of the secondary along the road to evaluate the influence of misalignments in overall performance.
- Investigate the impact on power transfer as a function of vehicle speed with transient state methods.

Chapter 2

Inductive Power Transfer System

The energy transfer from the primary coupler to the secondary coupler is done thanks to inductive coupling. As such, this chapter will cover the basic magnetic notions behind inductive power transfer (IPT) systems and will explain the principle of operation of the dynamic IPT system with a focused explanation towards the magnetic couplers.

2.1 Electromagnetic notions

The inductive power transfer phenomena is governed by two fundamental principles: the Ampère's law and the principle of magnetic induction discovered by Faraday. As such, the integral form of Ampère's law, also known as the 4th Maxwell equation, can be expressed as

$$\oint_C \boldsymbol{B} \cdot d\boldsymbol{\ell} = \mu_0 \sum i \tag{2.1}$$

which states that the line integral of the magnetic flux density around a coil is equal to the total current multiplied by the magnetic permeability of free space. From this notion, the concept of magnetic flux can be stated as being equal to

$$\Phi = \oint_S \boldsymbol{B} \cdot d\boldsymbol{s} \tag{2.2}$$

from which it can be concluded that the magnetic flux through a surface is proportional to its magnetic field, which in turn is proportional to the conductor current. Thus, $\Phi \propto B \propto i$. This relationship can be written as

$$\Phi = Li \tag{2.3}$$

with L being the inductance of the circuit. This expression is very important for this work, as will be clear in chapter 5. On the other hand, the Faraday's law of induction has its basis

on the concept that an electromotive force (emf) is induced in a coil when a time-variant magnetic flux is passing through it. This can be expressed as

$$e = -\frac{d\Phi}{dt} \tag{2.4}$$

The previous equation gives the induced emf for just one turn if a coil has N turns then the induced emf will be N times as much. On the other hand, the inductance L can also be expressed as a ratio of the differential change in the flux linkages to the differential change in the current. That is,

$$L = N\frac{d\Phi}{di} \tag{2.5}$$

Combining equation 2.2 with equation 2.5 and knowing that $\mathbf{H}\cdot\ell = Ni$ and $\mathbf{B} = \mu_0\mathbf{H}$ yields

$$L = \frac{\mu_0 N^2 A}{\ell} \tag{2.6}$$

The self inductance is a purely geometric parameter and is dependent on the number of turns N, the cross section A and the length ℓ of the coil. Let us now consider two coils that are close enough to induce any voltage on each other. A time-variant current i_1 in coil-1 establishes a magnetic flux Φ_1. This flux induces an emf in coil-1. A part of the flux, Φ_{12}, links coil-2 and as a result induces an emf in coil-2

$$e_2 = N_2\frac{d\Phi_{12}}{dt} = N_2\frac{d\Phi_{12}}{di_1}\frac{di_1}{dt} = M_{12}\frac{di_1}{dt} \tag{2.7}$$

this means that M_{12} is given as

$$M_{12} = N_2\frac{d\Phi_{12}}{di_1} \tag{2.8}$$

In a similar manner, if coil-2 carries a current i_2 while coil-1 is left open and creates a flux Φ_2, then Φ_2 induces emf in coil-2. Conversely, M_{21} is equal to

$$M_{21} = N_1\frac{d\Phi_{21}}{di_2} \tag{2.9}$$

Finally, if we write $\Phi_{12} = k_1\Phi_1$, where k_1 defines the fraction of the flux of coil-1 linking coil-2 and $\Phi_{21} = k_2\Phi_2$, where k_2 determines the portion of the flux of coil-2 linking coil-1, then the above expression can be simply written as

$$M_{12}M_{21} = k_1k_2L_1L_2 \tag{2.10}$$

In a linear system $M_{12} = M_{21} = M$, where M is the mutual inductance of coils 1 and 2. Equation 2.10 reduces to

$$M = k\sqrt{L_1L_2} \tag{2.11}$$

where $k = \sqrt{k_1 k_2}$ is known as the coefficient of coupling. Both k and M are very important in the context of inductive power transfer systems, due to their influence in the overall energy transfer capabilities. k can have values between 0 (magnetically isolated coils) and 1 (tightly coupled coils) and is a variable that provides a useful measure for directly comparing magnetic properties of different structures. It is the ratio of the flux that links the coils within a pad to the total flux produced by the opposite pad. High values are desired because less magnetomotive force is required to get the same power transfer [15].

2.2 Principle of operation

Now that the basic electromagnetic theory has been introduced, it is easier to understand how the IPT system works. Fig. 2.1 illustrates the complete system for continuous charging of EVs [16]. Typically, the system supplying power is stationary and can be named primary, transmitter or source. The 3-phase power input is converted from alternating current (AC) to direct current (DC) through a AC/DC converter and then to high frequency AC current by a DC/AC converter. This current I_p will drive the primary track through a compensation network and create a time-variant magnetic field around it, in accordance with Ampère's law. As vehicles pass on top of the primary track, a voltage will be induced in the secondary or pickup coils, as Faraday's law of induction states. Thus, energy is wirelessly delivered from the primary track to the secondary pickup, through the air. The AC secondary current I_s can then be rectified to charge the batteries inside the vehicle. There may exist a further DC-DC converter to reduce or increase the DC voltage in order to charge the battery pack

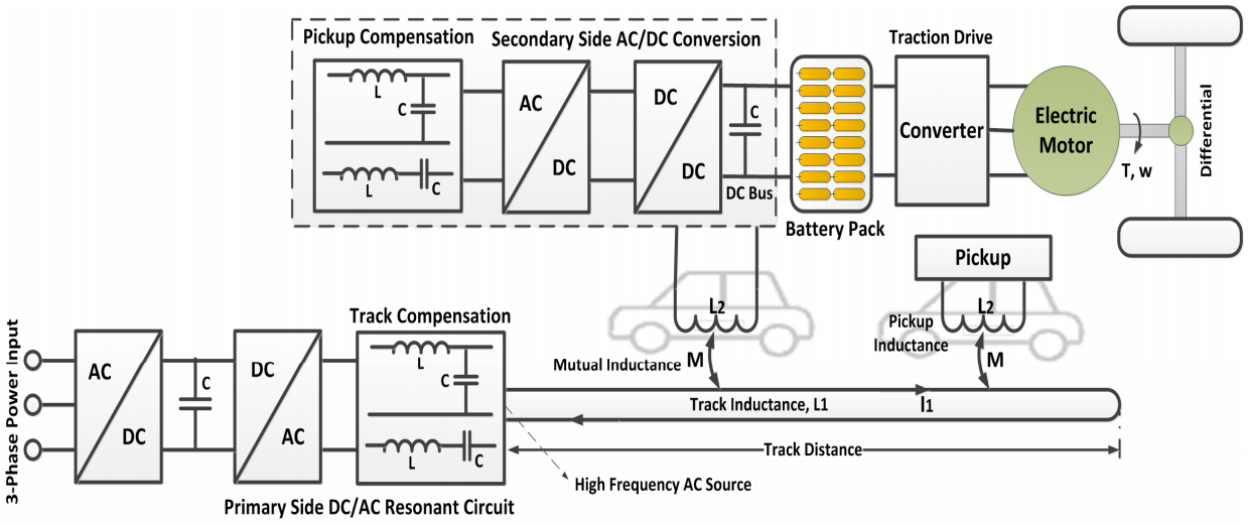

Figure 2.1: IPT system for dynamic charging of EVs.

at a rated voltage. Electricity from these batteries can be used to power electric motors and other loads in the EV.

A major difference from this system to the one found in common transformers is the coupling factor k. The primary track built underground is some 100-300 mm away from the secondary pickup, therefore the path between these structures is mainly composed of air, which has a high reluctance. Consequently, it is more difficult to transmit energy to the secondary coil. Moreover, dynamic charging gets more challenging because of the constant movement of the vehicle. The two inconveniences previously pointed out are responsible for lower values of M between the primary track and the pickup coil. As a result, in a dynamic IPT system the coupling factor ranges from 0.1 to 0.3 which makes these coils loosely coupled.

2.3 Magnetic couplers

The magnetic structure is composed of primary and secondary coils. Figure 2.2 shows the equivalent circuit of the magnetic coupler model at resonant frequency. The subscript p refers to the primary, while the subscript s refers to the secondary. Having considered the various hindrances in regards to the transfer of energy stated in the previous section, some actions are taken to minimize those pitfalls.

- *frequency*: the frequency of operation is usually in the VLF range (3-30 kHz), with the most common values ranging around 20 kHz due to the acoustic noise in lower frequencies. More recently, however, the SAE international J2954 task force for WPT has agreed in their guideline to push the frequencies of operation to 85 kHz in stationary IPT systems [17]. This is a much higher value that translates into better performances, less magnetic flux leakages, less copper usage, smaller ferrites and smaller inductors. This means that the pickup structures can be made potentially smaller and lighter, which impacts the system cost and efficiency. The power supplies rated for dynamic IPT are in the hundreds of kVA or more due to the higher power demands of the EVs, but it is difficult to operate at such high frequencies with the current semiconductor technologies. Moreover, the use of longer track transmitters requires proper compensation with capacitors in series with the track. They need to be able to support high frequencies and high voltage levels, which can be costly and problematic. On the other hand, equations 2.12 and 2.13 from Fig. 2.2 show that an increase in the system's frequency results in greater induced voltages which ultimately improves energy transfer.

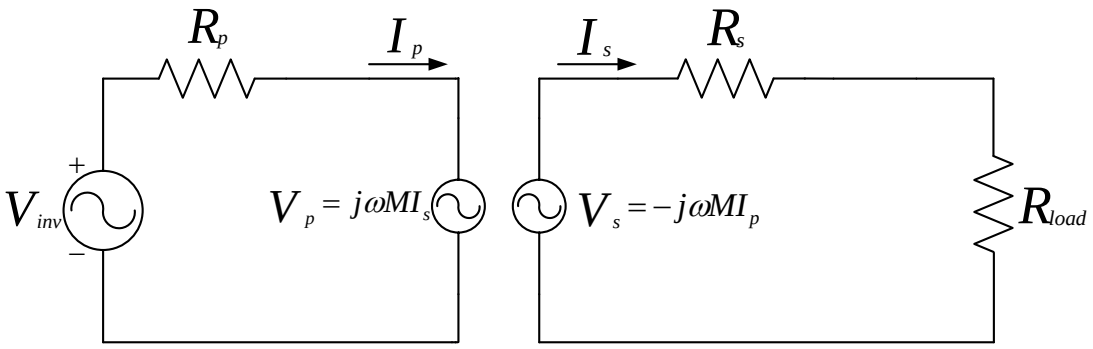

Figure 2.2: Ideal equivalent circuit in perfect resonance.

This can counter the low mutual inductances that are characteristic of these systems. With the advent of modern semiconductor devices, the frequency limits are increasing and consequently, cost effective, high power near MHz WPT for EV applications is not very far away [18].

$$V_p = jwMI_s \tag{2.12}$$

$$V_s = jwMI_p \tag{2.13}$$

- *compensation network*: the use of compensation networks in both the primary track and the pickup coils stems from the fact that these systems can have a significant reactive characteristic that is responsible for low power transfer levels. Indeed, by increasing the operating frequency the volt-ampere (VA) ratings required to drive the current also increase with a particularly dominant inductive system [4]. The loosely coupled coils with large leakage inductance require the use of compensation networks in both the primary and secondary coils to have a more flexible and advanced characteristic [19]. The simplest way to compensate a leakage inductance is to place a capacitor in series with each coil, as shown in Fig. 2.3. Depending on how the capacitors are connected to the coils, there are four basic compensation topologies: series-series (SS), series-parallel (SP), parallel-series (PS) and parallel-parallel (PP) [20]. Typically the capacitor would be tuned with the self inductance of the coil in order to function at resonant frequency. To operate on resonance the imaginary parts of the impedances must cancel each other. For instance, in the circuit of Fig. 2.3 both C_p and L_p as well as C_s and L_s have to cancel out to give a purely resistive circuit, like the one in Fig. 2.2. Equating the inductive and capacitive reactances to zero, like in equations 2.14

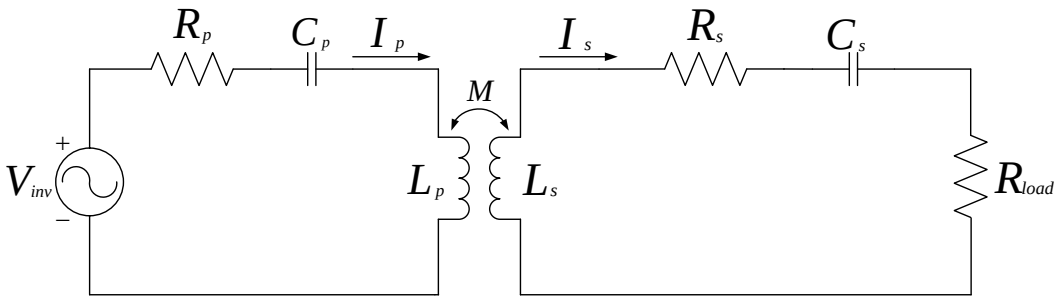

Figure 2.3: Actual equivalent circuit with compensation.

and 2.15, results in equation 2.16 which corresponds to the resonant frequency. Since the self inductances are usually known and the circuit is tuned to have the operating frequency match the resonant frequency, it is not difficult to find the necessary capacitor by applying equation 2.16. Owing to this, the reactive component gets reduced, the power factor improves and most importantly the power transfer levels get considerably increased.

$$\frac{1}{j\omega_0 C_p} + j\omega_0 L_p = 0 \tag{2.14}$$

$$\frac{1}{j\omega_0 C_s} + j\omega_0 L_s = 0 \tag{2.15}$$

$$\omega_0 = \frac{1}{\sqrt{L_x C_x}}, \quad x \in \{p, s\} \tag{2.16}$$

- *magnetic structure geometry*: this is the focus of this work. The geometry of the primary and secondary structures, i.e. their coil placement, dimensions as well as the materials used have a great impact on the system performance. In particular, the coupling factor can be improved by proper design of the magnetic couplers. Next chapters will have a thorough investigation regarding various topologies of magnetic couplers.

It is also relevant for the previous explanations the expression for the maximum power that the system can transfer

$$P_{out} = \omega \frac{M^2}{L_s} I_p^2 Q_s = V_p I_p k^2 Q_s \tag{2.17}$$

where V_p is equal to the voltage at the primary coil (Fig. 2.2) and Q_s is the quality factor of the secondary coil, which can be expressed as

$$Q_s = \frac{\omega L_s}{R} \tag{2.18}$$

with R being the series resistor with the inductor L_s. It can be concluded from 2.17 that increasing any of ω, M, I_p or Q_s will improve the power delivered to the load. However, there are limits to the frequencies of operation. Increasing the primary current I_p leads to a loss in efficiency. Improving the quality factor might be a good solution but can lead to narrow bandwidth and tuning problems [21]. Increasing k is definitely a doable approach as it is dependent on the air gap and the design of the magnetic structures.

Chapter 3

Topologies for magnetic structures

The transfer of energy from an electrical source to a load in an inductive power transfer system requires the project and construction of a suitable configuration. For that reason, it is important to compare and study the different types of topologies that are relevant in the on-line charging of electric vehicles. This chapter will cover some of the architectures behind the design of these structures and the various types of viable configurations. Furthermore, this chapter will also explain and characterize the materials used in these systems. The chapter ends with considerations regarding the use of air cores in dynamic IPT systems and their characteristics.

3.1 Design considerations

In a dynamic EV charging system, the main components are composed of a primary side coupler named transmitter, which is placed under the road, and a secondary side called pickup, which is mounted under an EV chassis. Coils are wound on top of magnetic cores on the primary and below magnetic cores on the secondary. The systems proposed for several IPT applications usually have poor coupling factors k and mutual inductances M due to the significant magnetic reluctance of the large air gaps involved (100-300 mm) and misalignments between the primary and secondary. Despite that, recent developments in IPT systems have made possible the transfer of power in the MW level with efficiencies of more than 80% [22].

A representation of two typical inductive power systems for RPEV is shown in Figure 3.1. Presently, the study of different topologies has revolved around these two main types. The primary coupler can be a long track, in which the secondary is significantly smaller than the track [13], [17], [23, 24] or a segmented series of tracks with roughly the same

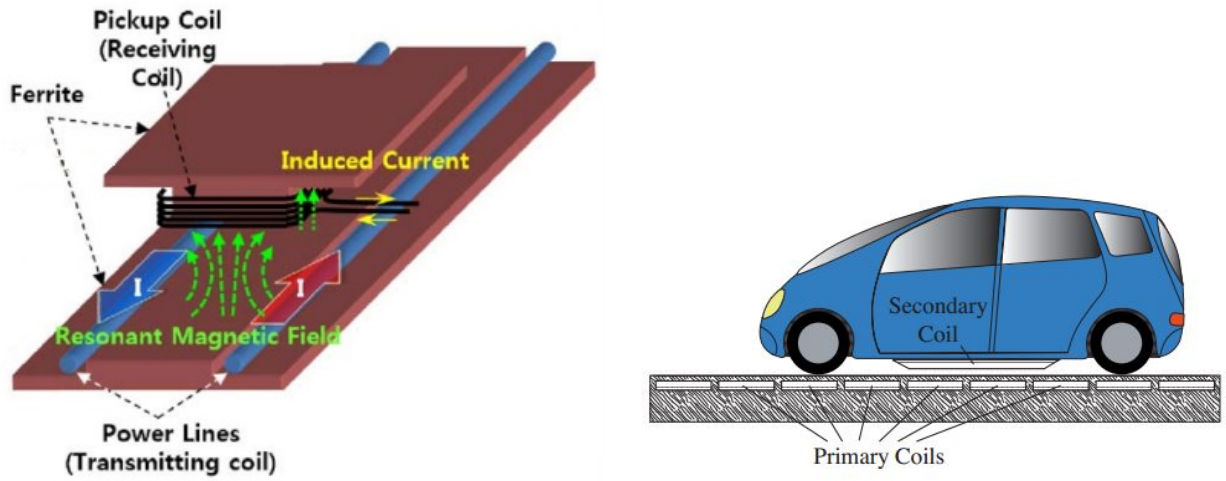

(a) Long topology. (b) Segmented topology

Figure 3.1: The two main types of configurations for dynamic IPT [29, 30].

size as the secondary pickup [25–28]. The design to be considered has greater requirements than those in the stationary inductive charging, such as larger lateral tolerance, higher air gap and lower construction cost. Moreover, the harsh conditions of the road in terms of temperature extremes and climate hazards, as well as the constant mechanical stress, mean that the system has to be robust but also compact to make it easy to install and maintain [10]. The design objectives of the IPT system can then be summarized as follows:

- Attain the best possible magnetic coupling so higher induced voltage can be obtained;
- Increase the power efficiency (>70%) for a given power capacity, device ratings and cost;
- Make modules as compact as possible to accommodate for given space and weight;
- Not increase EMF and preferably cancel it ($< 27\ \mu T$ for $20\ kHz$);
- Manage resonant frequency variation, changes in coupling factor, misalignments of pickup position and temperature shifts. [10]

The first prototypes and tests for powering vehicles while moving started with the use of long tracks with single stranded conductors on each lane [11]. The precursors of what would be the modern configurations were further developed in the PATH program at UC Berkeley [31]. The design used resembles the E-core and coil types that are commonly found in long track systems. Core shapes have letters as designation because of the similarities with them. For instance, ferrites of E [32], U [33], W [34], I [35] and S [36] types are used to increase the magnetic coupling and efficiency in long track systems. Researchers at KAIST have been working on these systems since 2009. Out of all the core configurations, the S type seems

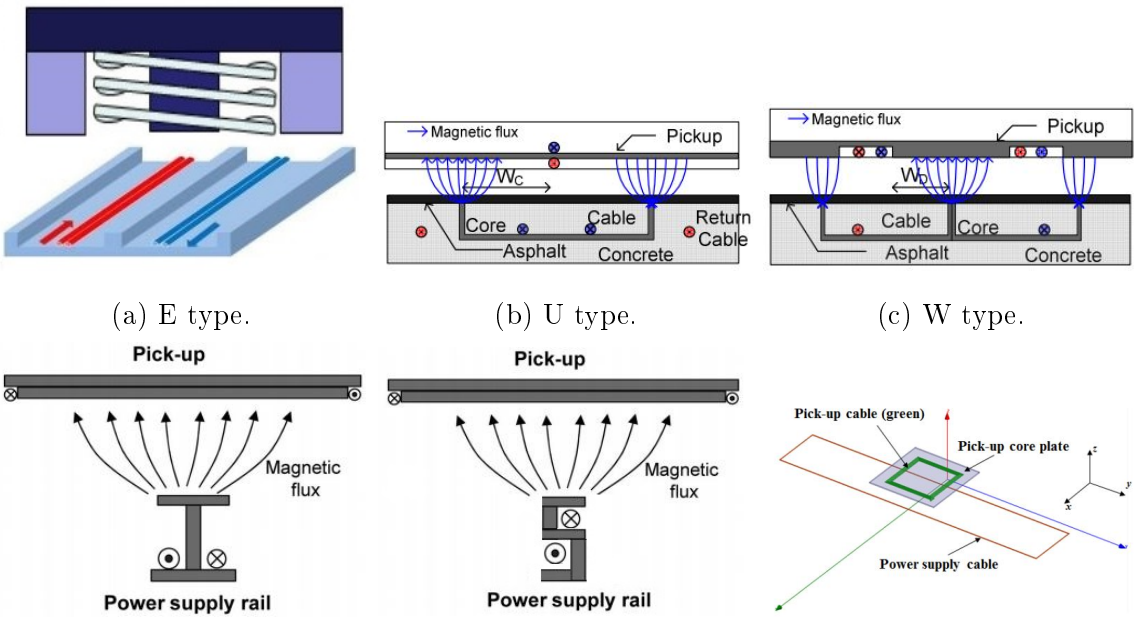

(a) E type. (b) U type. (c) W type.

(d) I type. (e) S type. (f) Coreless type.

Figure 3.2: The main types of configurations for long transmitter OLEV systems.

to be the most cost efficient as it has lower width than the others but has greater tolerance to misalignments and less EMF exposure to pedestrians. The aforementioned configurations are represented from E type in Fig. 3.2a to the coreless type in Fig. 3.2f. More recently, there have been efforts to implement coreless configurations [23], [37] since the deployment cost of the power rails and particularly the core materials are expensive. The coreless type has been showing great promise in high power railway applications, where the construction cost is high and can be much more time consuming if it is built with core systems. As will be further explained, the simulated long and segmented configurations studied have a common design based on Fig. 3.2f.

The most evident inconvenience of the long transmitter approach is the fact that the pickup is smaller than the track, which results in lower coupling factors and leakage inductances. Because of that, several studies have been made to use segments or power pads instead of long tracks.

Bhudia et al. had already proposed segmented systems that were later applied in stationary charging. Their prototypes initially used segmented tracks that have a circular shape with the coils wound on top of ferrite bars. This structure is compact and has low weight, however it is not the optimal choice given the limitations in power transfer and the low tolerance to misalignments. The use of larger pads could mitigate this issue but there is a limit of around 1 m^2 in pad area to place below the vehicle [38]. The design in Fig. 3.3e has

the same behaviors as a circular one. Instead of using a circular geometry, the pattern used was of a planar rectangular core structure with one coil wound on top of it. The geometric approximation can be done without significant loss of precision.

To reduce the flux leakages and improve the coupling coefficient as well as the power transfer capabilities, several geometries based on the DD design have been made [21]. This configuration is composed of two square coils connected in series and placed on the same planar core, hence the DD designation (Fig. 3.3i). Several researchers recommend the use of DD geometry on both the primary and secondary for dynamic charging of EV [39]. They argue that this type has more tolerance in the x and y directions which make it suitable particularly when the vehicle transitions between segments. Moreover the flux path reaches higher distances in the z direction with the DD configuration allowing for more magnetic coupling at greater air-gaps [19].

In essence there are two types of coils: unipolar and bipolar. An example of a unipolar coil is the circular design because of the presence of only one magnetic pole on each coil face. As for the bipolar type, the topology is more complex with coil faces having both north and south poles. The DD configuration has this characteristic where flux lines leave the pole face with the north pole and enter the pole face with the south pole. This creates a more confined space for the flux lines to travel.

The configurations to be studied and designed in the simulation software are presented in Fig. 3.3. From Fig. 3.3a to 3.3d, the long loop designs are illustrated, whereas from 3.3e to 3.3j the segmented types are displayed. As was previously pointed, the long tracks were designed based on Fig. 3.2f. The segmented system has three square shape structures in the

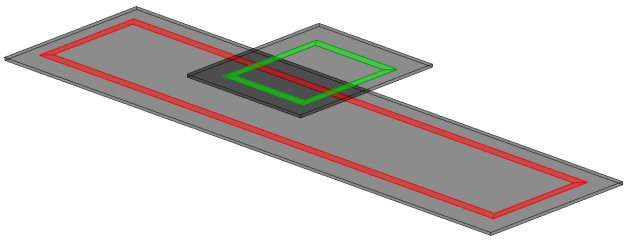

(a) R-R.

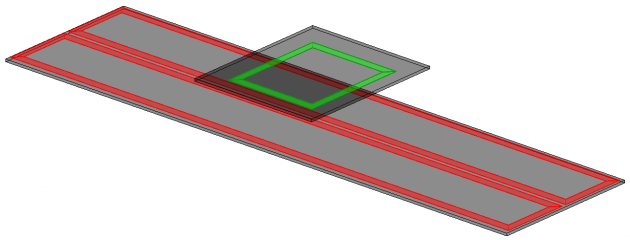

(b) DD-R.

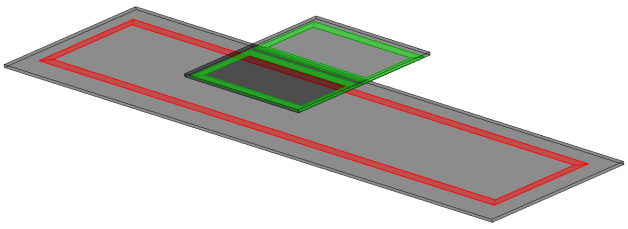

(c) R-DD.

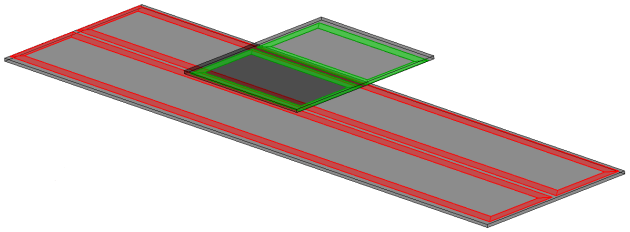

(d) DD-DD.

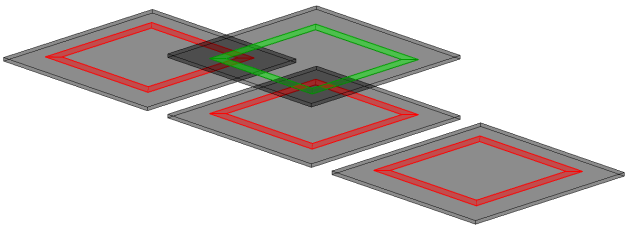

(e) R-R.

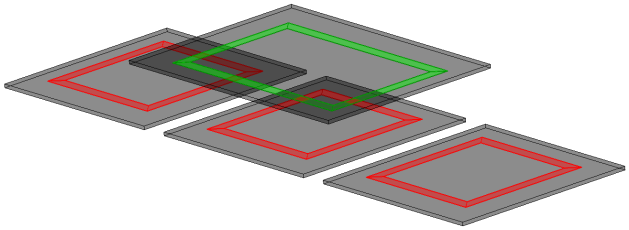

(f) R-R_+.

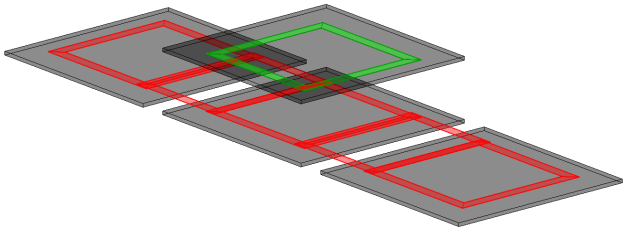

(g) BP-R.

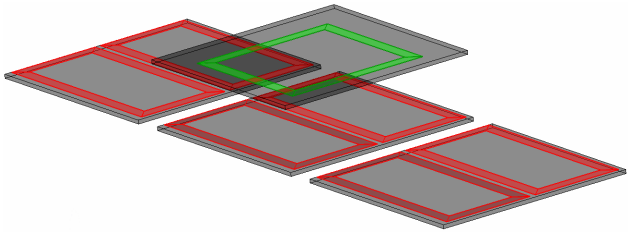

(h) DD-R.

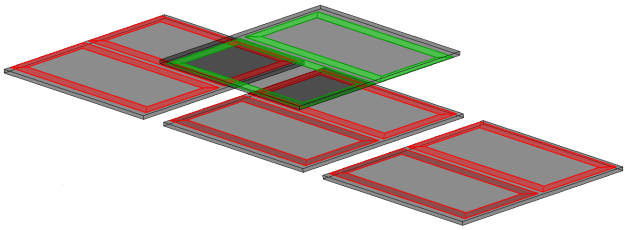

(i) DD-DD.

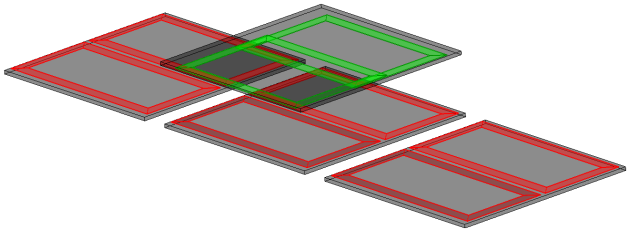

(j) DD-BP.

Figure 3.3: The configurations simulated in the finite element software.

primary that have the same dimensions as the secondary (except in Fig. 3.3f).

The primary coils are assigned the red color and the secondary coils the green color. The magnetic core considered for the simulations has a solid ferrite rectangular shape and is represented in gray color. The thickness of the coils was increased for better visualization.

Fig. 3.3b and 3.3c have a double coil configuration that is similar to the DD. In the first one it is employed in the primary, whereas in the second one it is applied in the secondary. The segmented variants are of the rectangular type in Fig. 3.3e and 3.3f, conversely DD types are presented from Fig. 3.3h to 3.3j. Fig. 3.3g shows a different approach on the primary side: there are overlapping coils between the segments. The last topology (Fig. 3.3j) has one coil that is overlapping the other in the secondary. This is commonly called the bipolar configuration.

All these configurations have a caption that relates to the configuration presented. For example, DD-DD stands for a DD configuration on the primary and on the secondary, R-R for a configuration with a rectangular coil on the primary and secondary and so on. The geometric analysis of these topologies will be further discussed in the next chapter. Table 3.1 compares the advantages and drawbacks of the two main types of geometries considered.

Table 3.1: Comparison between the two main types of dynamic IPT systems.

Type	Advantages	Disadvantages
Long track	• Lower construction cost. • Easier to control. • Continuous power transfer. • Constant coupling factor [18].	• Unwanted exposure to magnetic fields. • High track inductance will require compensation. • Low coupling factor. • Higher Joule and iron losses [16]. • Faults can make a large part of the road without power source.
Segmented pad	• Easier to replace faulty pads. • Higher coupling factor and mutual inductance. • Better system efficiency. • Powering several pads can create a longer track [40].	• Necessary to detect approaching and leaving vehicles from segments [41]. • Requires optimization for the distance between segments. • Difficult to control and is more expensive

3.2 Structure materials

On an IPT system it is necessary to choose the proper materials to be able to transfer power effectively. This choice will greatly influence the way the system works. Because of the constant movement of the electric vehicle and the considerable air gap between the primary and secondary, the coupling factor is low and the power transfer capability is severely affected. Furthermore, if the vehicle is misaligned in respect to the primary track or segment, the coupling and power transfer is further diminished. As previously pointed, the geometries play an important role in mitigating this effect. On the other hand, the materials to be used also have an important role in the overall performance of the system.

For a high system efficiency it is important to have high coupling factor k and quality factor Q. Generally, the larger the size to gap ratio of the coupler, the higher the k is. The thicker the wire and the larger the ferrite section area the larger the Q is. Increasing material size, however, is not a good engineering approach [19]. Not only because of the increased costs, but also due to the weight and space constraints especially under the vehicle.

Since this system has large air gaps, power transfer can be difficult. As such, the magnetic field created by the primary current will have high reluctance path to the secondary. Reluctance is a property of the magnetic materials analogous to the resistance in an electrical

circuit and is expressed by

$$\Re = \frac{\ell}{\mu A} \tag{3.1}$$

By using magnetic materials with high permeability μ it is possible to decrease reluctance and thus confine and guide the magnetic flux lines. Moreover, the presence of a magnetic core increases substantially the magnetic field generated which will improve the mutual and self inductance of magnetically coupled coils. These cores are usually made with the same ferromagnetic materials found in other magnetic devices, i.e. iron, silicon steel and ferrite types, with the latter type used in high frequency applications.

However, core losses are significant and since an IPT system operates at high frequencies, they get even more noticeable. These losses can manifest themselves by Foucault currents in the magnetic material or hysteresis losses. If the flux density varies sinusoidally with time but is uniform at any instant over the cross-section of a magnetic core, it can be shown that the average power loss due to the Foucault currents is [42]

$$P_f = k_f f^2 \delta^2 B_m^2 V \tag{3.2}$$

with k_f being a constant that depends upon the conductivity of the material, f the frequency in Hertz, δ the lamination thickness in meters, B_m the maximum flux density in Tesla and V the volume of the magnetic material. Then, there is the hysteresis loss that is directly associated with the hysteresis loop of the material and can be expressed as

$$P_h = k_h B_m^n f V \tag{3.3}$$

where k_h is a constant that depends on the magnetic material and n is the Steinmetz exponent that can vary between 1.5 and 2.5. Both these equations have the similarity of being dependent on the volume of the material and the frequency of operation. Less magnetic material results in lower losses. If the magnetic core is composed of thin laminated sheets (which reduces δ), the overall resistivity can be improved and ultimately reduce the Foucault currents.

The coils in these systems also have to be different due to the special conditions of powering vehicles on the move. Light and durable coils capable of operating at high frequencies with low losses are preferable. The type of conductor used is commonly made out of copper or aluminium. Copper has a lower resistivity but is more expensive, while aluminium is lighter and cheaper but has a worse electrical conductivity. In any case, the skin and proximity effect will exist and be significant due to the higher frequencies of operation and

the existence of Foucault currents. The skin effect is also a consequence of the existence of Foucault currents in the conductors. Instead of being uniform throughout the section of the conductor, the current density is larger at the surface and almost no current flows at greater depths in the conductor. This effect causes the resistance of the conductor to increase at greater frequencies because the skin depth is smaller. With higher resistance the loss by Joule effect is greater, affecting the final efficiency of the system. When a coil carries a current, the magnetic field associated with it can induce Foucault currents in other adjacent conductors, altering the overall current density of those wires in what is called the proximity effect. It is also dependent on frequency and is responsible for the increase in resistance of the conductors.

To minimize these problems multiple strands of thin wire insulated electrically from each other called *Litz* wires are used. Skin and proximity effect are reduced and the quality factor increases. However, special care must be taken when placing the primary coils because *Litz* wires can not withstand high temperatures or mechanical stresses [13].

3.2.1 Air core

In certain applications where there are constraints in the building cost of the system, it might be an option to not use any type of core to guide the magnetic flux. Whether it is because of the increased cost or the difficulty in protecting the magnetic material against mechanical stresses, it can be a viable way to power EVs dynamically. Furthermore, in applications where it is required to transfer power over long distances, the primary is built without core leaving the secondary with core [37]. Since the dynamic IPT system will be a large scale application, it is necessary to find the most cost efficient solution that can provide sufficient power transfer for the EV. Table 3.2 presents the advantages and disadvantages of the air core design. Appendix A further develops the air core configuration.

Table 3.2: Advantages and disadvantages of using an air core.

Type	**Advantages**	**Disadvantages**
Air core	• Lower cost. • Similar performance with the core-type [37]. • Less sensitive to misalignments [23]. • Easier to build. • Absence of core loss.	• Lower coupling factor and mutual inductance • Higher leakage flux • Lower self inductance • More turns are required to achieve the same power transfer levels

Chapter 4

Model architecture

For a thorough comparison between the two main types of dynamic IPT systems it will be necessary to model and build the respective subtypes presented in the last chapter. In order to do that, a finite element analysis (FEA) software is used. This chapter will cover a brief introduction to the simulation software and the simulation types considered for this work. Moreover, several parameters and important settings for the modeling of the system will also be addressed. They will range from the quantitative values used in the geometry to the mesh and the materials considered. Finally, a breakdown regarding the influence of speed in the power transfer of this system is explained.

4.1 Simulation software

The study of the different subtypes considered in the last chapter is made by the construction of the respective models in a simulation environment. The finite element method (FEM) is a numerical method used to solve problems in engineering and mathematical physics. It is very difficult to get analytical solutions in complex designs with different materials, proprieties and geometries. A finite element analysis (FEA) tool is necessary to solve for approximate results, by subdividing the problem into several smaller finite elements that are created by the mesh generation. This results in a series of algebraic equations that are more easily computed [43].

There are several software tools that have FEA. In this case, the chosen software was FLUX (by CEDRAT) because of its ability to solve electromagnetic systems with 2D or 3D models in static, harmonic or transient analysis. The FEA ensures a better understanding of all the magnetic and electrical variables that are present, while having an inductive coupling between a primary and a moving secondary. Furthermore, it is relatively straightforward to

assign materials to the different system components, change the system's dimensions and vary the speed at which the secondary is moving, among many other functionalities that will be covered in the following sections.

4.2 Simulation types

The simulation software divides the types of simulations in three major choices: 2D, Skew or 3D types. All of the models considered for this thesis were made in the 3D environment. Having chosen the 3D simulation type, the user is prompted to select the proper application for the model. The choice of an application depends on the problem type and on the desired results.

Fig. 4.1 presents the physical applications on the FLUX software. They are subdivided into four options that can be chosen according to the application. The aim of this work is to investigate the magnetic characteristics and properties of the dynamic IPT system. As such, the magnetic subtype was selected. Electric, thermal and thermal coupling are out of the scope of this work.

Magnetic applications can be further specified according to the field states as static, transient or steady state. Static, as the name implies, deals with phenomena where field sources are time independent. Steady state is related with devices where time variation of the field sources is sinusoidal. Finally, transient applications treat variables where field sources are time dependent (*in help file - CEDRAT*). Since the Magnetostatic 3D option is related to the presence of DC currents (stationary currents), it will not be used in this work as this

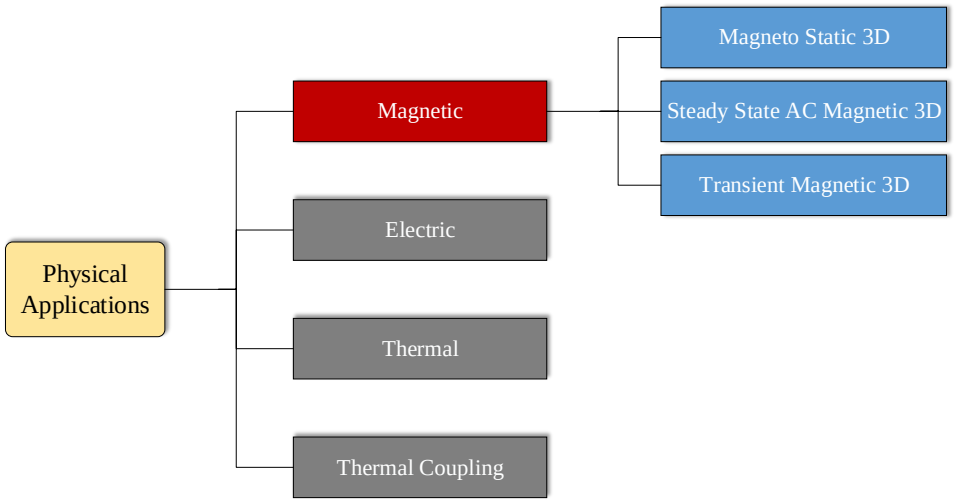

Figure 4.1: Physical applications available in the simulation software.

system will be working with AC power. As for steady state, Maxwell's equations consider that all physical quantities are time-variant for a given frequency. Also, the computed variables are obtained in discrete points chosen by the user and can be represented by their complex form or by the root mean square (RMS) value. Transient analysis has the particularity of allowing the user to establish a motion in a structure. In this case, the secondary will be moving in an arbitrary path and it is possible to impose a speed for that structure. The ability to investigate how the system works as a function of the secondary speed is of great interest. In that sense, simulations will be made in steady state and transient application models.

4.3 Infinite box

The infinite box is a "container" in which the whole structure is placed. The way this works is that the software uses a transformation to model an infinite domain. By using an infinite box, it is established that there is a null field at infinity, thus beyond the box dimensions there is no field and potential. These transformations can be of parallelepiped or cylinder layers and have two superimposed parallelepipeds or cylinders as can be seen in Fig. 4.2. For more clarity, the box shown below is ten times smaller than the one used. The inner box contains the magnetic field that is considered to be relevant to the study, whereas the outer box has magnetic field but with lesser strength.

There is no general rule for the overall dimensions of the infinite box and the user may build one with arbitrary values. It depends on the application and the magnetic or electric variables to study. However, to observe all the magnetic effects with greater detail outside the structure it is recommended to design one box much larger than the system which is the case for this work. Table 4.1 displays the numerical values for the dimensions of each

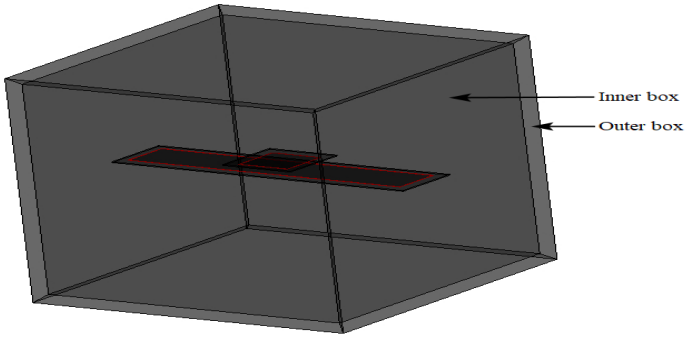

Figure 4.2: Infinite box of this work.

Table 4.1: Infinite box dimensions.

Axis	Inner box	Outer box
X	12000/15000	13000/16000
Y	12000/15000	13000/16000
Z	12000/15000	13000/16000

half side of the box considered in this work. The constant values of 12000 mm, 13000 mm, 15000 mm and 16000 mm were used because of the total length of the primary structure. In the long type it is 3000 mm (see Fig. 4.3), while on the segmented type it is 2300 mm (see Fig. 4.5). Essentially it was decided that, as a general rule for this work, the dimensions of the half sides of the box would be five times the length of the primary so 12000 mm for the segmented primary and 15000 mm for the long primary. Despite this, it is important to note that the dimensions used are directly connected to the mesh so having a considerable infinite box will require more computational effort when the software starts the solving process (*in help file - CEDRAT*).

4.4 Geometry

The different geometries considered for this comparison were introduced in the previous chapter. This section will further explain some of the design options taken for both the long and segmented types of dynamic IPT, as well as details regarding the geometric variables and values.

All the geometric dimensions considered for the long R-R configuration are presented in Fig. 4.3. They are based on the 6th generation of RPEV found in [23]. For better clarity, the dimensions for the thickness of the components are not specified. The thickness of the iron plates is the same on the primary and secondary and is equal to 13 mm. Moreover the coils on both the primary and secondary sides have a 4, 8 or 16 mm^2 cross section depending on the configuration used. These three different areas were chosen due to problems in the simulation software. When the conductor has a 4 mm^2 cross section in double coil (DD) types, the software would give an error because of the probable existence of so called

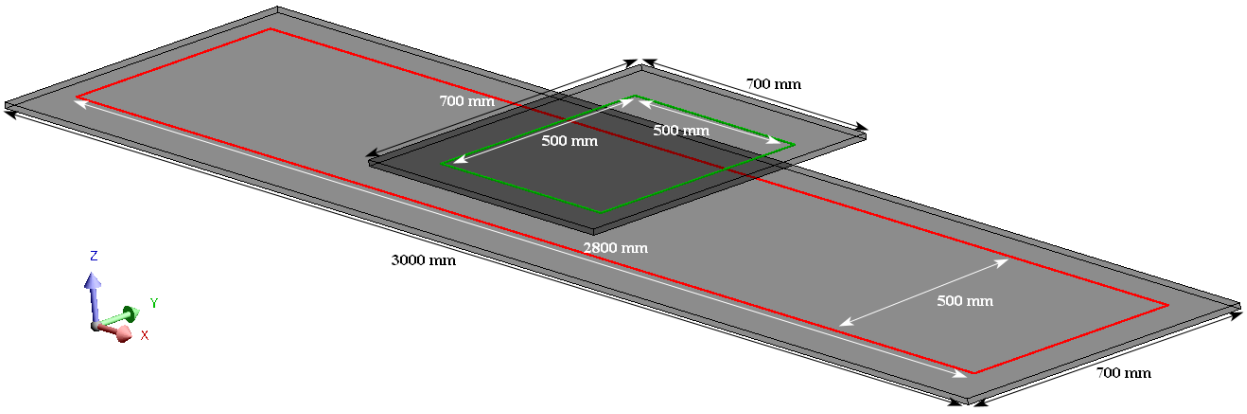

Figure 4.3: Dimensions considered for the long R-R configuration.

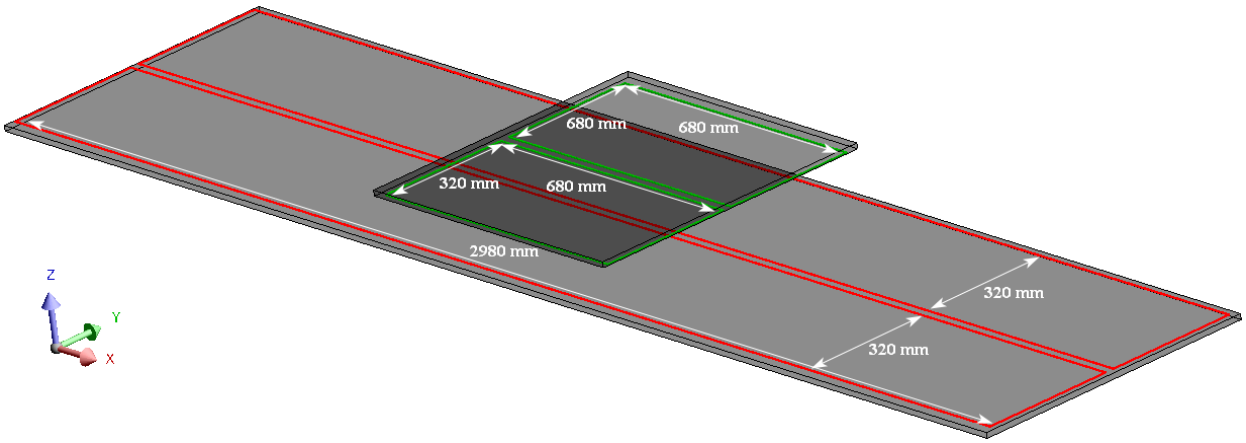

Figure 4.4: New dimensions for the DD-DD long configuration.

superimposed faces, presumably because of the very small area considered.

The long configurations are derived from the one shown in Fig. 4.3, from which several modifications are made as can be seen in Figs. 3.3b, 3.3d and 4.4. They are based on the rectangular and DD designs proposed in segmented configurations but adapted to the long profile. Although the geometry is different, the material used is the same to make sure that all the comparisons are made with an equivalent amount of materials.

The number of coils used for both the primary and secondary was also based on the bibliography [23]. Knowing that the primary has 2 turns and the secondary 15 turns, it is possible to design a configuration like the one in Fig. 4.4 by simple calculation. The primary coil in Fig. 4.3 is 2800x500 mm and has 2 turns. So, converting to a DD configuration requires the division of the turns into two separated coils of 2980x320 mm with one turn each. This results in the exact same length of coil (ℓ_p) used but with a different geometry, as can be seen from equation 4.1 with $N_p = 2$.

$$\begin{cases} \ell_p = \overbrace{\Big(\big(2800+500\big)\times 2\Big)}^{Length\ of\ one\ turn} \times N_p = 13200\ mm \\ \ell_p = \Big(\big(2980+320\big)\times 2\Big) \times N_p = 13200\ mm \end{cases} \quad \begin{cases} \ell_s = \overbrace{\Big(\big(500+500\big)\times 2\Big)}^{Length\ of\ one\ turn} \times N_s = 30000\ mm \\ \ell_s = \Big(\big(680+320\big)\times 2\Big) \times N_s = 32000\ mm \end{cases} \tag{4.1}$$

Same train of thought applies for the secondary coil length (ℓ_s) with $N_s = 15$, where turns are converted into 8 in each coil and the dimensions change from 500x500 mm to 680x320 mm. It is better to put 8 turns in each DD coil (16 total) for better symmetry, although with a slight increase in total length. The other long layouts of Fig. 3.3c and 3.3b have a similar design process.

As for the segmented designs, some different variations were considered, besides the

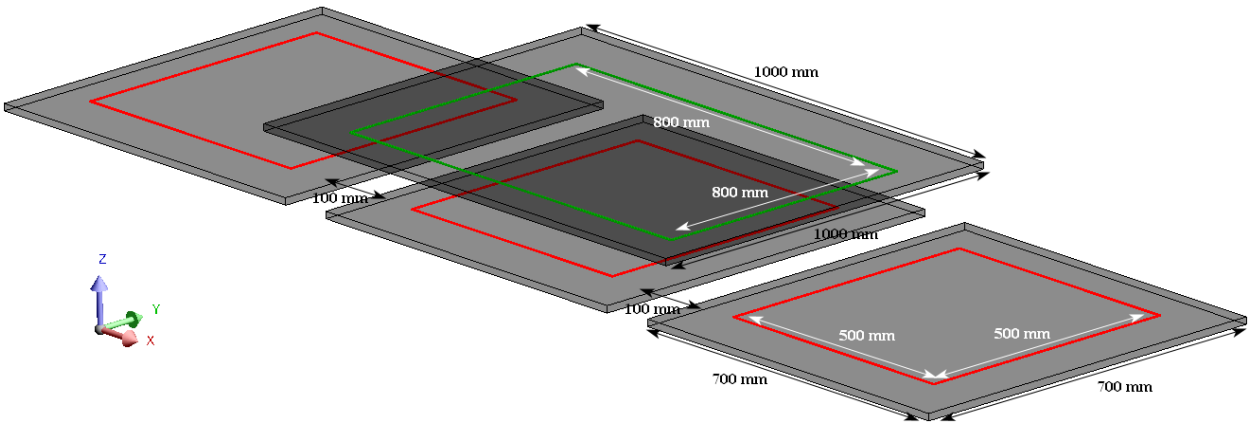

Figure 4.5: Dimensions for the segmented R-R_+ type with larger secondary.

already discussed rectangular and DD type. The one shown in Fig. 4.5 has a bigger secondary with the core plate being 1000x1000 *mm* instead of 700x700 *mm* and the coil modified to 800x800 *mm* from 500x500 *mm*. The distance between primary segments is the same in all topologies and is equal to 100 *mm*. Like in the long types, 2 turns were used in each primary segment and 15 in the secondary, except in double coil secondaries where it is 16.

The BP-R arrangement pictured in Fig. 4.6 is an exception to all primary geometries, with two additional coils that are placed between the 3 segments. They also have 2 turns each and are 400x500 *mm*. The designation of bipolar (BP) comes from the other type that also has overlapping coils in the secondary (Fig. 4.7). That type is known as DD-BP and was designed with the same intent of maintaining the coil length when changing from rectangular to DD or bipolar.

The conversion from rectangular to DD or rectangular to bipolar on segmented systems is also done with respect to equation 4.1 with the necessary adaptations. So, in the case of a conversion from a rectangular to a DD primary, coils will change from 500x500 *mm*

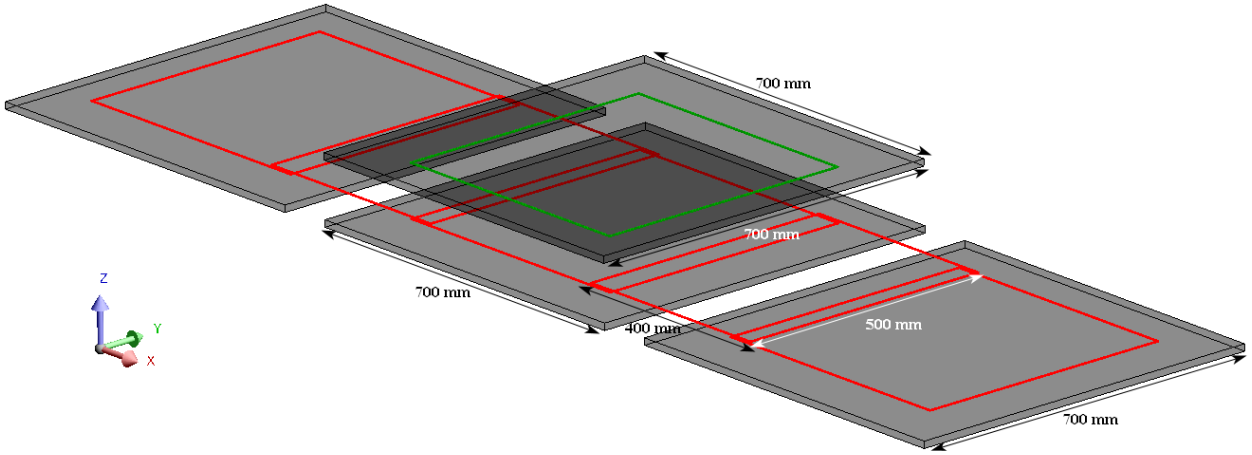

Figure 4.6: Dimensions for the segmented BP-R type.

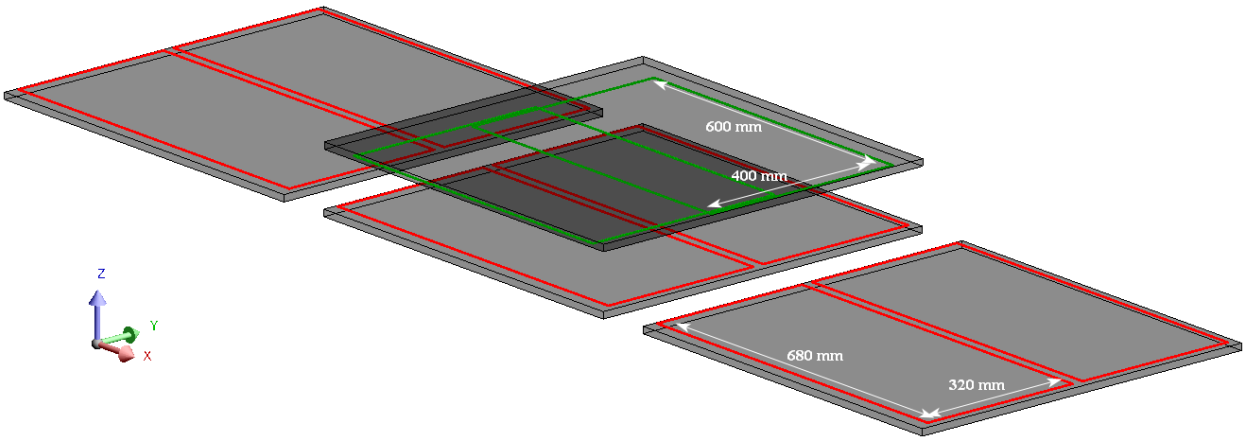

Figure 4.7: Dimensions for the segmented DD-BP type.

to 680x320 mm. This notion can then be applied to the other segmented variants. The ferromagnetic material for the segments remained the same in all segmented types and is 700x700 mm with the exception of R_+ (Fig. 4.5).

R-R and DD-DD systems have the same dimensions on primary and secondary, so previous explanations regarding their dimensions are sufficient.

Finally, it is important to note that the total length of the primary is different in the long and segmented configurations. It is 3000 mm in the long types and 2300 mm in the segmented types.

4.5 Material

The geometry used has great impact in the system behavior, either by different electric and magnetic characteristics, or capabilities of better coupling and power transfer. In spite of that, the materials used for the primary and secondary structures need to be adequate for a good overall system quality and efficiency.

In the primary and secondary structures the magnetic core has to have a good magnetic permeability μ_r and low losses but also good resistance against mechanical stresses. N87 by Epcos was the material chosen for the simulations due to its ability to work in high frequency applications with low core losses. Fig. 4.8a shows the dynamic magnetization curves of N87 at 10 kHz and 25^{o}C. The relative core losses as a function of frequency can be seen at Fig. 4.8b.

The stranded coil conductor used for both the primary and secondary was made out of copper with an isotropic resistivity linearly proportional to the temperature. The filling factor was not specified for this work. The magnetic and electric properties of the materials

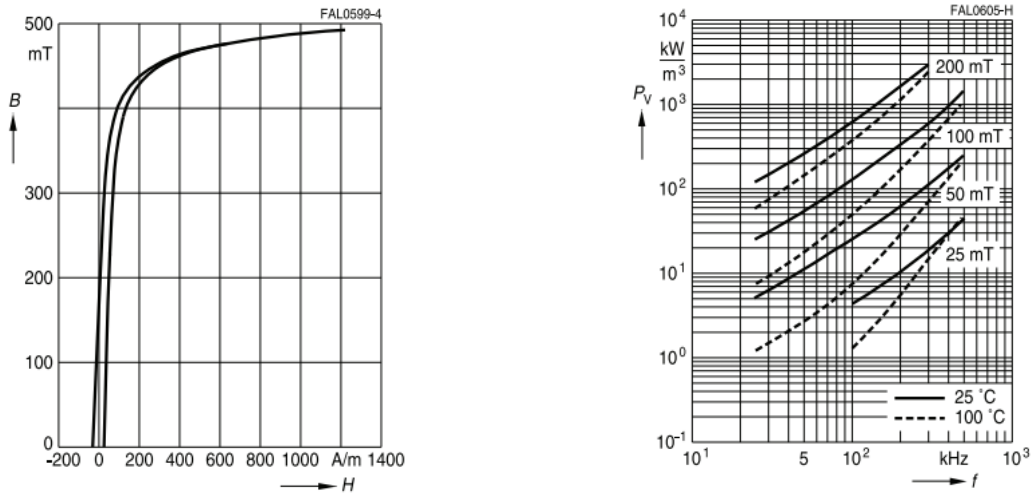

(a) B-H curve.

(b) Core losses.

Figure 4.8: N87 material [44].

used are specified in Appendix B.

4.6 Mesh

After building the geometry and specifying the materials for the electromagnetic study of a system, the suitable mesh must be proposed. The finite element analysis will divide the study domain into mesh elements for computation. These elements are divided into volume, surface and line. The mesh is directly related to the quality of the solution, so to have a more precise calculation the mesh element quality has to be good. However, increasing the quality of the mesh has the downside of also increasing the computation time. A compromise must be made between computation time and precision of results.

The automatic mesh generator was used for all geometries to mesh the whole domain because of its versatility, ease of use and overall good performance. Furthermore it is robust, fast and does not require any tweaking with the refinement options. Fig. 4.9a exhibits the

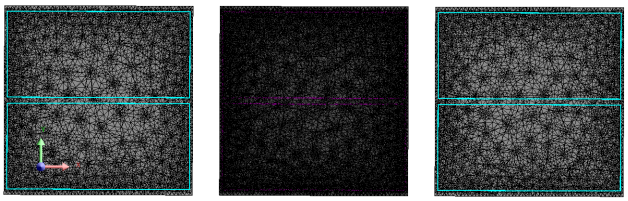

(a) Meshed domain.

```
Volume elements :
   Number of elements not evaluated     : 0  %
   Number of excellent quality elements : 14.01  %
   Number of good quality elements      : 27.22  %
   Number of average quality elements   : 41.22  %
   Number of poor quality elements      : 17.56  %
```

(b) Mesh details.

Figure 4.9: Mesh information for DD-DD segmented type.

meshed geometry of the DD-DD segmented type seen from above. The meshing is done with triangle elements for faces and tetrahedrons for volumes. Fig. 4.9b displays the elements' quality in percentage of the total number of elements. Since the automatic mesh is a balanced option, the overall quality is reflected on that by having more than 40% of average quality elements. Nevertheless, more than 75% of elements are of average or better quality. The mesh percentages for the other topologies are similar.

4.7 Electric circuit

The designed coils have to be assigned to an electric circuit that represents the system. Only the coupling system associated with the power transfer will be simulated i.e. primary and secondary. The primary side will be fed with an effective current of $I_p = 20\ A$ at 85 kHz for all the topologies studied in the steady state domain. For the transient study, a time-variant current source with $20\sqrt{2}\ A$ of amplitude is used. At the secondary coil the AC current must be rectified to charge the DC batteries of the EV. However, the respective converters were replaced with an equivalent single resistor that is named R_{load}. One of the main disadvantages of the segmented design is the supposed need of separate source converters for each segment. While it could be simulated that way, it was instead modeled with the primary coils all connected in series being powered simultaneously, as shown in Fig. 4.10 for the DD-DD topology.

The resistance of the stranded coil conductors was defined to be a constant value equal to 0,1 Ω and the load will be 100 Ω, or 10 $M\Omega$ whether it is a normal load test or an open circuit test.

The polarity of the coils is also subject to testing because of its influence on how the system will perform. It is possible to alter the direction of the current by orienting coils manually in the graphic environment, or by switching the polarity of the coil elements that

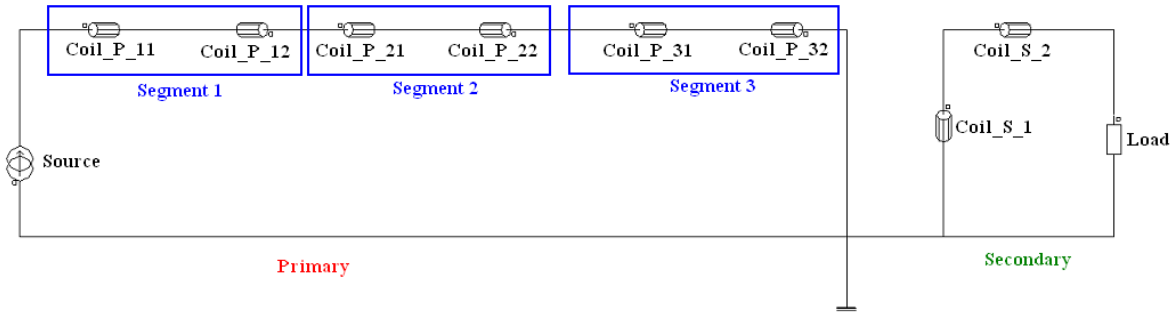

Figure 4.10: Electric schematic for the DD-DD segmented topology.

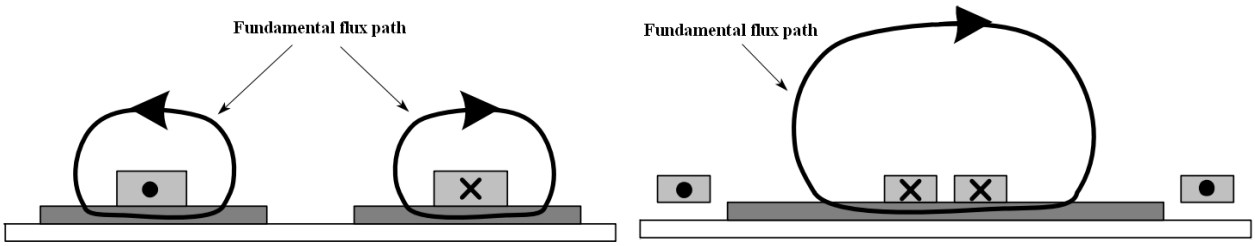

(a) Flux path for rectangular coils.

(b) Flux path for DD coils.

Figure 4.11: Flux path for rectangular and DD coils [19].

are presented in Fig. 4.10. Depending on the direction of current, the magnetic flux lines will also have a different direction as per the right hand rule. On the rectangular architectures, the direction of the magnetic flux lines was designed to be upwards (Fig. 4.11a). For DD types the coils were connected with opposing directions of current, so that a closing magnetic field is obtained, as shown in Fig. 4.11b. Note how the coils are connected in Fig. 4.10 with opposing polarities. If the DD coils were to have the same direction of current, the magnetic flux lines would cancel each other at the center of the structure. This would affect severely the fundamental magnetic field and, consequently, the coupling between the primary and secondary.

4.8 Speed of the secondary structure

The speed of the secondary structure is an important variable in the dynamic charging of electric vehicles and will definitely influence the performance of the system. The need to be able to deliver large power levels to vehicles on the road, when they could be traveling at speeds of up to 120 km/h, requires great engineering and high technological optimization. Powering an electric vehicle on the road is dependent on several factors [45]:

- Traffic on the road;
- Percentage of EVs to total vehicles passing;
- Length of the power track or pad;
- Speed of the EV.

The first two points are not related to this work. Last two, however, are discussed by comparing a long and segmented track and by varying the vehicle's velocity to evaluate the differences in power transfer.

A vehicle that moves at higher speeds will need more power than at slower speeds. Therefore, the power levels of the transmitting tracks must be designed as a function of

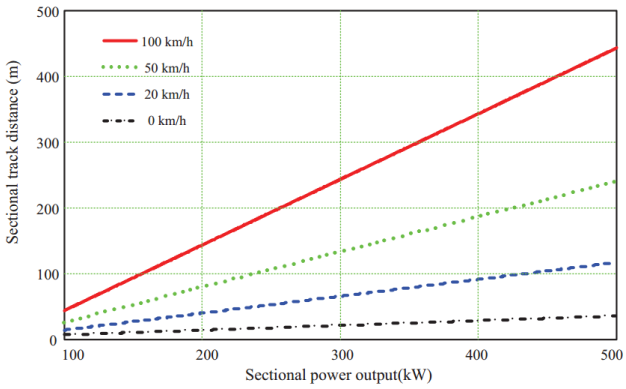

Figure 4.12: Power levels of sectional tracks as a function of velocity [46].

vehicle speed. Fig. 4.12 shows the relationship between vehicle speed, track length and segment power output. It can be inferred that the power output per sectional track distance decreases with increasing speed. The sectional track utilization is also lower with increased vehicle speed.

To adjust the vehicle speed in the FEA software, the application must be in transient mode and it is necessary to specify the mechanical sets of the environment. In this case, the system will have three mechanical sets: a fixed (primary), a moving (secondary) and a compressible part (area of air in which the moving part is moving). It is possible to specify which type of motion the moving part has, therefore a translation motion along the x axis was chosen. As for the imposed speed, it is a constant velocity in relation to the fixed part. The computation is carried out in a series of steps that are defined as a function of the source current period. Getting a lot of points per period will increase the precision of the resulting signals, at the cost of greater computation time. On top of that, the frequency of operation is 85 kHz, so to have a considerable number of points per period and simulate a fair speed (120 km/h) is extremely demanding to the hardware available.

4.8.1 Kinematic models

Flux software by CEDRAT allows the use of two main kinematic models to study the movement of objects. Those two models coincide with the ones chosen for this work which are:

- Multi-static model: consists of a static study of the movement. The computations for the electromagnetic field are carried out for various arbitrary relative positions of the moving parts. The position of the moving part is a varying parameter.
- Imposed speed model: the moving part travels at a constant speed relative to the fixed

part. Only available in transient mode.

These two models and their characteristics will be further explored in the next chapter.

Chapter 5

Simulation results

With the project model developed for all topologies, it is now necessary to compare and discuss the respective results for the simulations. As previously stated, the simulations were done in both steady state and transient. For steady state analysis, a set of discrete points in the Ox, Oy and Oz directions were specified. This allows the study of the different behaviors of the topologies to aligned and misaligned situations. With the insertion of a time-variant current source and the respective imposed speed for the secondary structure, it is possible to make a correlation between the results obtained in the steady state and transient simulations.

5.1 Steady state analysis

The computation in steady state gives access to a series of parameters that allow the user to obtain other variables. These are important for the analysis of the dynamic system. After proper construction of the system, a solving process begins. Depending on several factors like the mesh refinement, the infinite box and the complexity of the system, the solving may take from some hours to several days.

The post-processing (Fig. 5.1) of the system has a wide range of variables that are available when the solving process ends. Among them the rms values of magnetic flux Φ, current I, voltage V and reactive power Q_{source} are the most requested and necessary for

Figure 5.1: Overall flowchart for FEA.

the derivation of other parameters. To carry out the calculation of the coupling factor k and the mutual inductance M between primary and secondary, equations 2.11, 2.12 and 2.13 will be applied. In order to calculate the mutual inductance, two tests must be done which are the secondary and primary open circuit tests. After that, it is possible to calculate M_{ps} and M_{sp} and do the average between them to finally obtain M. The coupling factor is calculated with equation 2.11 and with M known, there is only L_p and L_s left to discover. The self inductances can be calculated through equation 2.3 with rms values of i and Φ. If the configuration to study uses only one coil at the primary and secondary, then the self inductance of each coil is given by that equation (2.3). However, given that in the majority of studied cases there are multiple coils connected in series in the primary or secondary coils, a different method for the effective self inductance must be used. The reactive power at the source can be expressed as a function of the reactance as

$$Q_{source} = I_x^2 \omega L_x, \quad x \in \{p, s\} \tag{5.1}$$

with I_x^2 being the rms current and L_x the effective inductance of the primary or secondary.

The characteristics and intrinsic differences between the two main types of primaries require that they are analyzed separately. In particular, due to the difference in their lengths, the discrete points at which the simulations were carried out are different in segmented and long types. For that reason and also to make the analysis easier, the separation is made.

5.1.1 Long types

There are 4 types of long configurations that were simulated. They are represented from Fig. 3.3a to 3.3d and will be named in the graphic legends as R-R to Fig. 3.3a, DD-R to Fig. 3.3b, R-DD to Fig. 3.3c and DD-DD to Fig. 3.3d. Important parameters regarding these

Table 5.1: Parameters for long types.

Parameters	Value	Description
t_{sim}	1-5 h	Simulation time
f	85 kHz	Frequency of operation
N_p	2	Primary turns
N_s	15/16	Secondary turns
I_{source}	20 A	Rms source current
R_p	0,1 Ω	Resistance of primary coil
R_s	0,1 Ω	Resistance of secondary coil
R_{load}	10 $M\Omega$	Load resistance

configurations are summarized in table 5.1. The secondary is placed with 100 mm of air gap at coordinates (0,0,100) in the aligned position, as can be seen in Fig. 3.3. The simulations were done considering 3 types of movement. Firstly, along the Ox axis and maintaining the other coordinates unchanged. After that, in the Oy direction, in which the secondary is only moved along the y axis. Finally, in the Oz axis that is equivalent to the variation of the air gap.

Results in the Ox direction

A set of points that goes from the beginning of the primary track till its end was simulated. The movement along the Ox axis is the most important result since vehicles will be running along the Ox axis. Knowing that the total length of the track is 3000 mm, an interval of 11 points equally distanced from themselves was considered, so that $x \in [-1500, 1500]$.

Fig. 5.2 shows the self inductances of the primary and secondary for the 4 types considered. In general, across all configurations, the inductance remains relatively constant throughout the x axis. This is important for the eventual capacitive compensation of the primary and secondary coils. Even though it was not considered for this work, the dynamic IPT system needs to be working at resonance frequency to achieve maximum power transfer and better efficiency. To do that the primary and secondary are compensated with capacitors that can be connected in series or parallel. These small variations in the self inductances mean that the resonance frequency is constantly changing, which in turn causes the system to not be in resonance if it has a constant frequency.

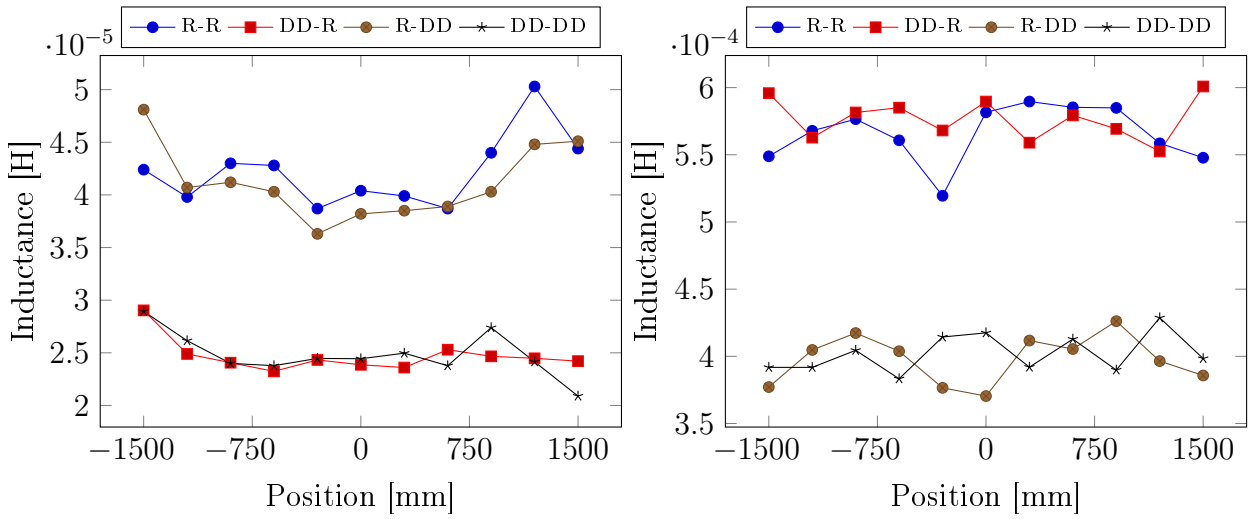

(a) Primary self inductance.

(b) Secondary self inductance.

Figure 5.2: Self inductances for long configurations as a function of x.

The self inductance depends on the material used, the number of turns, the geometry of the coils and how they are placed in the iron core. It is possible to conclude that the rectangular coils render a higher self inductance than the DD coils with this happening on both the primary and secondary. Moreover, it seems that the self inductance is independent of the configuration of the homologous structure. For instance, the self inductance of the primary R coil is essentially the same when the system is R-R or R-DD. Finally, the self inductance in the secondary is higher due to the greater number of turns there.

The mutual inductance and coupling factor of the long configurations as a function of the position along the track are plotted in Fig. 5.3a and 5.3b, respectively. The relationship between mutual inductance and coupling factor is evident and corroborates the equation 2.11. Mutual inductance and coupling factor remained constant as long as the secondary is above the track. At -1500 and 1500 mm, right at the end of the track, the misalignment is such that the coupling and mutual inductance are reduced significantly.

The mutual inductance depends very much on the positioning of the primary and secondary coils. If they are too far apart, or the geometry doesn't favor the induction of emf, then the mutual inductance will be low. For the DD-R configuration, the fact that the secondary is always at the center of the track in between the two DD primary coils ($y = 0$), makes it so that the flux of the primary has difficulty going through the secondary coil in that central position. The direction of flux is horizontal along that path (Fig. 4.11b) and the secondary coils are also placed parallel to the primary structure so the flux isn't perpendicular to the coils As a result, the flux that goes through the coil will be equal to the

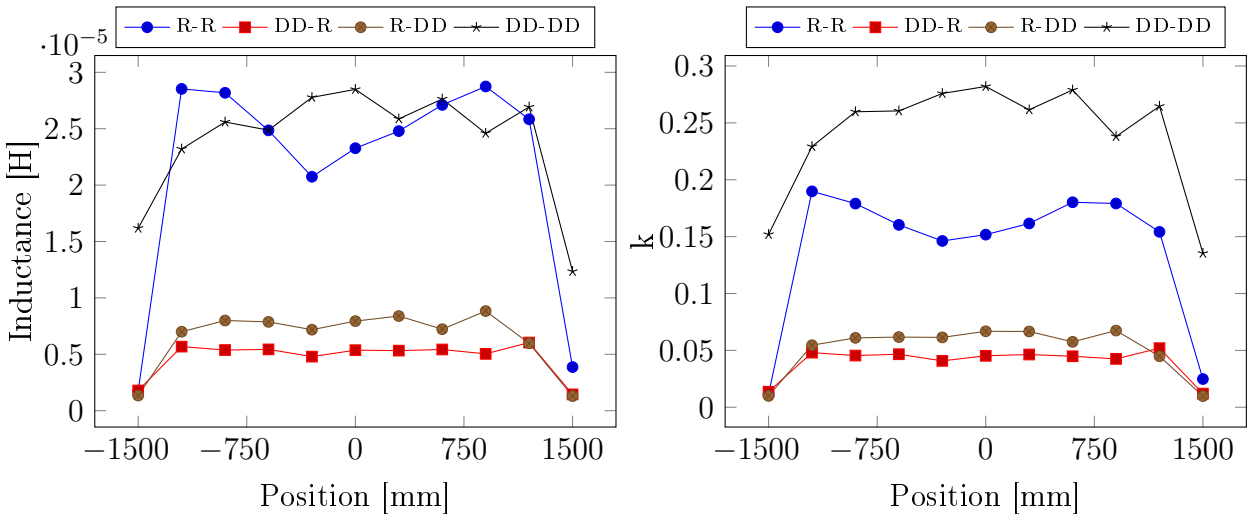

(a) Mutual inductance.

(b) Coupling factor.

Figure 5.3: Mutual induction and coupling factor for long configurations as a function of x.

one that leaves it, which causes the emf to be low. Same behaviour is noticed at the R-DD configuration, although in the reverse working condition. In this case the resulting emf is low when the primary is left open, so M_{sp} is also low and the coupling factor is similar to the DD-R topology.

Out of these 4 types, the R-R and DD-DD offered better coupling along the x axis. The simplest R-R configuration had a k between 0.15 and 0.2, while DD-DD almost reached a coupling factor of 0.3. The largest k is related to the characteristics of the magnetic flux in the DD configuration, as was explained in Chapter 4. This is expected as the size difference of the primary and secondary is large, and so is the leakage flux.

Results in the Oy direction

When traveling across a road, it is normal for the vehicle to not be perfectly aligned with the traffic lane. This results in a misalignment in the y direction and the coupling will be affected. To evaluate what happens with each configuration, 5 simulations of equal intervals were carried out from 0 to 500 mm. Fig. 5.4a and Fig. 5.4b show the influence of misalignments in the y direction on the self inductance of the coils.

In a similar behaviour to the previous situation, the self inductances of the primary and secondary coils are relatively constant throughout the 5 points considered. In fact, the values are similar even though in this case the x coordinate remains equal to zero at all points. The configurations with R coils remain with a superior self inductance.

Fig. 5.5 shows the mutual inductance and coupling factor for misalignments in the y

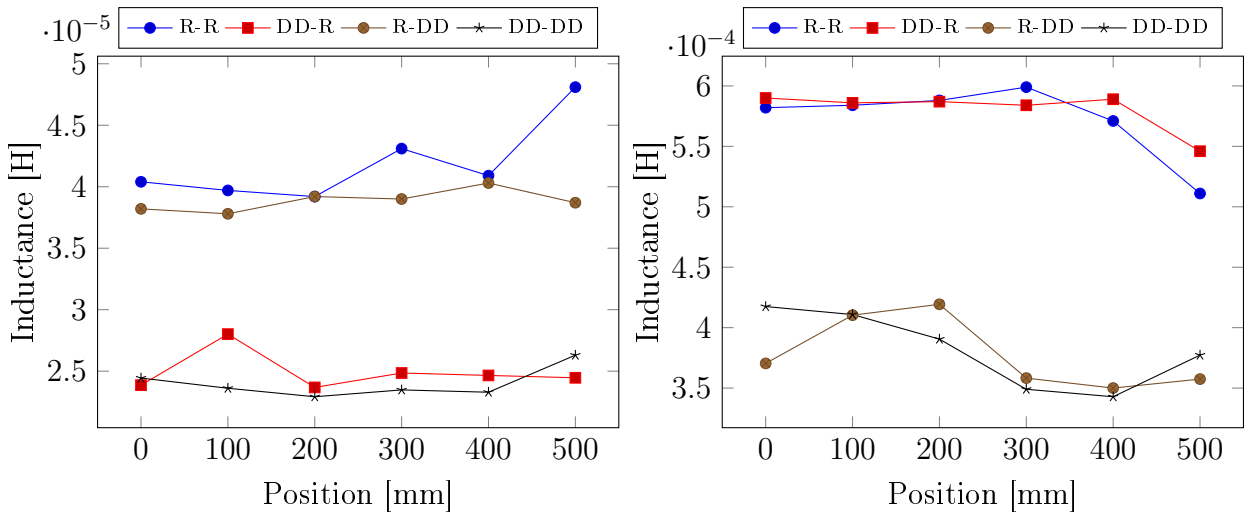

(a) Primary self inductance.

(b) Secondary self inductance.

Figure 5.4: Self inductances for long configurations as a function of y.

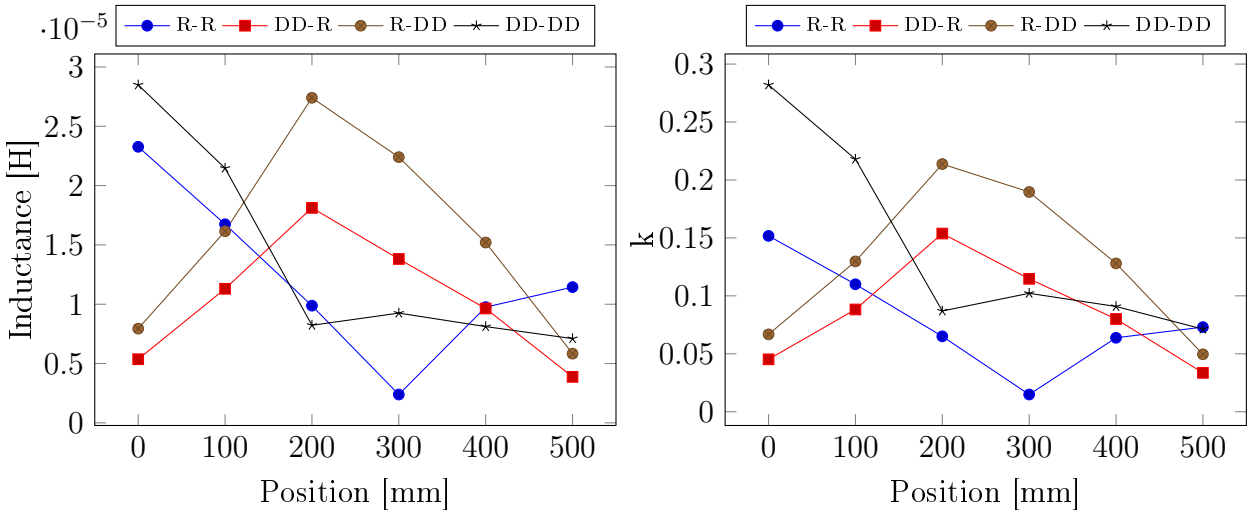

(a) Mutual inductance.

(b) Coupling factor.

Figure 5.5: Mutual induction and coupling factor for long configurations as a function of y.

direction. As can be inferred, there are two main differences in the types considered. Those with a decaying of mutual inductance and the others that have a fairly decent tolerance to deviations in the y axis.

Both R-R and DD-DD topologies have low tolerance in the y direction, with a lower coupling factor when the secondary gets farther from the primary track. Less magnetic flux lines will go through the couplers when the secondary is shifted, thus the mutual inductance diminishes. Yet, there is a point around 250 *mm* where that reduction is halted. Those are known as null points and will be addressed in the next analysis of the segmented designs. Two diagrams pertaining to the DD-R and R-DD configurations are pictured in Fig. 5.6, for a better understanding of the deviations considered. The magnetic characteristic of those two types is illustrated in Fig. 5.7.

It was clear from the results in the x domain that DD-R and R-DD had low coupling

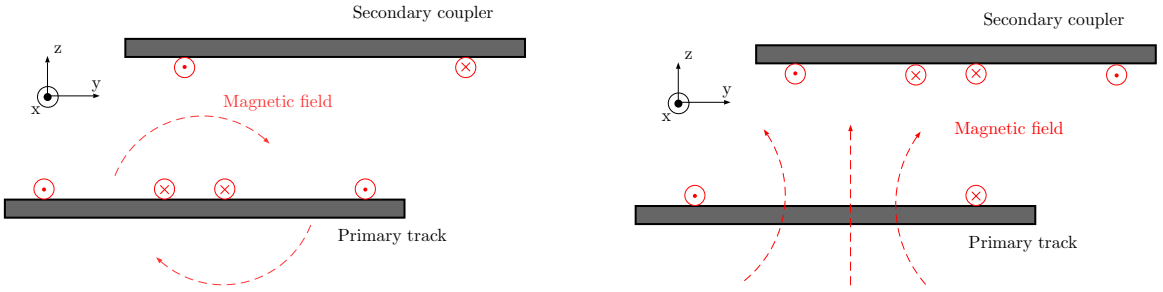

(a) DD-R.

(b) R-DD.

Figure 5.6: Deviation on y axis for long configurations.

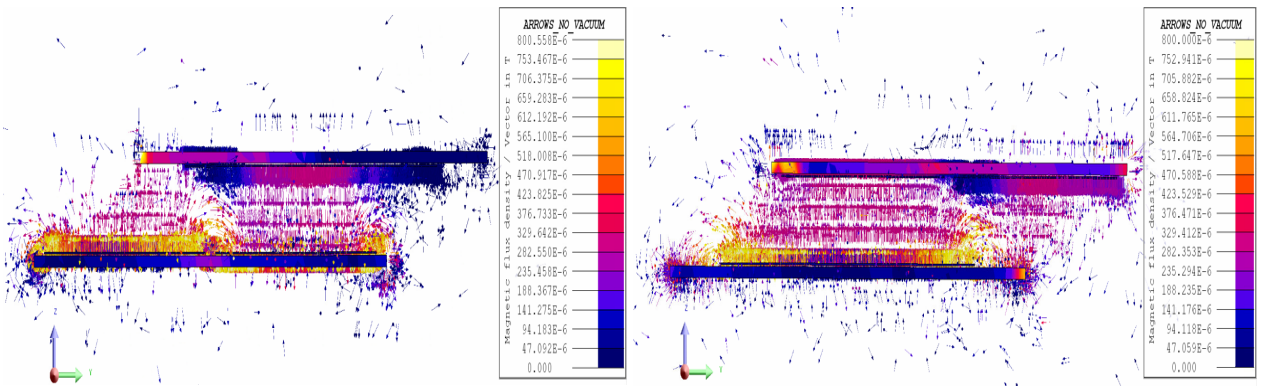

(a) DD-R topology. (b) R-DD topology.

Figure 5.7: Magnetic flux lines for a misalignment of $y = 200\ mm$.

factor and therefore are unsuitable for dynamic charging, at least in a centered position with $y = 0$. However, the results in the y domain show that those two configurations have better coupling with slight misalignments of around 200 mm.

The diagrams in Fig. 5.6 and 5.7 help understand how this increase in k possible. What happens is that on Fig. 5.6a the magnetic flux does not enter and exit the same coil like it does in $y = 0$. As such, the magnetic flux lines can go through the secondary coil without having a full cancellation effect. As for Fig. 5.6b, the conclusion is similar (note that these two types are symmetrical with respect to their configurations on primary and secondary). At a slight misalignment, the vertical primary flux goes through the left D coil and then pass through the right D coil with the downward flux (Fig. 5.7b). This suggests that these configurations would be suitable in dynamic charging for a two or one lane highway, depending on the combination used. With that in mind and knowing that these configurations have poor coupling at a central position in the track, two solutions are presented in Fig. 5.8. For a two lane highway, it is possible to avoid the poor coupling along x by designing both systems in that manner.

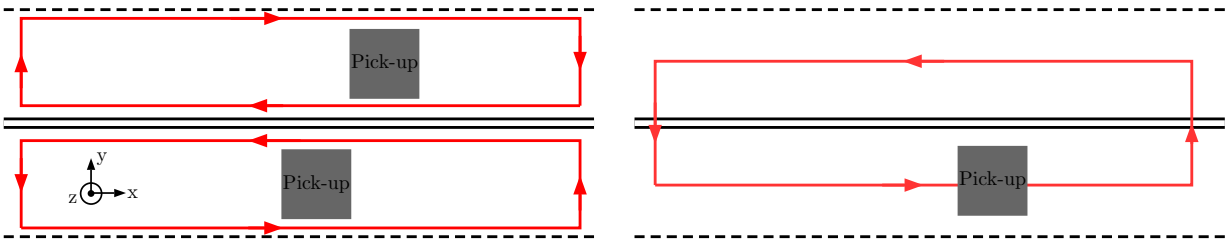

(a) Highway for DD-R topology. (b) Highway for R-DD topology.

Figure 5.8: Possible highway applications for DD-R and R-DD configurations.

Results in the Oz direction

In a real life situation the air gap stays relatively unchanged. However, five levels of distance in the z axis, from 100 to 200 *mm* were simulated. This was done to evaluate the difference in magnetic coupling as the air gap increases.

Fig. 5.9 shows the self inductances of secondary and primary coils as a function of air gap. The study for three different movements (x,y,z) was done and the results have in common the fact that the self inductances remains, for the most part, constant. On this case, there is a considerable decline as the vertical distance increases and the effect of the primary and secondary magnetic flux is weakened.

The effects in mutual inductance and coupling factor are also expected to decline as the magnetic field intensity is inversely proportional to the distance. Fig. 5.10 confirms this with a steady decrease in mutual inductance in all four configurations. It is important to note that changing from 100 to 200 *mm*, yields an almost 50% decrease in coupling factor from approximately 0.3 to 0.15 on the best design studied (DD-DD). This means that even above all situations previously discussed, the highest decrease per distance covered is in the z direction. Of course there is a limit to how close a secondary can get to the primary. Nevertheless, the aim should be to make them as close as possible. Overall, all the other configurations suffer from the same consequences, albeit with smaller decreases.

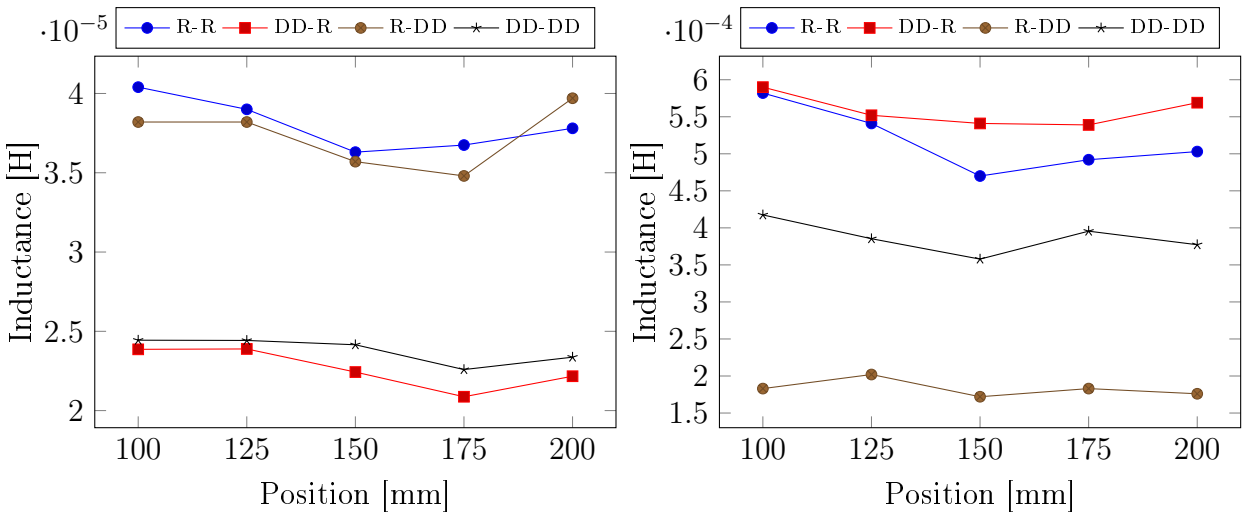

(a) Primary self inductance.

(b) Secondary self inductance.

Figure 5.9: Self inductances for long configurations as a function of z.

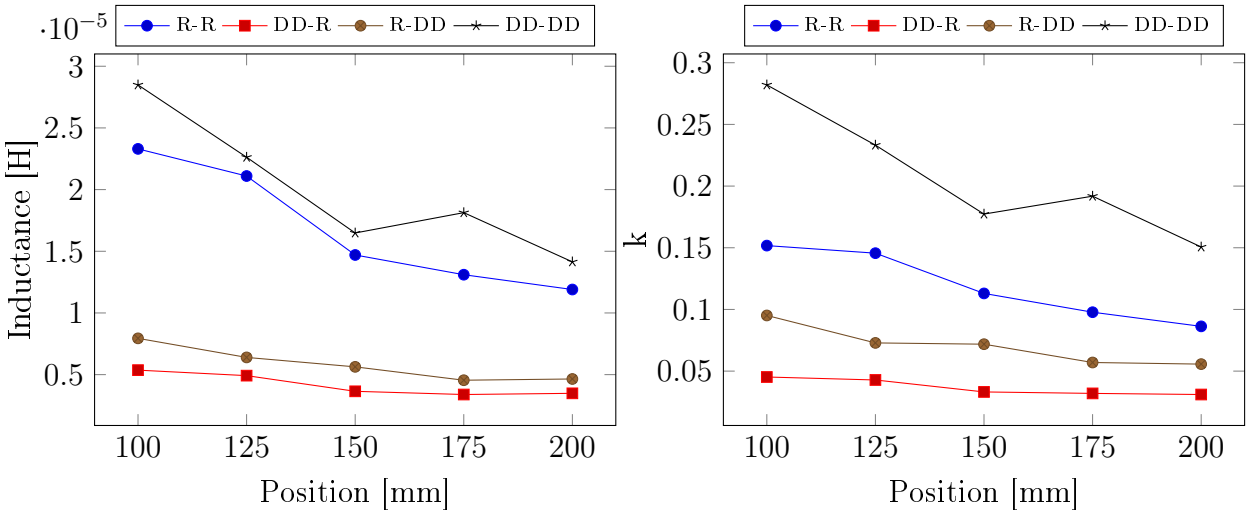

(a) Mutual inductance.

(b) Coupling factor.

Figure 5.10: Mutual induction and coupling factor for long configurations as a function of z.

5.1.2 Segmented types

Even though the long types have their advantages, most of the scientific research has been conducted on designs with less material usage and, most importantly, better coupling factors. The subdivision of the primary track into segments has been proven to be a good option for RPEVs. Chapter 3 already introduced the segmented designs, so in total there are 6 types: R-R, R-R_+, BP-R, DD-R, DD-DD and DD-BP from Fig 3.3e to 3.3j. R_+ stands for the larger secondary structure. This section will cover the same solving process as previously explained with minor changes due to the system's geometry. The main variables for the solving process are the same as the ones in Table 5.1 with the difference being that each primary segment has 2 turns, which makes the total number of turns above the one in the long system. Moreover, the coil segments are connected in series and so to calculate the self inductance, equation 5.1 was used.

Results in the Ox direction

Like in the previous simulations, the study along the x axis was done in a set of equally distanced points along three track sections. Since the total length of the primary is 2300 mm, including the gaps between segments, the movement in the x direction was considered from -1200 to 1200 mm, with 13 points. This will include positions that are between segments and also perfectly aligned with them, in order to evaluate what happens when a vehicle goes through several segments.

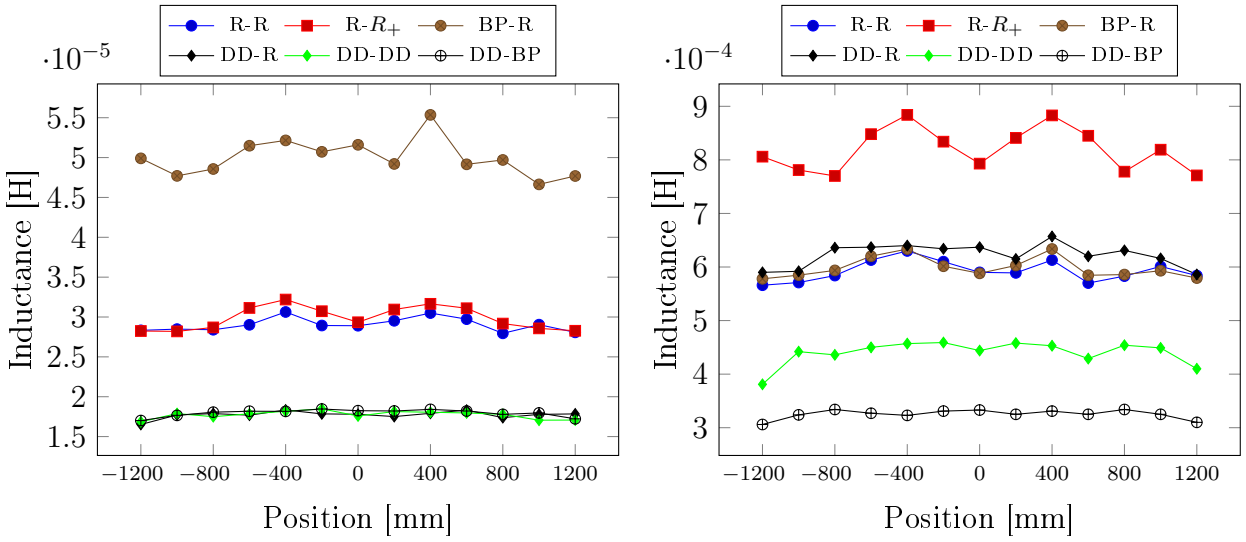

(a) Primary self inductance.

(b) Secondary self inductance.

Figure 5.11: Self inductances for segmented configurations as a function of x.

The relationship between self inductance and longitudinal movement is pictured in Fig. 5.11. Like in the previous analysis, the self inductance does not suffer a significant deviation throughout the x axis. In terms of the values obtained, the BP-R configuration has the larger L_p, due to the additional coils that were placed between segments. The configurations with a common rectangular primary (R-R and R-R_+) have similar values of primary inductance, as expected. R_+ has the highest L_s due to the longer secondary used. This increase seems to raise the fluctuation in self inductance. As the coils get more compact, their inductance is more stable.

As for the DD coils, because of the smaller length of each coil, the self inductance is also smaller. The same thought is applied to the L_s representation of Fig. 5.11b, where the secondary configurations are clearly independent of the primary ones.

Studying the influence on coupling and mutual inductance as a vehicle goes through a segmented track is the most important thing to evaluate the viability of the various configurations. The mutual inductance and coupling factor are represented in Fig. 5.12a and 5.12b, respectively, and show that these variables are very influenced by the type of geometry used. The three primary segments are placed at the origin and ±800 mm away from it. Results show that there are some architectures unsuitable for dynamic charging and others that may have good coupling in certain points. Some, however, suffer from high variation when transitioning between power pads.

Similarly to the previous long configuration, the DD-R topology has an equivalent performance to the long counterpart, with low coupling in a x aligned position throughout all

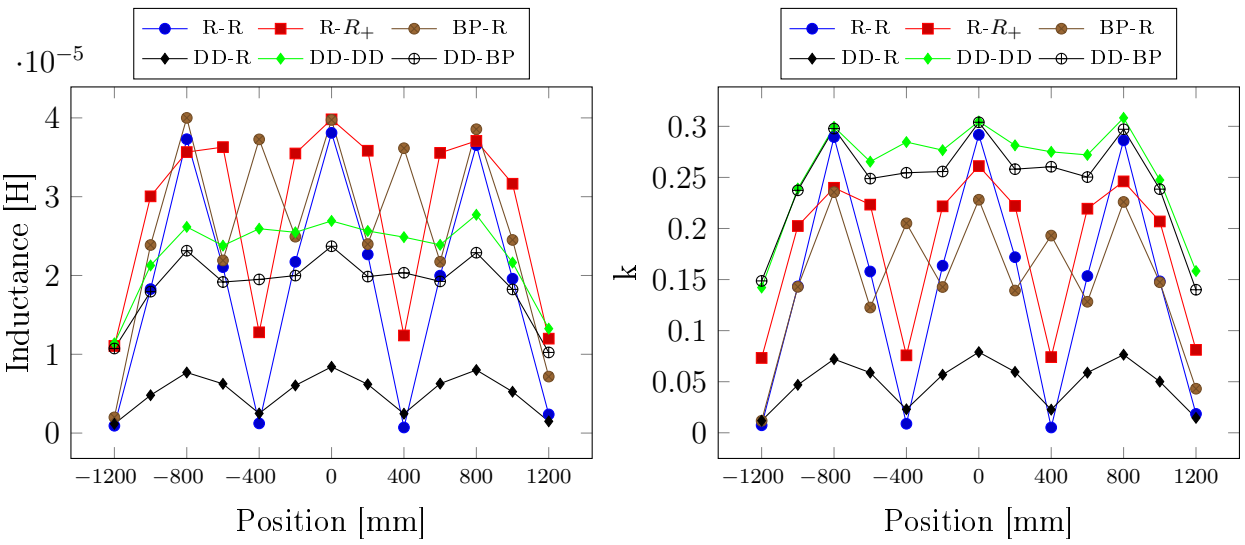

(a) Mutual inductance.

(b) Coupling factor.

Figure 5.12: M and k for segmented configurations as a function of x.

points. The rectangular coils are simple to build and construct, however their use in a segmented track would be unsafe because of their poor tolerance to misalignments in x. Blue, red and brown plots show the three topologies with a rectangular secondary coil: R-R, R-R_+ and BP-R. They all have something in common, which is the fact that coupling is quite good when the secondary is perfectly aligned with either one of the three segments, but drops tremendously when going between them. In perfectly aligned positions, the coupling factor is above 0.25, however at $\pm$400 it is almost 0. This can be observed from Fig. 5.13a, in which flux lines enter and leave the same coil resulting in a null voltage. This highly changeable characteristic was also confirmed with studies in segmented IPT systems [28] and by researchers at the Oak Ridge National Laboratory [47]. Using these configurations in a real life scenario would have an undesirable effect in the power electronics involved, by virtue of the constantly changing coupling factor which translates to highly changing (from 0 to some value and vice versa) voltage induction in the pickup coils. This in turn will reduce power transfer because during those gaps there is no coupling. Increasing the secondary size will moderate this issue but it is, nevertheless, still present. Using the BP-R topology, with intermediate rectangular coils placed in these gaps, may prevent some of this variation. However, this is not a cost effective solution.

On the other hand, simulations with DD coils achieve good coupling factors that remain high and relatively tolerant to misalignments along x (Fig. 5.13b). Examples of that are the DD-DD and DD-BP structures which have the highest overall coupling factors, almost reaching 0.3 whatever the position is along the three segments (Fig. 5.12b). Even though

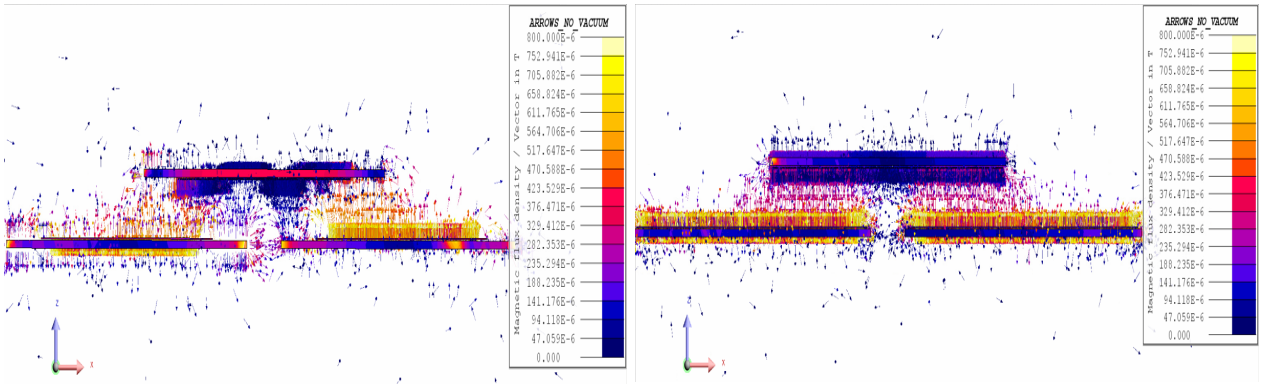

(a) R-R topology.

(b) DD-DD topology.

Figure 5.13: Magnetic flux lines in a transition between two segments ($x = -400\ mm$).

the primary is segmented, the coupling factor remains stable in those topologies. This means that the voltage induced will be relatively constant, which is pretended for a smooth power profile.

Results in the Oy direction

The majority of the configurations studied have poor tolerance for lateral movements and the magnetic coupling is almost negligible past 500 mm of the segment's center. In a highway, vehicles stay quite aligned in one lane, only moving laterally to overtake. As such, having good lateral tolerance is not the main goal in these systems.

Despite that lack of importance, better lateral tolerance may allow for cost reduction of infrastructure, if one primary group of segments is able to power different lanes, for example.

The parameters used remain the same, however, compared to the values of self inductances obtained in the lateral movement for long types, these ones are slightly smaller (Fig. 5.14). The reduced size of the primary segments is the main culprit in that result. Both primary and secondary self inductances are in compliance with the previous explanations.

As for the mutual inductance and coupling factor (Fig. 5.15), they have an almost negative linear relationship with the distance to the origin. All configurations suffer from a great decrease in magnetic coupling, due to the overall greater distance to the primary coils. They also reach a point where the magnetic coupling is the lowest (null-point), but *surprisingly* bounces back to higher values. Except for BP-R, where the decrease happens at a constant rate. In the rectangular types (R-R and R-R_+), this happens between 300 and 500 mm, which coincides with an alignment of the secondary structure and the primary conductor. The rectangular coil is ideal to the capture of vertical flux lines and at 400 mm

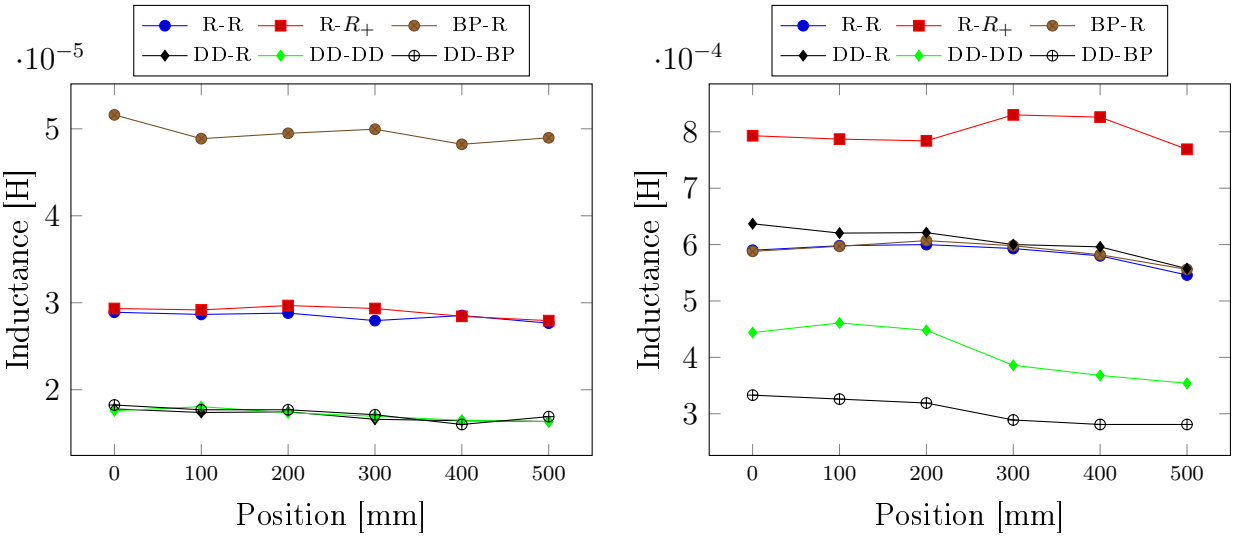

(a) Primary inductance.

(b) Secondary inductance.

Figure 5.14: Self inductances for segmented configurations as a function of y.

the flux is primarily horizontal which results in poor coupling. Thus the behaviour is similar to the one in Fig. 5.13a, with a null voltage occurring at that point. Once the secondary goes further away, some of the flux lines go through the secondary coil only once which increases the induced voltage.

The same situation happens with the DD configurations at a much closer point. Near the 200 *mm* point, the lowest coupling between the two structures occurs. DD coils are suitable to capture horizontal flux when they are perfectly aligned (see Fig. 5.16a and 4.11b), but with slight lateral movements the magnetic flux can enter and leave the same coil, resulting

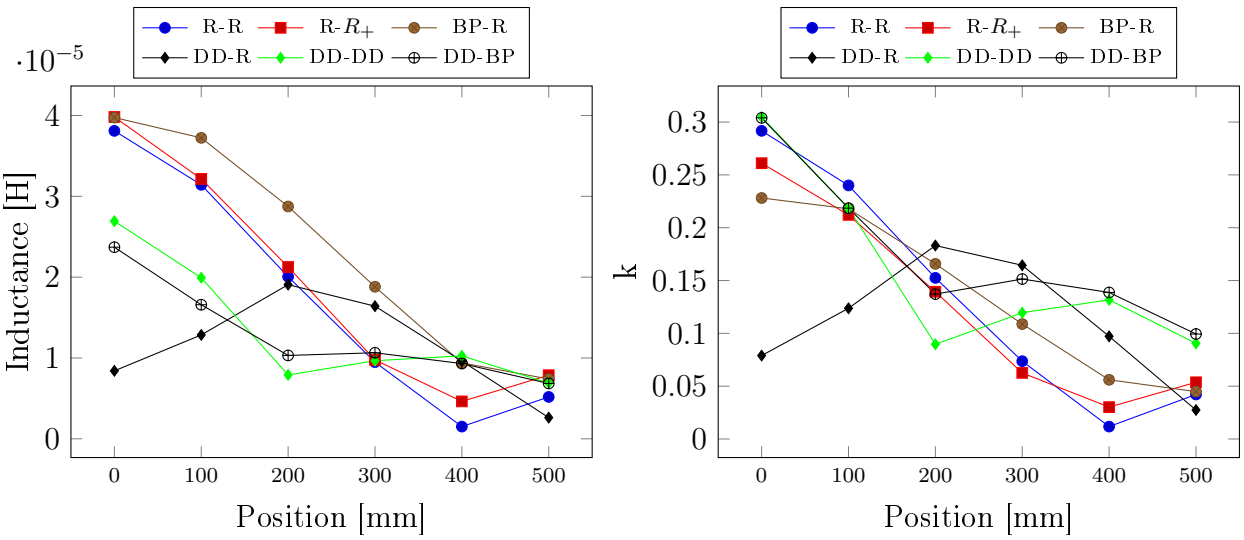

(a) Mutual inductance.

(b) Coupling factor.

Figure 5.15: M and k for segmented configurations as a function of y.

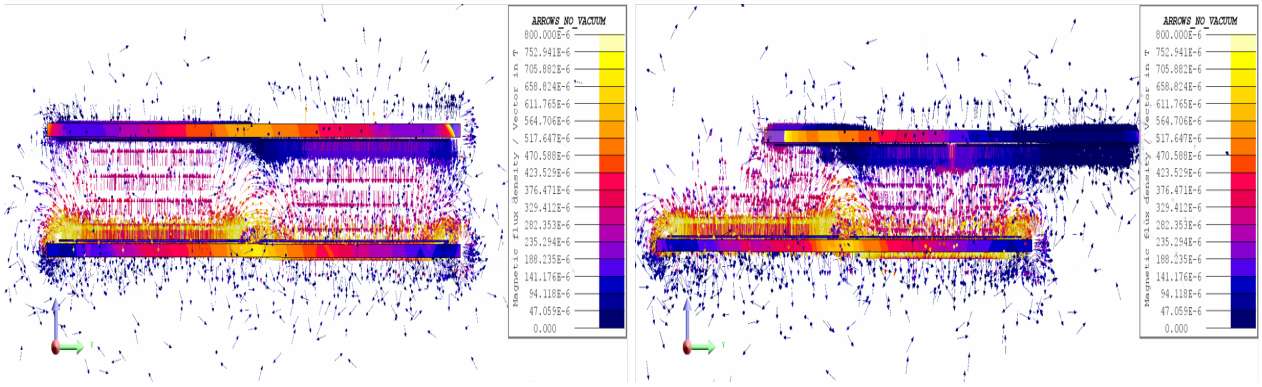

(a) Aligned position. (b) Misaligned position ($y = 200$).

Figure 5.16: Magnetic flux lines for the segmented DD-DD configuration.

in no induced voltage (Fig. 5.16b). As a result, one DD coil (coil 1 in Fig. 5.17a) will have no mutual inductance with the primary structure, while in the other (coil 2 in Fig. 5.17a) the same problem occurs, so the coupling will be low. At this point the tolerance to misalignment ends up being lower than the rectangular architectures. Increasing the lateral offset will lead to some improvements because coil 1 will get aligned with the right primary coil and some coupling will exist. Furthermore, overlapping the secondary coils (bipolar secondary) will soften this effect providing the best overall solution, if there are only two coils in the secondary.

On the other hand, having a single secondary rectangular coil results in good lateral tolerance, at the cost of having negligible magnetic coupling in an aligned position as can be seen on the plot of DD-R at Fig. 5.15. The null point along y-axis represents a large drawback in any configuration studied because of the limitations it imposes in the freedom of movement.

Specifically for the DD-DD type, which has one of the best performances, this problem

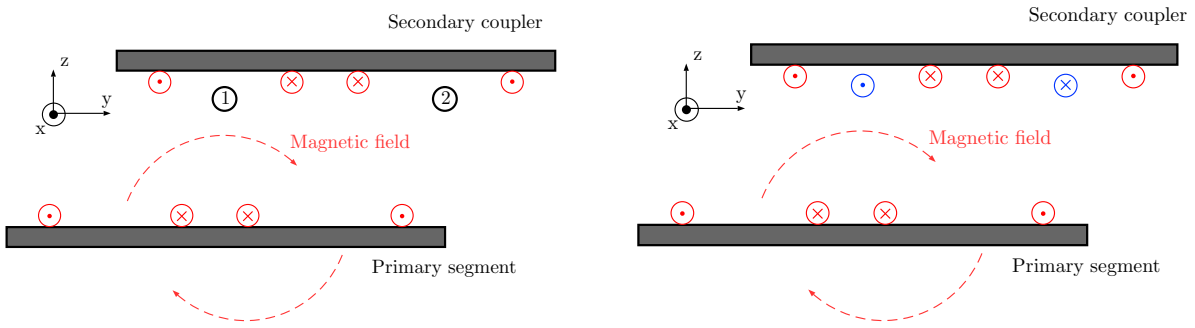

(a) Null point. (b) Quadrature coil.

Figure 5.17: Representation of the misalignment in y and possible null point solution.

can be attenuated with a primary made with a larger width, or better yet, by overlapping the secondary coils (DD-BP). However, an optimal solution would be a secondary that could couple both the horizontal and vertical flux components. This is done by placing a rectangular coil on top of the DD secondary coils as shown in Fig. 5.17b with blue color, resulting in a solution with good tolerance in x and y axis. It is commonly called quadrature coil [48, 49] and represents the possibility of having the best of both worlds.

Results in the Oz direction

The results were done in a similar manner to the long ones. The air gap was modified from 100 to 200 mm, in five equal intervals, and the structure remained aligned with the central primary segment. L_p stays constant and has equal values of self inductance regardless of the secondary location (Fig. 5.18a). Conversely, the pickup L_s is seemingly affected by the air gap, with a decrease in all configurations (Fig. 5.18b). In any case, like the homologous test for the long configurations, the self inductances are constant.

The mutual inductance M is, as expected, affected strongly by the increase in air gap. Since the coupling factor k is derived directly from it, there is a corresponding consequence (Fig. 5.19). This test proves the higher tolerance to greater air gaps in the DD configurations. Indeed, these topologies provide an higher coverage for flux in the z axis (Fig. 4.11) and allow for better coupling compared to the rectangular ones.

The BP-R configuration has proven to be the least viable and even though the aligned

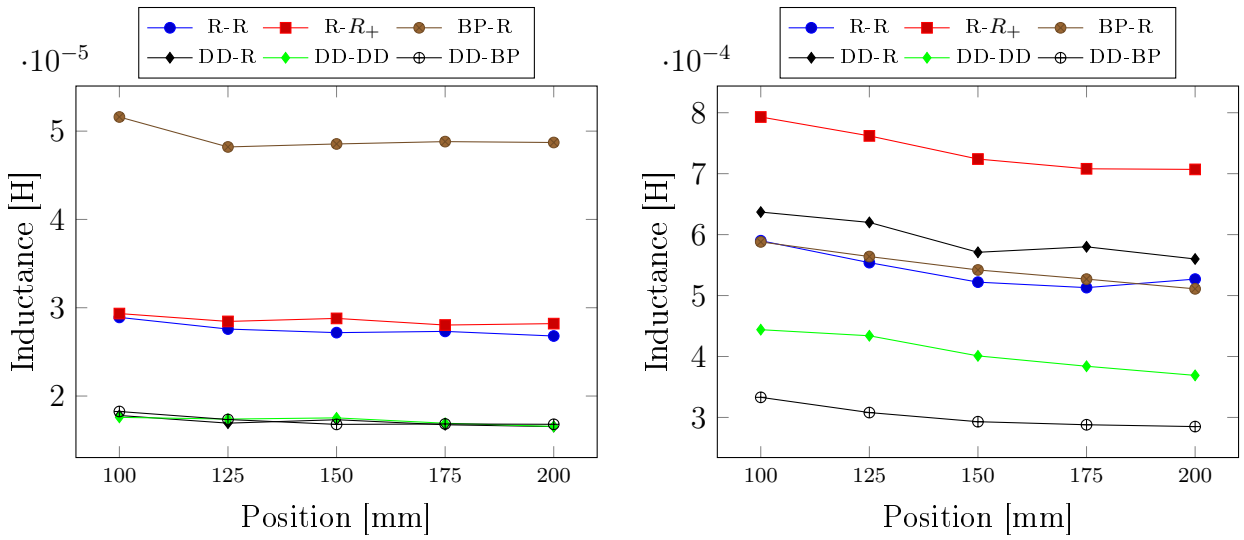

(a) Primary self inductance.

(b) Secondary self inductance.

Figure 5.18: Self inductances for segmented configurations as a function of air gap.

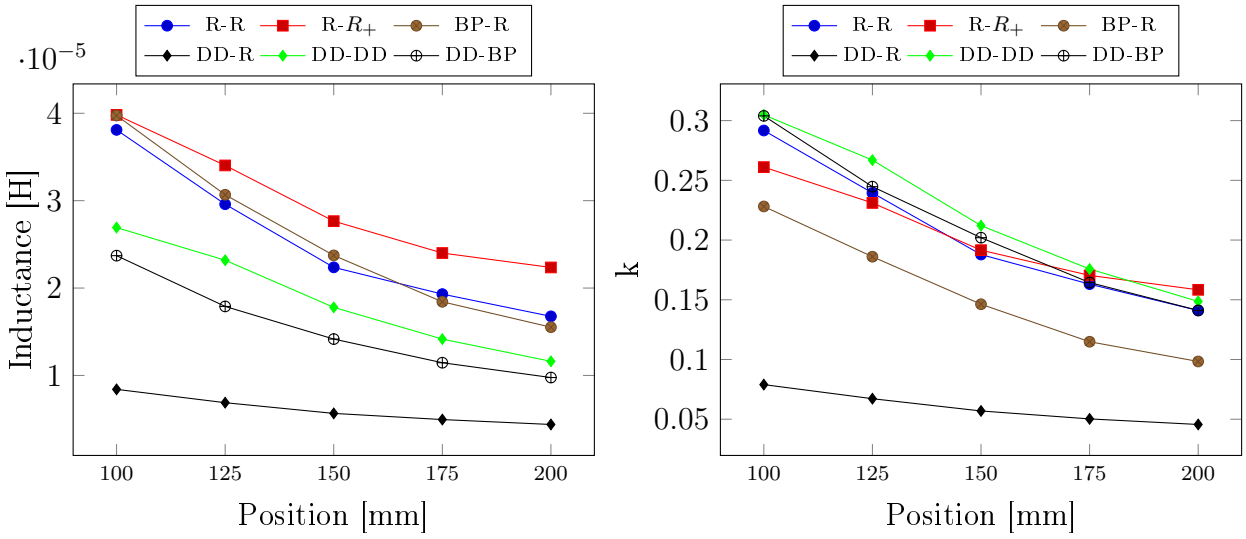

(a) Mutual inductance.

(b) Coupling factor.

Figure 5.19: M and k for segmented configurations as a function of air gap.

coupling is not the best, after increasing the air gap it gets much worse. Although the rectangular coils are not ideal for continuous charging of electric vehicles, due to their inherent lack of magnetic coupling in the x and y direction, they are a good option for stationary cases. That can be concluded by seeing that k is high in an aligned position and has almost the same values compared to the DD types with increased air gaps (Fig. 5.19b). Increasing the secondary size is also a good option to counter the air gap at longer distances (R-R_+). However, compared to other architectures the small improvements over longer distances do not justify the greater structure cost. All the data necessary to the graphical analysis done in this section is compiled in Appendix C.

Overall the performance of all geometries between 100 and 200 mm is better, with higher coupling factor compared to the long types. Table 5.2 summarizes the previous section by marking the recommended configuration with an emoticon ☺ and not recommended configurations with ☹ for dynamic charging of EVs.

Table 5.2: Performance of all configurations studied.

Type	R-R	R-DD	DD-R	DD-DD	R-R_+	BP-R	DD-BP
Long	☹	☹	☹	☺	—	—	—
Segmented	☹	—	☹	☺	☹	☹	☺

5.2 Transient analysis

Previous simulations did not specify the speed at which the secondary pickup is moving. The parameters were obtained in specific points and calculations were made with *rms* values. Tests in transient mode are much more demanding and require a lot of computational power, due to the need to remesh the displacement area (air). Sadly, that translates to long simulation times which prohibit the study of different movement types. For that reason, simulations were made only along the x axis.

The aim of this study is to evaluate the wireless power transfer as a function of speed, with a special preference in speeds that are realistic (120 km/h). Unfortunately, the high frequency used (85 kHz) and the necessity of having fairly good waveforms (20 points per period) mean that a lot of steps will be computed. The amount of steps to compute, in addition to the already long time they take to complete, add up to simulation times unreasonably long. Because of that, the infinite box was reduced significantly and the speed had to be increased so that the number of points to simulate was lessened.

The settings used for the transient simulations are displayed in table 5.3. 20 points were considered for each period in order to have a reasonable waveform. Furthermore, R_{load} is 100 Ω and is equivalent to the resistance seen from the secondary coil. It was established that the segmented configurations are more advantageous to dynamic charging of electric vehicles because of the overall better coupling factors in all movement types (x,y,z). So, for this study two architectures were studied: R-R and DD-DD. The number of turns in the primary and secondary is the same as previous simulations. As for the speed, a comparison was done with regard to two different values, in order to evaluate the power transfer as a function of speed. The total length of the route is 2400 mm (*different* from 2300 mm because

Table 5.3: Parameters used in transient state.

Parameters	Value	Description
t_{sim}	10-15 days	Simulation time
f	85 kHz	Frequency of operation
I_{source}	$20\sqrt{2}\sin(2\pi ft)$	Current source
T_s	$\frac{1}{85000}$ s	Source period
u_s	$\frac{T_s}{20}$ s	Time step
R_p	0.1 Ω	Resistance of primary coil
R_s	0.1 Ω	Resistance of secondary coil
R_{load}	100 Ω	Load resistance

the pickup starts moving 100 mm before reaching the first segment and moves an additional 100 mm after the last segment) but the plots were done for 1600 mm which is relative to a covered distance of two segments. This is enough to observe the behavior while moving through several segments. The speeds used are 6800 m/s and 10000 m/s which correspond to a waveform with $20T_s$ and one with approximately $13.6T_s$, respectively. These speeds are obviously faster than any vehicle available, however the study isn't compromised by that.

5.2.1 Rectangular-Rectangular Geometry

After the solving process is concluded, several 2D plots can be computed. Voltage, flux, current, among other variables can be plotted as a function of time. For all intents and purposes, only the voltage and power transfered to the secondary coil will be discussed. Firstly, as can be seen on Fig. 5.20, the instantaneous induced voltages follow the same behavior as the mutual inductance from Fig. 5.12a, which is expected. As a vehicle passes through each segment, the induced voltages reach 0. Then, when the alignment is perfect, maximum induced voltage happens. This way of operating is the main reason the R-R geometry is not recommended for dynamic charging. The values of induced voltage are in consonance with the steady state values obtained in the solving process. As can be seen by Fig. 5.21, in steady state the rms voltage reaches around 125 V on aligned position (x=±800 and x=0). Conversely, in transient state the maximum and minimum voltages are achieved at those points as well due to the maximum magnetic coupling. As such, the rms voltage at those points is simply $\frac{166.1}{\sqrt{2}}$ which results in 117.8 V. This result is very much similar to the one obtained in steady state (123.1 V), as it should be. Note, however, that this is valid for

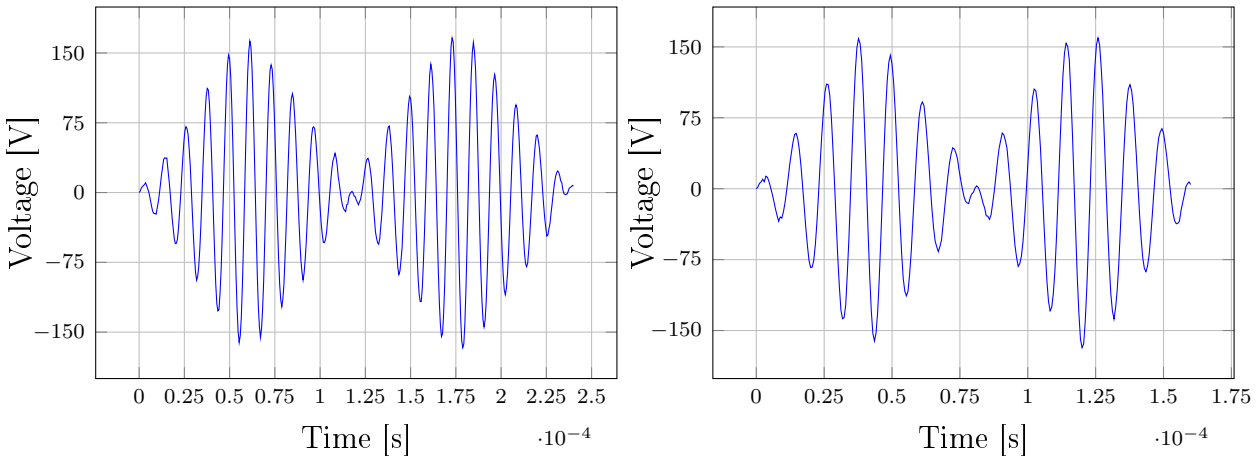

(a) 6800 m/s (b) 10000 m/s

Figure 5.20: Load voltage in R-R configuration.

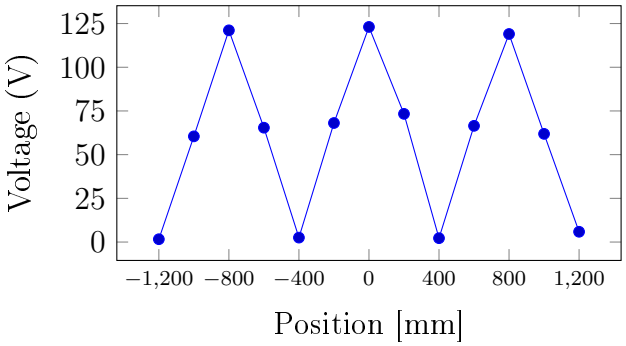

Type	V_{max}	V_{min}	V_{rms}
Steady (x=0)	-	-	123.1
Transient	166.1	-166.6	117.8

Figure 5.21: Voltage values in steady state compared to transient mode.

a comparison of specific points along the segmented track, but does not represent the *rms* voltage of the whole curve.

The power delivered to the load (P_{load}) was the other variable computed in this study. In this case, the load remained constant and equal to 100 Ω. Fig. 5.22 represents the instantaneous P_{load} as a function of time. It can be seen that the faster secondary takes 160 μs to go across 1600 mm while the slower one takes 240 μs. The power profile follows the voltage one. A vehicle moving at a slower speed can be more easily charged than a fast moving vehicle. It was explained in section 4.8 that speed is highly influential in the average power transferred to the load. A slower speed means that the vehicle will spend more time on top of each segmented structure. Fig. 5.22a shows that, for the same distance, more periodic waveforms exist (note that the period is always T_s) and therefore the energy transfered will be greater.

The power transfered to the load was also calculated in steady state and is shown in

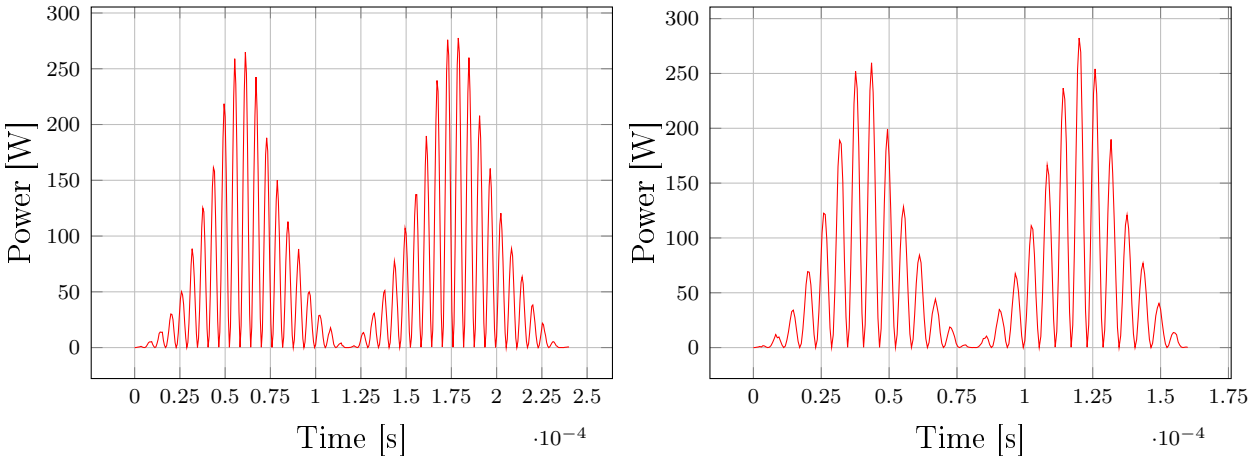

(a) 6800 m/s (b) 10000 m/s

Figure 5.22: Load power in R-R configuration.

the graph of Fig. 5.23. After obtaining the load current in the post processing results, $P_{load} = I_{load}^2 R_{load}$ was applied for every point. Fig. 5.23 also shows a table with P_{avg} and the energy transfered E_{transf} for the two speeds considered in transient state. The average powers obtained are nearly the same, because the integral calculation is done over the full periodic waveform. Doing this for a wave with 30 periods is no different than doing it for 20. The E_{transf} variable represents the energy value in millijoules. While the average power is always the same regardless of the speed of the vehicle, *energy transfered* is dependent on the simulated time

$$E_{transf} = P_{avg} \cdot \Delta t \tag{5.2}$$

with Δt being the elapsed time to run across the two segments. This means that, for the same average power, a greater time to go through the specified course will result in a larger energy value. That can be confirmed by the values obtained in the table of Fig. 5.23, in which the slower speed corresponds to a greater energy transfer. Refer to Appendix D for an additional simulation result with explanations regarding the speed and power transfer relationship.

5.2.2 DD-DD geometry

Steady state results have shown that DD-DD geometries have great magnetic coupling along the x axis. That is primarily why they have great potential for applications in dynamic WPT. The load voltage over two segments is represented in Fig. 5.24. It can be immediately asserted that the voltage follows the characteristics of the steady state simulations, namely the fact the voltage curve is a sinusoid with no pulsating characteristics. This is ideal for a smooth voltage source at the secondary coil that can then be rectified and provided to charge the batteries. Again, a slower speed as represented in Fig. 5.24a corresponds to

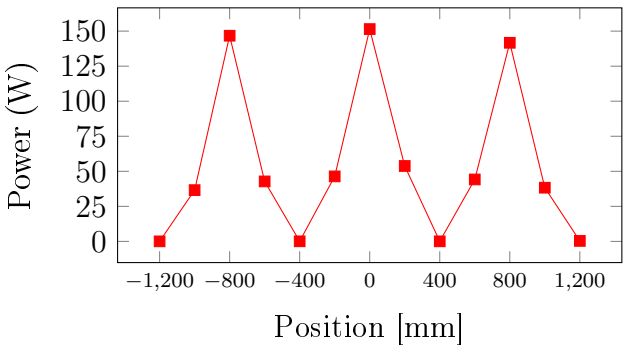

Speed (m/s)	P_{avg} (W)	E (mJ)
6800	54.357	13.04
10000	54.261	8.68

Figure 5.23: Power values in steady state compared to transient for R-R geometry.

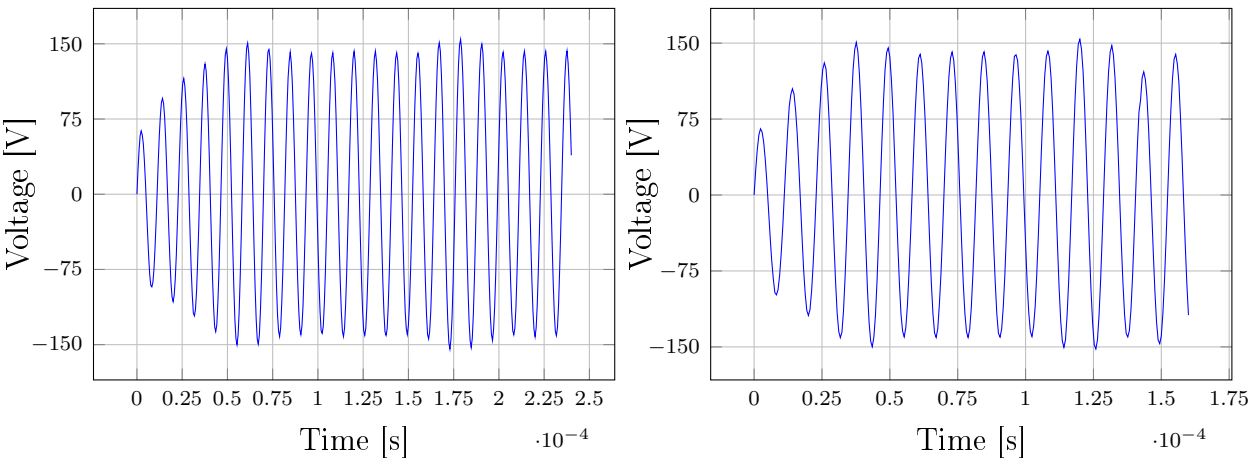

(a) 6800 m/s (b) 10000 m/s

Figure 5.24: Load voltage in DD-DD configuration.

a higher number of periods (20) compared to 5.24b, in which approximately 13.6 periods are computed. As for the steady state graphical representation of the load voltage, it is displayed in Fig. 5.25. The *rms* values of voltage in steady state are in accordance to the coupling factor and mutual inductance profiles discussed in the previous section (Fig. 5.12). At the best alignments effective voltage reaches maximum values, but does not decrease that much when moving between segments. Applying the same calculations on the instantaneous values, with t equal to the point where the secondary is aligned with the primary, yields a value of 101.8 V that is close to the 111.8 V obtained at $x = 0$ in steady state.

The secondary structure starts its movement at $x = -1200$ mm and for that reason the initial induced voltage is low (perfect alignment with the first segment occurs at -800 mm). As the distance covered increases, the secondary reaches alignment with the first segment at around 60 μs with 6800 m/s and 40 μs with 10000 m/s. These points coincide with higher power transfers of around $P_{max} = 225$ W as can be seen on Fig. 5.26. It is important to note that this system has no compensation in primary and secondary, which explains the relatively

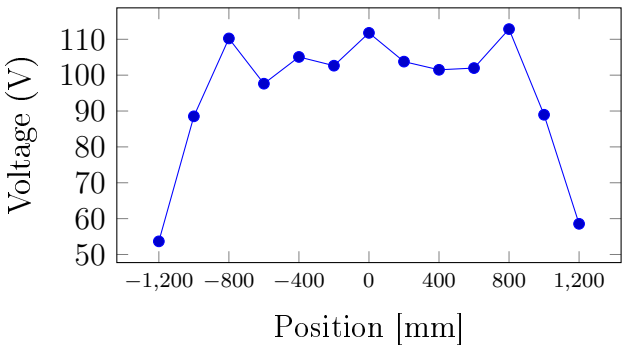

Type	V_{max}	V_{min}	V_{rms}
Steady (x=0)	-	-	111.8
Transient	154.3	-154.4	101.8

Figure 5.25: Voltage values in steady state compared to transient for DD-DD geometry.

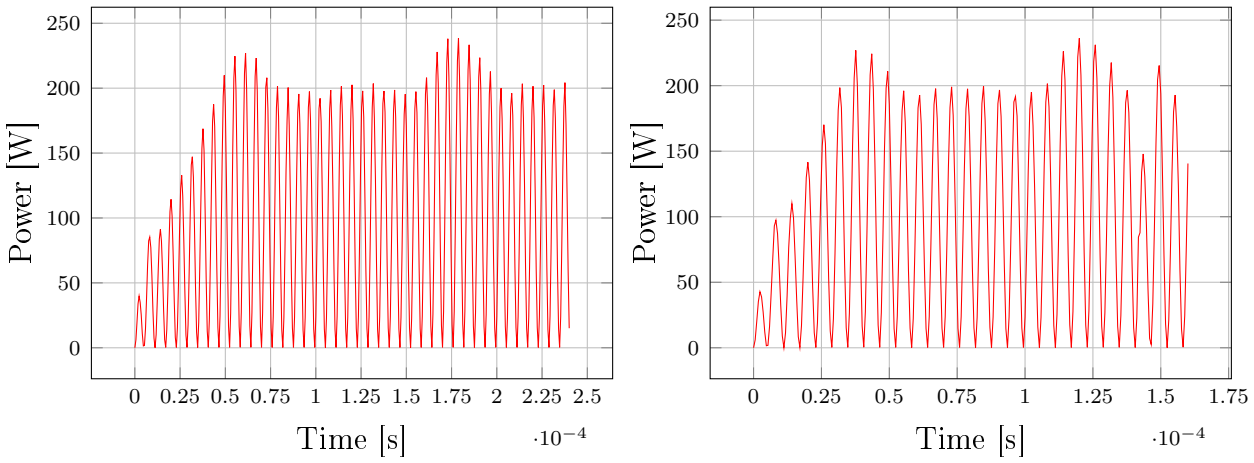

(a) 6800 m/s (b) 10000 m/s

Figure 5.26: Load power in DD-DD configuration.

low power levels. The secondary then reaches perfect alignment with the second segment at around 180 μs with 6800 m/s and 120 μs with 10000 m/s with the same maximum values. The plot representation ends with the secondary at the position exactly between the second and third segments. Even between transitions from segment to segment the average power delivered to the load does not get significantly affected.

Both speeds have a similar waveform with the main difference being on the amount of energy that can be transferred as a function of time. As Fig. 5.26 points out, more waveforms per distance covered means that the energy transfer along that time will be greater. This quantity is proportional to the amount of time a vehicle is on top of the structures. The same calculations for the energy transfered across the segments were done and are shown in the table of Fig. 5.27. Similarly to the previous R-R test, a slower speed results in a greater energy transfer of 23.3 mJ compared to 15.11 mJ because of the greater Δt associated with slower speeds. For the steady state study of the power dissipated by the load (Fig. 5.27),

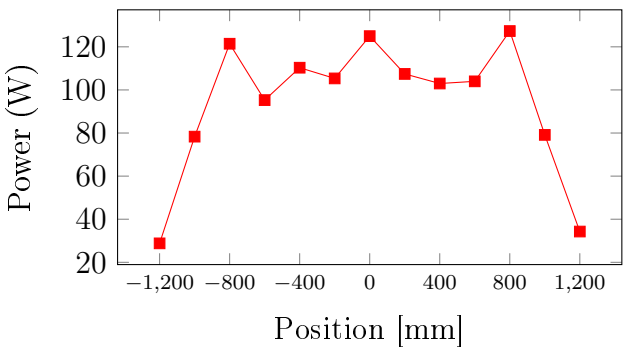

Speed (m/s)	P_{avg} (W)	E (mJ)
6800	97.1	23.3
10000	94.45	15.11

Figure 5.27: Load power in steady state compared to transient for DD-DD geometry.

the characteristic is similar to what was already observed.

Comparing the average power consumed by the load in both R-R and DD-DD geometries reveals something important. By employing a DD-DD configuration, that has the same amount of materials as the R-R but different placement of coils, leads to an almost increase of 100% average power transfered to the load. As a consequence the energy transfer levels are also increased considerably. This is because of the greater tolerance in the x axis for this geometry, which prevents the voltage levels to reach very low values between segments. It is concluded that to achieve better energy transfers several options can be made, like greater size of segments, slower secondary speeds and proper geometry of the primary and secondary couplers.

Chapter 6

Conclusions and future work

6.1 Conclusions

Inductive power transfer has been used effectively in stationary environments, that is, a primary magnetic coupler is placed in a charging station and the secondary magnetic coupler that is under an EV simply has to be above it in a static manner. However, this does not eliminate completely some of the drawbacks faced when using EVs, namely the long charging times and the annoyance of having to stop to recharge. For that reason, dynamic wireless charging of EV started to be investigated. The continuous charging of EV on the road can, effectively, eliminate the need to use expensive and bulky batteries that are responsible for the EV greater costs. The principle of operation is the same as the one in static IPT, but has to be more resistant to possible secondary misalignments because a vehicle is constantly changing position along a roadway.

This work focused on the geometry of the magnetic couplers both in the primary and secondary sides. The transmitter can be made of a long track or a set of segmented pads spaced equally between them. Moreover, different coil arrangements and designs can be made in both the primary and secondary in order to influence the energy transfer of the system. To quantify how viable a system is for dynamic IPT several variables were studied, with special attention towards the coupling factor and mutual inductance. Because of the large air gaps, the mutual inductance between primary and secondary is low and to improve it careful design of the couplers is necessary.

A total of four long configurations and six segmented topologies were considered based on recent research. They differ on the placement of the primary and secondary coils but are otherwise equivalent in material usage. It is possible to conclude from the simulation

results that the most advantageous configuration for the long types is the DD-DD topology because it offers the best coupling along the x axis and does not suffer too much from misalignments in the y direction. Regarding the segmented types, both DD-DD and DD-BP are good options for roadway IPT systems compared to the other rectangular types because of their great tolerance when traveling from segment to segment. The ultimate choice is very dependent on the application, but with less materials, the segmented topologies have better energy transfer than the long types. It is also concluded that the self inductances are independent of the secondary position.

A transient study for the relationship between the speed of the vehicle and the energy transfer values was also addressed. The conclusion is that higher vehicle speeds yield a lower energy transfer while lower speeds and/or greater primary size help improve the amount of energy transfered.

6.2 Future work

The work presented in this thesis helped get a close understanding regarding the operation of dynamic IPT systems, in particular the different magnetic couplers used. To continue this work some of these suggestions can be taken:

- Explore the possibility of using air cores, and what implications that choice has in the characteristics of the system.
- Implement the recommended designs in a real experimental setting.
- Investigate possible compensation networks to be used in dynamic IPT.
- Evaluate the impact of electromagnetic radiation in dynamic IPT and study ways of minimizing it.
- Integrate the designs proposed into a high power system with the compensation networks and all the electronics associated.

References

[1] Z. Pantic, S. Bai, and S. M. Lukic. Inductively coupled power transfer for continuously powered electric vehicles. In *2009 IEEE Vehicle Power and Propulsion Conference*, pages 1271–1278, Sept 2009.

[2] C. Park, S. Lee, G. H. Cho, and C. T. Rim. Innovative 5-m-off-distance inductive power transfer systems with optimally shaped dipole coils. *IEEE Transactions on Power Electronics*, 30(2):817–827, Feb 2015.

[3] F. Musavi, M. Edington, and W. Eberle. Wireless power transfer: A survey of ev battery charging technologies. In *2012 IEEE Energy Conversion Congress and Exposition (ECCE)*, pages 1804–1810, Sept 2012.

[4] S. Lukic and Z. Pantic. Cutting the cord: Static and dynamic inductive wireless charging of electric vehicles. *IEEE Electrification Magazine*, 1(1):57–64, Sept 2013.

[5] X. Liu and S. Y. R. Hui. Equivalent circuit modeling of a multilayer planar winding array structure for use in a universal contactless battery charging platform. *IEEE Transactions on Power Electronics*, 22(1):21–29, Jan 2007.

[6] E. Waffenschmidt and T. Staring. Limitation of inductive power transfer for consumer applications. In *2009 13th European Conference on Power Electronics and Applications*, pages 1–10, Sept 2009.

[7] Q. Chen, S. C. Wong, C. K. Tse, and X. Ruan. Analysis, design, and control of a transcutaneous power regulator for artificial hearts. *IEEE Transactions on Biomedical Circuits and Systems*, 3(1):23–31, Feb 2009.

[8] Stanimir Valtchev, Elena Baikova, and Luis Jorge. Electromagnetic field as the wireless transporter of energy. 25:171–181, 01 2012.

[9] V. Cirimele, F. Freschi, and M. Mitolo. Inductive power transfer for automotive applications: State-of-the-art and future trends. In *2016 IEEE Industry Applications Society Annual Meeting*, pages 1–8, Oct 2016.

[10] S. Y. Choi, B. W. Gu, S. Y. Jeong, and C. T. Rim. Advances in wireless power transfer systems for roadway-powered electric vehicles. *IEEE Journal of Emerging and Selected Topics in Power Electronics*, 3(1):18–36, March 2015.

[11] J. G. Bolger, F. A. Kirsten, and L. S. Ng. Inductive power coupling for an electric highway system. In *28th IEEE Vehicular Technology Conference*, volume 28, pages 137–144, March 1978.

[12] S. Y. Choi, B. W. Gu, S. Y. Jeong, and C. T. Rim. Trends of wireless power transfer systems for roadway powered electric vehicles. In *2014 IEEE 79th Vehicular Technology Conference (VTC Spring)*, pages 1–5, May 2014.

[13] K. Throngnumchai, A. Hanamura, Y. Naruse, and K. Takeda. Design and evaluation of a wireless power transfer system with road embedded transmitter coils for dynamic charging of electric vehicles. In *2013 World Electric Vehicle Symposium and Exhibition (EVS27)*, pages 1–10, Nov 2013.

[14] S. Jeong, Y. J. Jang, and D. Kum. Economic analysis of the dynamic charging electric vehicle. *IEEE Transactions on Power Electronics*, 30(11):6368–6377, Nov 2015.

[15] M. Budhia, J. T. Boys, G. A. Covic, and C. Y. Huang. Development of a single-sided flux magnetic coupler for electric vehicle ipt charging systems. *IEEE Transactions on Industrial Electronics*, 60(1):318–328, Jan 2013.

[16] M. Yilmaz, V. T. Buyukdegirmenci, and P. T. Krein. General design requirements and analysis of roadbed inductive power transfer system for dynamic electric vehicle charging. In *2012 IEEE Transportation Electrification Conference and Expo (ITEC)*, pages 1–6, June 2012.

[17] L. Chen, G. R. Nagendra, J. T. Boys, and G. A. Covic. Double-coupled systems for ipt roadway applications. *IEEE Journal of Emerging and Selected Topics in Power Electronics*, 3(1):37–49, March 2015.

[18] DM Vilathgamuwa and JPK Sampath. Wireless power transfer (wpt) for electric vehicles

(evs)—present and future trends. In *Plug in electric vehicles in smart grids*, pages 33–60. Springer Singapore, 2015.

[19] S. Li and C. C. Mi. Wireless power transfer for electric vehicle applications. *IEEE Journal of Emerging and Selected Topics in Power Electronics*, 3(1):4–17, March 2015.

[20] Chwei-Sen Wang, G. A. Covic, and O. H. Stielau. Power transfer capability and bifurcation phenomena of loosely coupled inductive power transfer systems. *IEEE Transactions on Industrial Electronics*, 51(1):148–157, Feb 2004.

[21] G. A. Covic and J. T. Boys. Modern trends in inductive power transfer for transportation applications. *IEEE Journal of Emerging and Selected Topics in Power Electronics*, 1(1):28–41, March 2013.

[22] J. H. Kim, B. S. Lee, J. H. Lee, S. H. Lee, C. B. Park, S. M. Jung, S. G. Lee, K. P. Yi, and J. Baek. Development of 1-mw inductive power transfer system for a high-speed train. *IEEE Transactions on Industrial Electronics*, 62(10):6242–6250, Oct 2015.

[23] V. X. Thai, S. Y. Choi, B. H. Choi, J. H. Kim, and C. T. Rim. Coreless power supply rails compatible with both stationary and dynamic charging of electric vehicles. In *2015 IEEE 2nd International Future Energy Electronics Conference (IFEEC)*, pages 1–5, Nov 2015.

[24] S. Lee, W. Lee, J. Huh, H. J. Kim, C. Park, G. H. Cho, and C. T. Rim. Active emf cancellation method for i-type pickup of on-line electric vehicles. In *2011 Twenty-Sixth Annual IEEE Applied Power Electronics Conference and Exposition (APEC)*, pages 1980–1983, March 2011.

[25] Z. Chen, W. Jing, X. Huang, L. Tan, C. Chen, and W. Wang. A promoted design for primary coil in roadway-powered system. *IEEE Transactions on Magnetics*, 51(11):1–4, Nov 2015.

[26] G. Buja, M. Bertoluzzo, and H. K. Dashora. Lumped track layout design for dynamic wireless charging of electric vehicles. *IEEE Transactions on Industrial Electronics*, 63(10):6631–6640, Oct 2016.

[27] K. Song, C. Zhu, Kim Ean Koh, T. Imura, and Y. Hori. Wireless power transfer for running ev powering using multi-parallel segmented rails. In *2015 IEEE PELS Workshop on Emerging Technologies: Wireless Power (2015 WoW)*, pages 1–6, June 2015.

[28] K. Lee, Z. Pantic, and S. M. Lukic. Reflexive field containment in dynamic inductive power transfer systems. *IEEE Transactions on Power Electronics*, 29(9):4592–4602, Sept 2014.

[29] M. Kim, H. Kim, D. Kim, Y. Jeong, H. H. Park, and S. Ahn. A three-phase wireless-power-transfer system for online electric vehicles with reduction of leakage magnetic fields. *IEEE Transactions on Microwave Theory and Techniques*, 63(11):3806–3813, Nov 2015.

[30] J. A. Russer, M. Dionigi, M. Mongiardo, F. Mastri, A. Costanzo, and P. Russer. A system for dynamic inductive power supply of electric vehicles on the road. In *2016 IEEE Wireless Power Transfer Conference (WPTC)*, pages 1–4, May 2016.

[31] D.M. Empey, Inc Systems Control Technology, Partners for Advanced Transit, Highways (Calif.), and Berkeley. Institute of Transportation Studies University of California. *Roadway Powered Electric Vehicle Project: Track Construction and Testing Program. Phase 3D.* PATH research report. California PATH Program, Institute of Transportation Studies, University of California, Berkeley, 1994.

[32] J. T. Boys, G. A. Covic, and A. W. Green. Stability and control of inductively coupled power transfer systems. *IEE Proceedings - Electric Power Applications*, 147(1):37–43, Jan 2000.

[33] J. Shin, S. Shin, Y. Kim, S. Ahn, S. Lee, G. Jung, S. J. Jeon, and D. H. Cho. Design and implementation of shaped magnetic-resonance-based wireless power transfer system for roadway-powered moving electric vehicles. *IEEE Transactions on Industrial Electronics*, 61(3):1179–1192, March 2014.

[34] S. Lee, J. Huh, C. Park, N. S. Choi, G. H. Cho, and C. T. Rim. On-line electric vehicle using inductive power transfer system. In *2010 IEEE Energy Conversion Congress and Exposition*, pages 1598–1601, Sept 2010.

[35] J. Huh, S. W. Lee, W. Y. Lee, G. H. Cho, and C. T. Rim. Narrow-width inductive power transfer system for online electrical vehicles. *IEEE Transactions on Power Electronics*, 26(12):3666–3679, Dec 2011.

[36] S. Y. Choi, S. Y. Jeong, B. W. Gu, G. C. Lim, and C. T. Rim. Ultraslim s-type power supply rails for roadway-powered electric vehicles. *IEEE Transactions on Power Electronics*, 30(11):6456–6468, Nov 2015.

[37] Chan-Bae Park. A study on the high-efficiency coreless-typed wireless power transfer system for railway transit. *Journal of Electrical Engineering and Technology*, 11(5):1305–1310, Jan 2016.

[38] M. Budhia, G. A. Covic, and J. T. Boys. Design and optimization of circular magnetic structures for lumped inductive power transfer systems. *IEEE Transactions on Power Electronics*, 26(11):3096–3108, Nov 2011.

[39] G. R. Nagendra, G. A. Covic, and J. T. Boys. Sizing of inductive power pads for dynamic charging of evs on ipt highways. *IEEE Transactions on Transportation Electrification*, 3(2):405–417, June 2017.

[40] W. Zhang, S. C. Wong, C. K. Tse, and Q. Chen. An optimized track length in roadway inductive power transfer systems. *IEEE Journal of Emerging and Selected Topics in Power Electronics*, 2(3):598–608, Sept 2014.

[41] G. R. Nagendra, L. Chen, G. A. Covic, and J. T. Boys. Detection of evs on ipt highways. *IEEE Journal of Emerging and Selected Topics in Power Electronics*, 2(3):584–597, Sept 2014.

[42] Bhag S. Guru and Huseyin R. Hiziroglu. *Electric Machinery and Transformers*. Oxford University Press, 2000.

[43] D.L. Logan. *A First Course in the Finite Element Method*. Cengage Learning, 5th edition, 2011.

[44] Epcos. *Siferrite material N87*, May 2017.

[45] T. E. Stamati and P. Bauer. On-road charging of electric vehicles. In *2013 IEEE Transportation Electrification Conference and Expo (ITEC)*, pages 1–8, June 2013.

[46] W. Zhang, S. C. Wong, C. K. Tse, and Q. Chen. A study of sectional tracks in roadway inductive power transfer system. In *2011 IEEE Energy Conversion Congress and Exposition*, pages 822–826, Sept 2011.

[47] O. C. Onar, J. M. Miller, S. L. Campbell, C. Coomer, C. P. White, and L. E. Seiber. A novel wireless power transfer for in-motion ev/phev charging. In *2013 Twenty-Eighth Annual IEEE Applied Power Electronics Conference and Exposition (APEC)*, pages 3073–3080, March 2013.

[48] M. Budhia, J. T. Boys, G. A. Covic, and C. Y. Huang. Development of a single-sided flux magnetic coupler for electric vehicle ipt charging systems. *IEEE Transactions on Industrial Electronics*, 60(1):318–328, Jan 2013.

[49] M. Budhia, G. A. Covic, J. T. Boys, and C. Y. Huang. Development and evaluation of single sided flux couplers for contactless electric vehicle charging. In *2011 IEEE Energy Conversion Congress and Exposition*, pages 614–621, Sept 2011.

[50] J. Sallan, J. L. Villa, A. Llombart, and J. F. Sanz. Optimal design of icpt systems applied to electric vehicle battery charge. *IEEE Transactions on Industrial Electronics*, 56(6):2140–2149, June 2009.

Appendix A

Air cores

Air cores can be a good option in IPT systems, especially in dynamic IPT. Since it is necessary to cover large parts of a road with transmitters in order to charge the batteries over long distances, using ferromagnetic materials for the magnetic cores can increase the costs of the overall system significantly.

Some calculations regarding the use of air cores and the influence in the induced voltage in the secondary pickup will be made. Moreover, a comparison between the calculation of the mutual inductance between two coils with several methods will also be addressed.

A.1 Coreless system

For the purpose of comparison the segmented DD-DD geometry was used (Fig. 3.3i). The core volumes pertaining to the magnetic core, in the simulation software, were simply replaced with air volumes. The sheets of magnetic material in IPT systems are usually placed below the primary track coils and above the secondary pickup coils. It is important to note that the number of turns in both the secondary and primary segments did not change. In this comparison the only modification was to the core type.

Fig. A.1 shows the primary and secondary self inductances of the core and coreless systems. The tests were done only in the longitudinal movement (x axis) and show that removing the ferromagnetic material reduces the self inductances of the coils. With a ferrite or an iron core the magnetic flux lines can be strengthened and the magnetic flux increases because of the magnetization of the core. Less magnetic flux means that the self inductance will also decrease (equation 2.3).

Comparing the mutual inductance and coupling factor with and without the magnetic

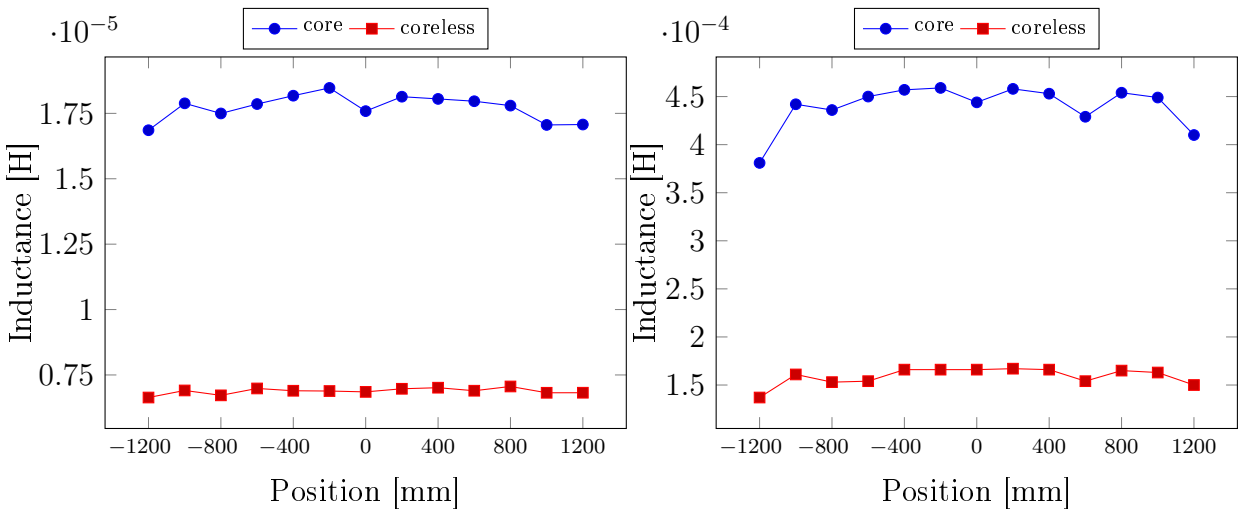

(a) Primary self inductance.

(b) Secondary self inductance.

Figure A.1: Self inductances for coreless and core based DD-DD topologies.

core shows that removing this component has a great impact on the performance of the system. The decrease in coupling and mutual inductance stems from the fact that the magnetic core, that has good relative permeability, concentrates the magnetic flux lines and without it, the leakage flux is greater. Energy transfer is tremendously compromised by this as the induced voltages are effectively reduced as can be seen in Fig. A.3. Because of this, several adjustments can be made in order to have induced voltages similar to the ones observed in a core configuration. The more obvious one is to increase the number of turns in the pickup coil (equation 2.4). Doing this ensures that only the secondary voltage is changed without affecting other parts of the system. Fig. A.3a shows the voltage profile with core

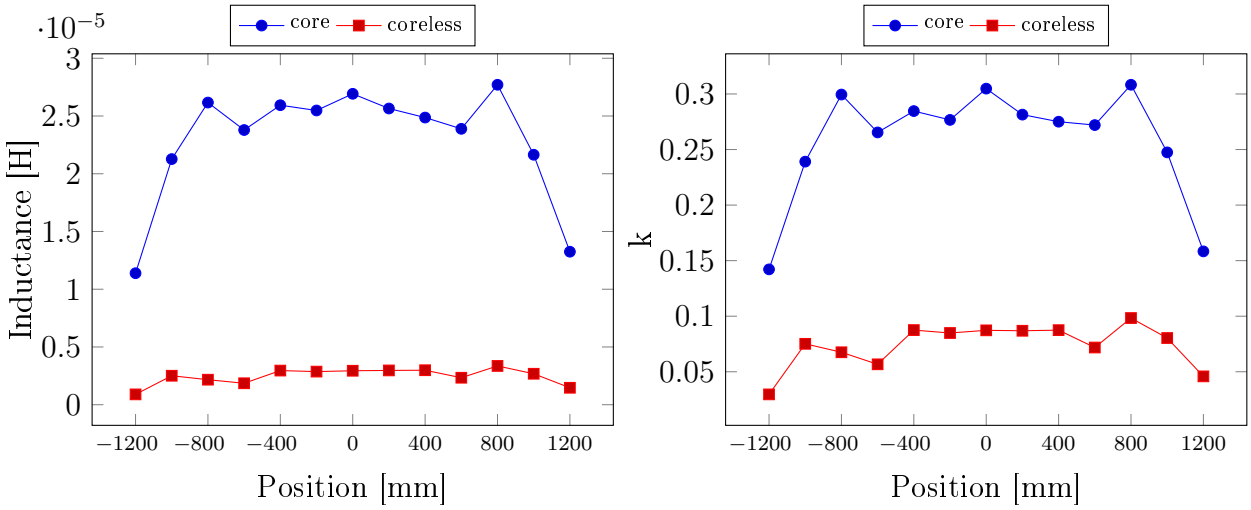

(a) Mutual inductance.

(b) Coupling factor.

Figure A.2: M and k with core and coreless DD-DD topologies.

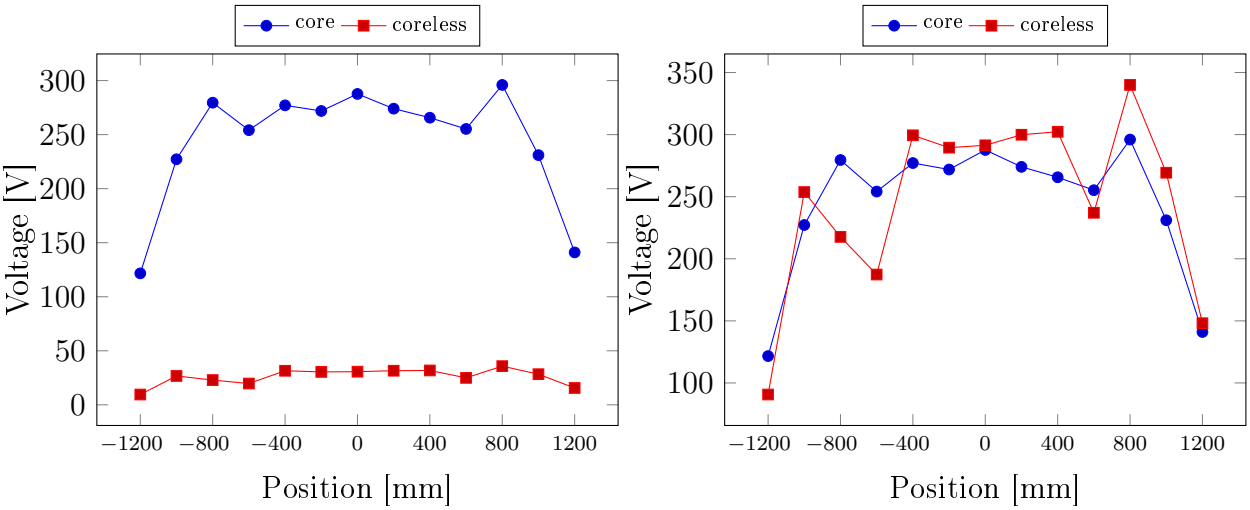

(a) Secondary voltages without adding turns.

(b) Secondary voltages with additional turns in the coreless type.

Figure A.3: Secondary voltages without adding turns vs adding turns.

and without core for the same amount of turns on the primary and secondary. Fig. A.3b, however, shows the same waveforms but with the difference that, this time, more turns were added to the secondary coil in the coreless type. From a total of 16 turns in the secondary, 8+8 for each D coil, a total of 76 turns (38+38) were now used. The induced voltages are close to the ones in the core type, however at the cost of much more wiring. Moreover, it seems that there is more variance in the voltages along the distance studied.

A.2 Mutual inductance in air core systems

In this section a comparison between different methods of calculating the mutual inductance for air core systems is done. There are different ways to calculate it analytically, i.e. by open circuit tests like the ones done in this thesis or by the Neumann's formula which is given by

$$M = \frac{\mu_0}{4\pi} N_p N_s \oint_\gamma \oint_\gamma \frac{dl \cdot dl'}{r} \tag{A.1}$$

The calculation was done in a single position with the segmented R-R topology. Perfect alignment with the middle primary segment was chosen. Moreover a third calculation method was considered that is expressed by

$$M = \frac{V_{oc}}{V_p} L_s \tag{A.2}$$

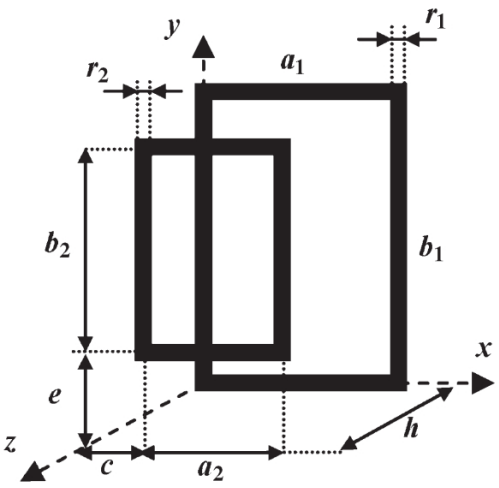

Figure A.4: Parameters for rectangular coils for any dimension and position.

in which V_{oc} is equal to the open circuit voltage of the secondary pick coil. A particular case of Neumann's formula [50] for rectangular coils allows the calculation of M as a function of the coils dimensions with the parameters represented in Fig. A.4 and is given by

$$d = a_1 - a_2 - c \qquad g = a_1 - c$$

$$m = a_2 + c \qquad p = b_1 - e$$

$$q = b_2 + e \qquad t = b_1 - b_2 - e$$

$$\begin{aligned}
M = \frac{\mu_0}{4\pi} N_p N_s \times \Bigg[\Bigg[& d \ln\left(\frac{d+\sqrt{h^2+(-t^2)+d^2}}{g+\sqrt{h^2+d^2+q^2}}\right) + h \ln\left(\frac{g+\sqrt{h^2+q^2+g^2}}{g+\sqrt{h^2+g^2+(-t^2)}}\right) + \\
& + c \ln\left(\frac{(-c)+\sqrt{h^2+q^2+c^2}}{(-c)+\sqrt{h^2+m^2+q^2}}\right) + m \ln\left(\frac{(-m)+\sqrt{h^2+(-t^2)+m^2}}{(-m)+\sqrt{h^2+m^2+q^2}}\right) + \sqrt{h^2+q^2+d^2} - \\
& - \sqrt{h^2+q^2+g^2} - \sqrt{h^2+q^2+m^2} + \sqrt{h^2+q^2+c^2} + \sqrt{h^2+(-t^2)+g^2} - \\
& - \sqrt{h^2+(-t^2)+d^2} + \sqrt{h^2+(-t^2)+m^2} - \sqrt{h^2+(-t^2)+c^2} \Bigg] - \\
& - \Bigg[d \ln\left(\frac{d+\sqrt{h^2+(-p)^2+d^2}}{d+\sqrt{h^2+d^2+e^2}}\right) + g \ln\left(\frac{h+\sqrt{h^2+e^2+g^2}}{g+\sqrt{h^2+h^2+(-p)^2}}\right) + \\
& + c \ln\left(\frac{(-c)+\sqrt{h^2+e^2+c^2}}{(-c)+\sqrt{h^2+c^2+(-p)^2}}\right) + m \ln\left(\frac{(-m)+\sqrt{h^2+(-p)^2+m^2}}{(-m)+\sqrt{h^2+m^2+e^2}}\right) + \sqrt{h^2+e^2+d^2} - \\
& - \sqrt{h^2+e^2+g^2} - \sqrt{h^2+e^2+m^2} + \sqrt{h^2+e^2+c^2} + \sqrt{h^2+(-p)^2+g^2} - \\
& - \sqrt{h^2+(-p)^2+d^2} + \sqrt{h^2+(-p)^2+m^2} - \sqrt{h^2+(-p)^2+c^2} \Bigg] + \\
& + \Bigg[t \ln\left(\frac{t+\sqrt{h^2+(-g)^2+t^2}}{t+\sqrt{h^2+t^2+c^2}}\right) + p \ln\left(\frac{p+\sqrt{h^2+p^2+c^2}}{p+\sqrt{h^2+(-g)^2+p^2}}\right) +
\end{aligned}$$

$$+ e\ln\left(\frac{(-e)+\sqrt{h^2+e^2+c^2}}{(-e)+\sqrt{h^2+e^2+(-g)^2}}\right) + q\ln\left(\frac{(-q)+\sqrt{h^2+(-g)^2+q^2}}{(-q)+\sqrt{h^2+c^2+q^2}}\right) + \sqrt{h^2+c^2+t^2} -$$
$$- \sqrt{h^2+c^2+p^2} - \sqrt{h^2+c^2+q^2} + \sqrt{h^2+e^2+c^2} + \sqrt{h^2+(-g)^2+p^2} -$$
$$- \sqrt{h^2+(-g)^2+t^2} + \sqrt{h^2+(-g)^2+q^2} - \sqrt{h^2+(-g)^2+e^2}\Big] -$$
$$- \Big[t\ln\left(\frac{(t)+\sqrt{h^2+(-d)^2+t^2}}{(t)+\sqrt{h^2+t^2+m^2}}\right) + p\ln\left(\frac{(p)+\sqrt{h^2+m^2+p^2}}{(p)+\sqrt{h^2+(-d)^2+p^2}}\right) +$$
$$+ e\ln\left(\frac{(-e)+\sqrt{h^2+e^2+m^2}}{(-e)+\sqrt{h^2+e^2+(-d)^2}}\right) + q\ln\left(\frac{(-q)+\sqrt{h^2+(-d)^2+q^2}}{(-q)+\sqrt{h^2+m^2+(-q)^2}}\right) + \sqrt{h^2+m^2+t^2} -$$
$$- \sqrt{h^2+m^2+p^2} - \sqrt{h^2+m^2+q^2} + \sqrt{h^2+e^2+m^2} + \sqrt{h^2+(-d)^2+p^2} -$$
$$- \sqrt{h^2+(-d)^2+t^2} + \sqrt{h^2+(-d)^2+q^2} - \sqrt{h^2+(-d)^2+e^2}\Big]\Big] \quad \text{(A.3)}$$

With a_1, a_2, b_1, b_2, c and e the variables shown in Fig. A.4. Since both primary and secondary coils have the same dimensions $a_1 = a_2 = 0.5\ m$ and $b_1 = b_2 = 0.5\ m$ which means that $c = e = 0$ thus d, m, q, g, p and t are given by

$$\begin{cases} d = t = 0 \\ m = g = p = q = 0.5 \end{cases}$$

Moreover, $h = 0.1\ m$, $N_p = 2$ and $N_s = 15$ so in table A.1 the comparison between the three methods of calculation is exposed. These were done in a single position coinciding with the alignment at $x = 0$ which corresponds with the middle primary segment. Overall, the three methods result in very approximate values and as such can be used depending on the situation. The open circuit test is straightforward in the sense that only a handful of calculations are necessary. However, both this and the method from equation A.2 need to power both the primary and secondary with a voltage or current source and do the specific calculations until M is obtained. That is not necessary with Neumann's equation so it is possible to obtain the mutual inductance without powering the any of the coils. Furthermore, the variables c an e are basically dimensions related to the misalignments in the x and y directions so it is also possible to apply this expression with misaligned coils.

Table A.1: Different methods for the calculation of mutual inductance.

Method	Open circuit test	$M = \frac{V_{oc}}{V_p} L_s$	Neumann's formula
Mutual Inductance (μH)	6.18	6.34	6.52

Appendix B

Material properties

This appendix contains additional information regarding the materials designated for the magnetic core and coils of the IPT system.

B.1 Coils

In the FEA software there are several parameters associated with the material used. Copper was chosen for the coil material and its electrical properties, namely the resistivity, are of the linear isotropic type proportional to the temperature (^{o}C) as shown in Fig. B.1. The curve is expressed by

$$\rho(T) = \rho_a(1 + a(T - T_0)) \tag{B.1}$$

with $\rho_a = 0.1564 \times 10^{-7}$ and $a = 0.00427$. ρ_a represents the resistivity of the material at $T = T_0$ while a is the slope coefficient. The thermal conductivity considered for the material is also

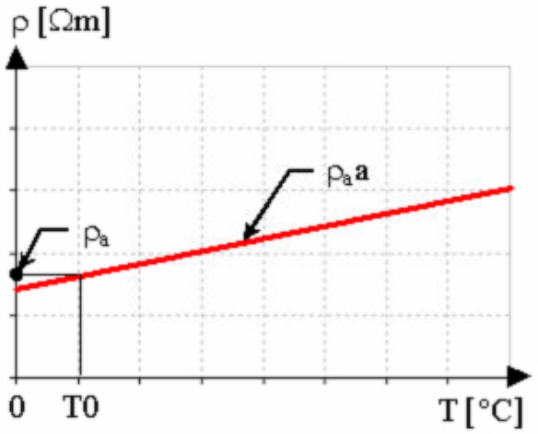

Figure B.1: Resistivity as a function of temperature.

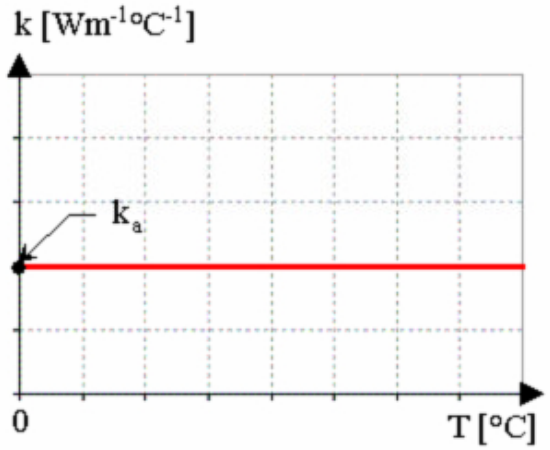

Figure B.2: Thermal conductivity as a function of temperature.

another parameter that can be specified in the coil material. For this case, it is considered to be isotropic, constant and independent of temperature with $k_a = 394\ Wm^{-1}°C^{-1}$. Finally,

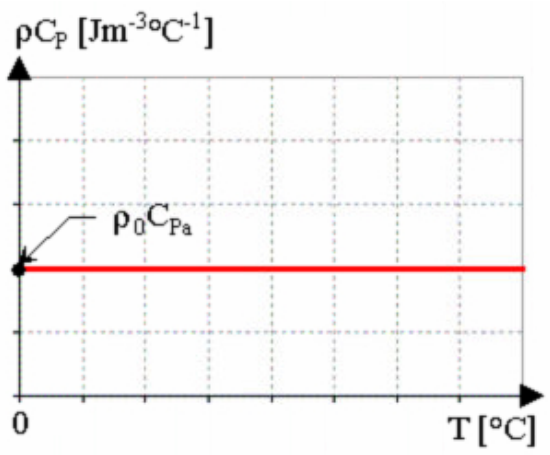

Figure B.3: Volumetric heat capacity as a function of temperature.

the volumetric heat capacity (Fig. B.3) was also specified to be independent of temperature and has a constant value of $\rho_a C_{Pa} = 3518000\ Jm^{-3}°C^{-1}$.

B.2 Magnetic core

As pointed out in chapter 4, the magnetic core used a material called N87. The magnetic property of the material can be specified in the simulation software. A curve represented in Fig. B.4 illustrates the B-H curve and the possibility of changing certain values. Its characteristic is *isotropic soft magnetic material analytic saturation curve*. With the equation for the curve given as

$$B(H) = \mu_0 H + \frac{2J_s}{\pi} \arctan\left(\frac{\pi(\mu_r - 1)\mu_0 H}{2J_s}\right) \tag{B.2}$$

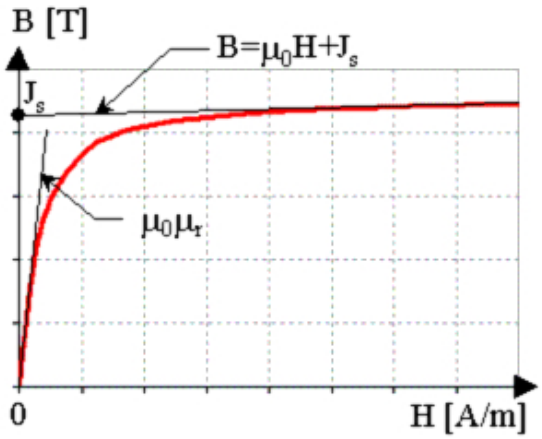

Figure B.4: B-H curve of the N87 material.

with the initial relative permeability μ_r equal to 2300 and the saturation magnetization J_s equal to 0.47 T.

Appendix C

Additional data

This appendix will compile the data that was used to compute the values discussed in chapter 5.

C.1 Long configurations

C.1.1 Ox

Desalinhamento X (mm)	-1500	-1200	-900	-600	-300	0	300	600	900	1200	1500
Tensão_p	452,836736	424,96371	459,079474	457,683713	413,859828	431,870731	426,467516	412,8845902	470,227022	536,992003	474,257599
Corrente_p	20	20	20	20	20	20	20	20	20	20	20
Fluxo_p	8,48E-04	7,96E-04	8,60E-04	8,57E-04	7,75E-04	8,09E-04	7,99E-04	7,73E-04	8,80E-04	0,00100546	8,88E-04
L_p	4,24E-05	3,98E-05	4,30E-05	4,28E-05	3,87E-05	4,04E-05	3,99E-05	3,87E-05	4,40E-05	5,03E-05	4,44E-05
Tensão_s	19,2457746	306,465441	301,160067	265,475413	222,294981	248,551527	264,814711	289,9713463	307,091618	277,387236	41,4345019
Corrente_s	1,92E-06	3,06E-05	3,01E-05	2,65E-05	2,22E-05	2,49E-05	2,65E-05	2,90E-05	3,07E-05	2,77E-05	4,14E-06
Fluxo_s	3,60E-05	5,74E-04	5,64E-04	4,97E-04	4,16E-04	4,65E-04	4,96E-04	5,43E-04	5,75E-04	5,19E-04	7,76E-05
$M_{p,s}$	1,8018E-06	2,8691E-05	2,8195E-05	2,4854E-05	2,0811E-05	2,327E-05	2,4792E-05	2,71473E-05	2,875E-05	2,5969E-05	3,8791E-06

(a) Open circuit on secondary (R-R).

Desalinhamento X (mm)	-1500	-1200	-900	-600	-300	0	300	600	900	1200	1500
Tensão_p	18,4227786	303,028609	300,937555	265,439408	220,76491	248,563861	264,749219	289,1597618	306,981999	274,627887	41,2016938
Corrente_p	1,84E-06	3,03E-05	3,01E-05	2,65E-05	2,21E-05	2,49E-05	2,65E-05	2,89E-05	3,07E-05	2,75E-05	4,12E-06
Fluxo_p	3,45E-05	5,67E-04	5,63E-04	4,97E-04	4,13E-04	4,65E-04	4,96E-04	5,41E-04	5,75E-04	5,14E-04	7,71E-05
Tensão_s	5862,81559	6065,48134	6157,82153	5989,63134	5548,90416	6212,22191	6298,12722	6252,122212	6247,55831	5966,04189	5851,33541
Corrente_s	20	20	20	20	20	20	20	20	20	20	20
Fluxo_s	0,0109776	0,01135707	0,01152997	0,01121505	0,01038983	0,01163183	0,01179268	0,011706542	0,011698	0,01117088	0,0109561
L_s	5,49E-04	5,68E-04	5,76E-04	5,61E-04	5,19E-04	5,82E-04	5,90E-04	5,85E-04	5,85E-04	5,59E-04	5,48E-04
$M_{s,p}$	1,7248E-06	2,837E-05	2,8174E-05	2,4851E-05	2,0668E-05	2,3271E-05	2,4786E-05	2,70713E-05	2,874E-05	2,5711E-05	3,8573E-06

(b) Open circuit on primary (R-R).

Desalinhamento X (mm)	-1500	-1200	-900	-600	-300	0	300	600	900	1200	1500
Tensão_p1	156,7632868	133,8530253	123,6049168	124,858588	130,3970323	128,616879	127,2397162	136,1353735	131,893074	131,802308	130,2427594
Corrente_p1	20	20	20	20	20	20	20	20	20	20	20
Fluxo_p1	2,94E-04	2,51E-04	2,31E-04	2,34E-04	2,44E-04	2,41E-04	2,38E-04	2,55E-04	2,47E-04	2,47E-04	2,44E-04
Tensão_p2	153,3672275	132,097853	133,464815	123,42329	129,4472249	126,312703	124,886005	134,1042717	131,5966572	129,695599	128,3872709
Corrente_p2	20	20	20	20	20	20	20	20	20	20	20
Fluxo_p2	2,87E-04	2,47E-04	2,50E-04	2,31E-04	2,42E-04	2,36E-04	2,34E-04	2,51E-04	2,46E-04	2,43E-04	2,40E-04
Tensão_s	4,364252659	1,217007534	6,824678113	10,03933	8,59427954	11,8691719	9,065813729	9,756097894	1,727256392	9,46659034	1,675480133
Corrente_s	4,36E-07	1,22E-07	6,82E-07	1,00E-06	8,59E-07	1,19E-06	9,07E-07	9,76E-07	1,73E-07	9,47E-07	1,68E-07
Fluxo_s	8,17E-06	2,28E-06	1,28E-05	1,88E-05	1,61E-05	2,22E-05	1,70E-05	1,83E-05	3,23E-06	1,77E-05	3,14E-06
Q	-6202,09429	-5318,415891	-5140,771282	-4964,9931	-5196,269346	-5097,9639	-5041,879724	-5404,200769	-5269,187354	-5229,3462	-5171,981892
Lp (efetivo)	2,90322E-05	2,48957E-05	2,40641E-05	2,3241E-05	2,43239E-05	2,3864E-05	2,36012E-05	2,52972E-05	2,46652E-05	2,4479E-05	2,42102E-05
$M_{p,s}$	4,08584E-07	1,13937E-07	6,3893E-07	9,3989E-07	8,04601E-07	1,1112E-06	8,48747E-07	9,13371E-07	1,61707E-07	8,8627E-07	1,56859E-07

(c) Open circuit on secondary (DD-R).

Desalinhamento X (mm)	-1500	-1200	-900	-600	-300	0	300	600	900	1200	1500
Tensão_p1	19,16735134	59,46360784	50,60275569	48,005131	42,62055834	57,2993493	47,82009606	48,2430599	52,11092496	64,3921074	15,62510124
Corrente_p1	4,38E-07	1,22E-07	6,82E-07	1,00E-06	8,58E-07	1,19E-06	9,05E-07	9,66E-07	1,66E-07	9,21E-07	2,06E-07
Fluxo_p1	3,59E-05	1,11E-04	9,47E-05	8,99E-05	7,98E-05	1,07E-04	8,95E-05	9,03E-05	9,76E-05	1,21E-04	2,93E-05
Tensão_p2	14,78758541	60,68656536	57,41916321	58,0370687	51,20313099	45,4326744	56,86770248	57,90319842	53,76825932	55,1805978	13,56359594
Corrente_p2	4,38E-07	1,22E-07	6,82E-07	1,00E-06	8,58E-07	1,19E-06	9,05E-07	9,66E-07	1,66E-07	9,21E-07	2,06E-07
Fluxo_p2	2,77E-05	1,14E-04	1,08E-04	1,09E-04	9,59E-05	8,51E-05	1,06E-04	1,08E-04	1,01E-04	1,03E-04	2,54E-05
Tensão_s	6364,698081	6011,330607	6211,175971	6249,20258	6068,105941	6298,03455	5971,178072	6188,062449	6081,061017	1,4886017788	6417,821494
Corrente_s	20	20	20	20	20	20	20	20	20	20	20
Fluxo_s	0,011917331	0,011255682	0,011629874	0,01170108	0,011361988	0,01179251	0,011180499	0,011586596	0,011386246	0,01105001	0,0120168
L_s	0,000595867	0,000562784	0,000581494	0,00058505	0,000568099	0,00058963	0,000559025	0,00057933	0,000569312	0,0005525	0,00060084
Q (Var)	-127293,9553	-120226,6055	-124223,513	-124984,05	-121362,1122	-125960,68	-119423,5547	-123761,2425	-121621,2138	-118029,765	-128356,4237
$M_{s,p}$	3,18E-06	1,12E-05	1,01E-05	9,93E-06	8,78E-06	9,62E-06	9,80E-06	9,94E-06	9,91E-06	1,12E-05	2,73E-06

(d) Open circuit on primary (DD-R).

Desalinhamento X (mm)	-1500	-1200	-900	-600	-300	0	300	600	900	1200	1500
Tensão_p1	514,1800715	434,627315	439,6679947	430,9729604	387,6159801	407,6795222	411,581235	415,947695	430,25916	478,1001472	481,8486482
Corrente_p1	20	20	20	20	20	20	20	20	20	20	20
Fluxo_p1	9,63E-04	8,14E-04	8,23E-04	8,07E-04	7,26E-04	7,63E-04	7,71E-04	7,79E-04	8,06E-04	8,95E-04	9,02E-04
L_p1	4,81E-05	4,07E-05	4,12E-05	4,03E-05	3,63E-05	3,82E-05	3,85E-05	3,89E-05	4,03E-05	4,48E-05	4,51E-05
Tensão_s1	8,334404681	74,7632923	85,32277391	75,02571136	69,72510939	84,82084881	80,0358948	77,1533186	76,874488	60,99657075	5,28543369
Corrente_s1	5,99E-07	5,20E-07	6,83E-09	9,07E-07	6,96E-07	1,44E-06	9,58E-07	4,71E-07	1,75E-06	2,84E-07	8,54E-07
Fluxo_s1	1,56E-05	1,40E-04	1,60E-04	1,40E-04	1,31E-04	1,59E-04	1,50E-04	1,44E-04	1,44E-04	1,14E-04	9,90E-06
Tensão_s2	14,32565999	69,5650459	85,39103046	84,09248772	76,68143446	70,46396045	89,6159568	72,446585	94,351893	63,83852101	13,8260996
Corrente_s2	5,99E-07	5,20E-07	6,83E-09	9,07E-07	6,96E-07	1,44E-06	9,58E-07	4,71E-07	1,75E-06	2,84E-07	8,54E-07
Fluxo_s2	2,68E-05	1,30E-04	1,60E-04	1,57E-04	1,44E-04	1,32E-04	1,68E-04	1,36E-04	1,77E-04	1,20E-04	2,59E-05
Tensão_s	22,66006467	144,328338	170,7138044	159,1181991	146,4065439	155,2848093	169,651852	149,599904	171,22638	124,8350918	19,11153329
Q	-10283,52364	-8692,45428	-8793,26892	-8619,366393	-7752,21641	-8153,49233	-8231,52752	-8318,8577	-8605,0902	-9561,91928	-9636,88995
$M_{p,s}$	2,12145E-06	1,3512E-05	1,59823E-05	1,48967E-05	1,37067E-05	1,45378E-05	1,5883E-05	1,4006E-05	1,603E-05	1,16871E-05	1,78923E-06

(e) Open circuit on secondary (R-DD).

Desalinhamento X (mm)	-1500	-1200	-900	-600	-300	0	300	600	900	1200	1500
Tensão_p1	5,982426408	5,20555124	0,071516907	9,06965247	6,951963972	14,35385894	9,57389518	4,73530007	17,443204	2,81163635	8,544455487
Corrente_p1	5,98E-07	5,21E-07	7,15E-09	9,07E-07	6,95E-07	1,44E-06	9,57E-07	4,74E-07	1,74E-06	2,81E-07	8,54E-07
Fluxo_p1	1,12E-05	9,75E-06	1,34E-07	1,70E-05	1,30E-05	2,69E-05	1,79E-05	8,87E-06	3,27E-05	5,26E-06	1,60E-05
Tensão_s1	2035,502085	2141,45734	2236,227697	2122,799375	1977,024792	2005,896456	2186,6997	2183,45695	2300,6945	2160,245561	2076,968208
Corrente_s1	20	20	20	20	20	20	20	20	20	20	20
Fluxo_s1	0,003811295	0,00400969	0,004187136	0,003974751	0,003701801	0,003755861	0,0040944	0,00408833	0,0043078	0,00404866	0,003888937
Tensão_s2	1992,79642	2181,79403	2221,476645	2190,530449	2044,951733	2158013969	2211,22116	2147,19952	2251,376	2074,422874	2043,420569
Corrente_s2	20	20	20	20	20	20	20	20	20	20	20
Fluxo_s2	0,003731332	0,00408521	0,004159516	0,004101572	0,003828988	0,00365254	0,00414031	0,00402044	0,0042155	0,003884171	0,003826122
Ls	0,000377131	0,00040475	0,000417333	0,000403816	0,000376539	0,00037042	0,00041174	0,00040544	0,0004262	0,000396452	0,000385753
Q	-80565,93037	-86464,9903	-89154,0509	-86266,55937	-80439,4907	-79132,2047	-87958,3808	-86613,093	-91041,374	-84693,3309	-82407,7367
$M_{s,p}$	5,60E-07	4,87E-07	6,70E-09	8,49E-07	6,51E-07	1,34E-06	8,96E-07	4,43E-07	1,63E-06	2,63E-07	8,00E-07

(f) Open circuit on primary (R-DD).

Desalinhamento X (mm)	-1500	-1200	-900	-600	-300	0	300	600	900	1200	1500
Tensão_p1	156,2794352	139,4407668	128,2722429	128,2695532	132,2605304	130,2550831	128,7714497	126,8463659	142,4356384	125,7635329	112,4254113
Corrente_p1	20	20	20	20	20	20	20	20	20	20	20
Fluxo_p1	2,93E-04	2,61E-04	2,40E-04	2,40E-04	2,48E-04	2,44E-04	2,41E-04	2,37E-04	2,67E-04	2,35E-04	2,10E-04
Tensão_p2	152,8907415	139,9384158	128,0937425	125,7555693	129,1296744	130,8293765	137,9375282	127,1486943	150,1781286	132,2220382	110,7616077
Corrente_p2	20	20	20	20	20	20	20	20	20	20	20
Fluxo_p2	2,86E-04	2,62E-04	2,40E-04	2,35E-04	2,42E-04	2,45E-04	2,58E-04	2,38E-04	2,81E-04	2,48E-04	2,07E-04
Tensão_s1	84,3638149	118,8938801	138,4538503	132,1469627	141,4388236	147,4794872	136,0451335	145,2430317	135,1234504	142,8289144	65,98205028
Corrente_s1	1,73E-05	2,48E-05	2,73E-05	2,66E-05	2,97E-05	3,04E-05	2,76E-05	2,95E-05	2,63E-05	2,88E-05	1,32E-05
Fluxo_s1	1,58E-04	2,23E-04	2,59E-04	2,47E-04	2,65E-04	2,76E-04	2,55E-04	2,72E-04	2,53E-04	2,67E-04	1,24E-04
Tensão_s2	88,49950194	129,0179109	135,011648	133,5809092	155,3676888	156,8793095	140,3502745	150,0324582	127,6745415	144,847642	65,96329597
Corrente_s2	1,73E-05	2,48E-05	2,73E-05	2,66E-05	2,97E-05	3,04E-05	2,76E-05	2,95E-05	2,63E-05	2,88E-05	1,32E-05
Fluxo_s2	1,66E-04	2,42E-04	2,53E-04	2,50E-04	2,91E-04	2,94E-04	2,63E-04	2,81E-04	2,39E-04	2,71E-04	1,24E-04
Tensão_s	172,8633168	247,9117909	273,4654983	265,7278719	296,8065124	304,3587967	276,395408	295,27549	262,7579918	287,6765564	131,9453463
Q	-6182,885898	-5587,010834	-5126,695446	-5079,87238	-5227,191726	-5221,076184	-5333,578795	-5079,27109	-5851,728042	-5159,09068	-4463,023366
Lp (efetivo)	2,89423E-05	2,61535E-05	2,39982E-05	2,3779E-05	2,44686E-05	2,444E-05	2,49666E-05	2,37762E-05	2,73921E-05	2,41498E-05	2,08915E-05
$M_{p,p}$	1,61836E-05	2,32096E-05	2,5602E-05	2,48776E-05	2,78722E-05	2,84942E-05	2,58763E-05	2,76439E-05	2,46033E-05	2,69324E-05	1,23528E-05

(g) Open circuit on secondary (DD-DD).

Desalinhamento X (mm)	-1500	-1200	-900	-600	-300	0	300	600	900	1200	1500
Tensão_p1	87,68607118	126,5390633	135,5075818	132,8201656	146,7904358	150,701995	138,7245444	145,1132721	134,362655	140,906211	64,94760196
Corrente_p1	1,73E-05	2,48E-05	2,73E-05	2,66E-05	2,97E-05	3,04E-05	2,76E-05	2,95E-05	2,63E-05	2,88E-05	1,32E-05
Fluxo_p1	1,64E-04	2,37E-04	2,54E-04	2,49E-04	2,75E-04	2,82E-04	2,60E-04	2,72E-04	2,52E-04	2,64E-04	1,22E-04
Tensão_p2	85,0608011	121,1708339	137,7885846	132,7841538	149,806234	153,4817989	137,5378287	150,0028421	128,317525	146,613211	66,85451907
Corrente_p2	1,73E-05	2,48E-05	2,73E-05	2,66E-05	2,97E-05	3,04E-05	2,76E-05	2,95E-05	2,63E-05	2,88E-05	1,32E-05
Fluxo_p2	1,59E-04	2,27E-04	2,58E-04	2,49E-04	2,80E-04	2,87E-04	2,58E-04	2,81E-04	2,40E-04	2,75E-04	1,25E-04
Tensão_s1	2076,31572	2094,245419	2176,619413	2029,83242	2178,28715	2238,614774	2079,976231	2206,048662	2094,360668	2290,704087	2137,988816
Corrente_s1	20	20	20	20	20	20	20	20	20	20	20
Fluxo_s1	0,003887715	0,003921287	0,004075525	0,003800679	0,004078647	0,004191605	0,003894569	0,004130628	0,003921502	0,004289138	0,004003192
Tensão_s2	2108,467979	2090,573653	2143,689345	2064,378879	2247,988528	2220,620611	2106,832227	2203,404463	2069,579968	2288,478151	2117,186535
Corrente_s2	20	20	20	20	20	20	20	20	20	20	20
Fluxo_s2	0,003947917	0,003914412	0,004013866	0,003865364	0,004209157	0,004157913	0,003944854	0,004125677	0,003875103	0,00428497	0,003964242
Q	-83695,63574	-83696,34321	-86406,13811	-81884,18689	-88525,47739	-89184,67181	-83736,13092	-88189,0262	-83278,77428	-91583,6098	-85103,46941
Ls (efetivo)	0,000391782	0,000391785	0,00040447	0,000383302	0,00041439	0,000417476	0,000391971	0,000412815	0,00038983	0,000428705	0,000398372
$M_{s,p}$	1,61727E-05	2,31907E-05	2,55861E-05	2,4866E-05	2,77675E-05	2,85E-05	2,58638E-05	2,76289E-05	2,45923E-05	2,69177E-05	1,23394E-05

(h) Open circuit on primary (DD-DD).

Figure C.1: Parameters along Ox for the long types.

Desalinhamento X (mm)	-1200	-1000	-800	-600	-400	-200	0	200	400	600	800	1000	1200
Tensão_p1	112,9327526	116,0604509	115,7560207	117,8969199	116,5475124	101,2984453	99,2944522	93,97346458	95,96204504	94,94834099	93,41936659	99,57870388	92,69207771
Corrente_p1	20	20	20	20	20	20	20	20	20	20	20	20	20
Fluxo_p1	2,11E-04	2,17E-04	2,17E-04	2,21E-04	2,18E-04	1,90E-04	1,86E-04	1,76E-04	1,80E-04	1,78E-04	1,75E-04	1,86E-04	1,74E-04
Tensão_p2	94,21860219	92,23225034	93,97503034	98,51635178	118,273731	116,1679114	113,9429881	118,531226	116,6813244	106,506221	92,35829185	95,74783897	95,80995529
Corrente_p2	20	20	20	20	20	20	20	20	20	20	20	20	20
Fluxo_p2	1,76E-04	1,73E-04	1,76E-04	1,84E-04	2,21E-04	2,17E-04	2,13E-04	2,22E-04	2,18E-04	1,99E-04	1,73E-04	1,79E-04	1,79E-04
Tensão_p3	95,47855342	95,98346224	93,7111053	93,63575094	92,42500022	91,64206371	95,5792781	102,9239109	113,1476457	116,1735148	112,8577259	114,9105694	111,4339917
Corrente_p3	20	20	20	20	20	20	20	20	20	20	20	20	20
Fluxo_p3	1,79E-04	1,80E-04	1,75E-04	1,75E-04	1,73E-04	1,72E-04	1,79E-04	1,93E-04	2,12E-04	2,17E-04	2,11E-04	2,15E-04	2,09E-04
Tensão_s	5,168459071	193,9465841	397,2104824	224,0267713	8,899782331	232,1340983	406,972307	242,2159794	7,578966457	213,1292749	389,4211809	208,1171793	19,26434641
Corrente_s	5,17E-07	1,94E-05	3,97E-05	2,24E-05	8,90E-07	2,32E-05	4,07E-05	2,42E-05	7,58E-07	2,13E-05	3,89E-05	2,08E-05	1,93E-06
Fluxo_s	9,68E-06	3,63E-04	7,44E-04	4,19E-04	1,67E-05	4,35E-04	7,62E-04	4,54E-04	1,42E-05	3,99E-04	7,29E-04	3,90E-04	3,61E-05
Q	-6051,40036	-6084,328009	-6067,644687	-6199,807759	-6543,81058	-6180,992513	-6175,16156	-6307,42007	-6514,70704	-6351,42019	-5971,491588	-6203,574503	-5997,51238
Lp	2,83268E-05	2,84809E-05	2,84028E-05	2,90215E-05	3,06318E-05	2,89334E-05	2,89061E-05	2,95252E-05	3,04955E-05	2,97312E-05	2,79527E-05	2,90391E-05	2,80745E-05
$M_{p,p}$	4,83874E-07	1,81574E-05	3,71871E-05	2,09735E-05	8,33203E-07	2,17325E-05	3,8101E-05	2,26764E-05	7,09547E-07	1,99533E-05	3,64578E-05	1,9484E-05	1,80354E-06

(a) Open circuit on secondary (R-R).

Desalinhamento X (mm)	-1200	-1000	-800	-600	-400	-200	0	200	400	600	800	1000	1200
Tensão_p1	9,195084307	187,6513638	388,9955881	196,3582851	5,671691769	33,62178888	12,03756238	7,344724123	5,172572791	0,249443052	1,070552466	1,107759323	1,114475078
Corrente_p1	5,29E-07	1,94E-05	3,97E-05	2,24E-05	8,90E-07	2,32E-05	4,07E-05	2,42E-05	7,57E-07	2,13E-05	3,89E-05	2,08E-05	1,93E-06
Fluxo_p1	1,72E-05	3,51E-04	7,28E-04	3,68E-04	1,06E-05	6,30E-05	2,25E-05	1,38E-05	9,69E-06	4,67E-07	2,00E-06	2,07E-06	2,09E-06
Tensão_p2	4,691173946	7,492915166	9,17564366	28,60867337	7,438674005	191,5116635	384,5303299	200,014556	3,579429157	32,14560696	8,761053535	6,566385471	6,02746131
Corrente_p2	5,29E-07	1,94E-05	3,97E-05	2,24E-05	8,90E-07	2,32E-05	4,07E-05	2,42E-05	7,57E-07	2,13E-05	3,89E-05	2,08E-05	1,93E-06
Fluxo_p2	8,78E-06	1,40E-05	1,72E-05	5,36E-05	1,39E-05	3,59E-04	7,20E-04	3,75E-04	2,96E-06	6,02E-05	1,64E-05	1,23E-05	1,13E-05
Tensão_p3	0,790052808	1,214985434	1,369866692	0,956279457	4,209388949	6,991675883	10,3811424	34,82028877	0,821026879	181,2178049	381,4533851	202,638028	24,16303558
Corrente_p3	5,29E-07	1,94E-05	3,97E-05	2,24E-05	8,90E-07	2,32E-05	4,07E-05	2,42E-05	7,57E-07	2,13E-05	3,89E-05	2,08E-05	1,93E-06
Fluxo_p3	1,48E-06	2,27E-06	2,57E-06	1,79E-06	7,88E-06	3,31E-05	1,94E-05	6,52E-05	1,54E-06	3,39E-04	7,14E-04	3,79E-04	4,52E-05
Tensão_s	6050,33263	6094,213104	6242,189584	6549,483616	6728,035605	6516,801739	6303,289532	6294,020354	6546,424559	6091,150928	6227,183363	6419,59113	6241,110187
Corrente_s	20	20	20	20	20	20	20	20	20	20	20	20	20
Fluxo_s	0,011328709	0,011410872	0,011687944	0,012263325	0,012597648	0,012202131	0,011802349	0,011784993	0,012257597	0,011405138	0,011659847	0,012020113	0,011685923
L_s	5,66E-04	5,71E-04	5,84E-04	6,13E-04	6,30E-04	6,10E-04	5,90E-04	5,89E-04	6,13E-04	5,70E-04	5,83E-04	6,01E-04	5,84E-04
Q	-121006,646	-121884,2555	-124843,7853	-130989,6662	-134660,0286	-132035,6286	-126065,784	-125880,401	-130928,485	-121823,012	-124543,6608	-128391,8164	-124822,197
$M_{s,p}$	1,374E-06	1,83833E-05	3,74053E-05	2,11511E-05	1,62149E-06	2,17317E-05	3,80988E-05	2,2673E-05	7,08991E-07	1,99986E-05	3,66323E-05	1,96895E-05	2,93079E-06

(b) Open circuit on primary (R-R).

Desalinhamento X (mm)	-1200	-1000	-800	-600	-400	-200	0	200	400	600	800	1000	1200
Tensão_p1	115,0589639	115,3566174	115,704881	123,9421941	124,3144189	114,9371445	93,80179704	98,15433561	94,56552173	95,1357158	96,601655	94,296221	93,17029181
Corrente_p1	20	20	20	20	20	20	20	20	20	20	20	20	20
Fluxo_p1	2,15E-04	2,16E-04	2,17E-04	2,32E-04	2,33E-04	2,15E-04	1,76E-04	1,84E-04	1,77E-04	1,78E-04	1,81E-04	1,77E-04	1,74E-04
Tensão_p2	93,0699372	95,07123929	98,55652262	117,5019123	123,4765513	121,0001749	119,9626728	119,3192807	122,0426809	114,305132	95,89727871	92,9023279	95,6925634
Corrente_p2	20	20	20	20	20	20	20	20	20	20	20	20	20
Fluxo_p2	1,74E-04	1,78E-04	1,85E-04	2,20E-04	2,31E-04	2,27E-04	2,25E-04	2,23E-04	2,28E-04	2,14E-04	1,80E-04	1,74E-04	1,79E-04
Tensão_p3	93,60394031	90,79814529	92,3149899	91,20571404	96,10359164	92,3108908	95,69247291	113,0610515	121,5651157	122,796991	119,211122	118,072172	113,2031788
Corrente_p3	20	20	20	20	20	20	20	20	20	20	20	20	20
Fluxo_p3	1,75E-04	1,70E-04	1,73E-04	1,71E-04	1,80E-04	1,73E-04	1,87E-04	2,12E-04	2,28E-04	2,30E-04	2,23E-04	2,21E-04	2,12E-04
Tensão_s	116,1955118	319,8469883	579,610301	385,1287703	15,38356528	379,0238852	425,3408744	382,7494557	17,77101391	375,98049	395,112018	336,298555	126,7340777
Corrente_s	1,16E-05	3,20E-05	3,80E-05	3,85E-05	1,54E-06	3,79E-05	4,25E-05	3,83E-05	1,78E-06	3,76E-05	3,95E-05	3,36E-05	1,27E-05
Fluxo_s	2,18E-04	5,99E-04	7,11E-04	7,21E-04	2,88E-05	7,10E-04	7,96E-04	7,17E-04	3,33E-05	7,04E-04	7,40E-04	6,30E-04	2,37E-04
Q	-6033,451916	-6023,30958	-6130,34271	-6651,894351	-6876,829219	-6563,85195	-6267,977329	-6609,596467	-6762,386492	-6643,66032	-6233,034	-6104,22058	-6040,119855
Lp	2,82428E-05	2,81953E-05	2,8696E-05	3,13377E-05	3,21906E-05	3,07256E-05	2,93408E-05	3,09397E-05	3,16549E-05	3,10995E-05	2,9177E-05	2,8574E-05	2,8274E-05
$M_{s,p}$	1,08783E-05	2,99443E-05	3,5539E-05	3,6058E-05	1,44022E-06	3,54844E-05	3,98206E-05	3,58332E-05	1,66373E-06	3,52E-05	3,6991E-05	3,1484E-05	1,18649E-05

(c) Open circuit on secondary (R-R_+).

Desalinhamento X (mm)	-1200	-1000	-800	-600	-400	-200	0	200	400	600	800	1000	1200
Tensão_p1	110,1299196	309,2612567	356,967546	333,8737464	121,1661154	46,12614191	27,31942637	13,55987837	6,43646205	3,87603585	1,33670749	1,71135725	1,31377592
Corrente_p1	1,16E-05	3,20E-05	3,79E-05	3,85E-05	1,55E-06	3,79E-05	4,25E-05	3,83E-05	1,78E-06	3,76E-05	3,94E-05	3,36E-05	1,27E-05
Fluxo_p1	2,06E-04	5,79E-04	6,68E-04	6,25E-04	2,27E-04	8,64E-05	5,12E-05	2,54E-05	1,21E-05	7,26E-06	2,50E-06	3,20E-06	2,46E-06
Tensão_p2	7,930966127	11,63621248	23,7583297	53,69718905	128,0698447	319,7045547	369,2639371	323,7529414	125,8791094	47,22610648	27,5632592	12,0045967	9,381682246
Corrente_p2	1,16E-05	3,20E-05	3,79E-05	3,85E-05	1,55E-06	3,79E-05	4,25E-05	3,83E-05	1,78E-06	3,76E-05	3,94E-05	3,36E-05	1,27E-05
Fluxo_p2	1,49E-05	2,18E-05	4,45E-05	1,01E-04	2,40E-04	5,99E-04	6,91E-04	6,06E-04	2,36E-04	8,84E-05	5,16E-05	2,25E-05	1,76E-05
Tensão_p3	1,863925868	1,081215797	1,45800812	2,547613283	8,576377192	13,16058368	28,69205494	45,40320967	114,5433709	332,561966	368,07724	325,932826	118,5821067
Corrente_p3	1,16E-05	3,20E-05	3,79E-05	3,85E-05	1,55E-06	3,79E-05	4,25E-05	3,83E-05	1,78E-06	3,76E-05	3,94E-05	3,36E-05	1,27E-05
Fluxo_p3	3,49E-06	2,02E-06	2,73E-06	4,77E-06	1,61E-05	2,46E-05	5,37E-05	8,50E-05	2,14E-04	6,23E-04	6,89E-04	6,10E-04	2,22E-04
Tensão_s	8607,826081	8345,738225	8227,73651	9055,575134	9439,110429	8904,939761	8468,065517	8986,041425	9433,590954	9024,19385	8309,11922	8743,47128	8233,055321
Corrente_s	20	20	20	20	20	20	20	20	20	20	20	20	20
Fluxo_s	0,016117389	0,015626652	0,0154057	0,016955759	0,017673895	0,016673708	0,015855699	0,016825563	0,01766356	0,016897	0,015555809	0,016373137	0,015411919
L_s	8,06E-04	7,81E-04	7,70E-04	8,48E-04	8,84E-04	8,34E-04	7,93E-04	8,41E-04	8,83E-04	8,45E-04	7,78E-04	8,19E-04	7,71E-04
Q	-172156,517	-166914,76	-164554,725	-181111,4983	-188782,2043	-178098,791	-169361,3056	-179720,824	-188671,8148	-180483,873	-166182,38	-174869,421	-164621,1016
$M_{s,p}$	1,12274E-05	3,01438E-05	3,578E-05	3,65231E-05	2,41365E-05	3,54834E-05	3,98145E-05	3,58301E-05	2,31111E-05	3,59189E-05	3,7165E-05	3,1788E-05	1,12103E-05

(d) Open circuit on primary (R-R_+).

Desalinhamento X (mm)	-1200	-1000	-800	-600	-400	-200	0	200	400	600	800	1000	1200
Tensão_p1	124,7524329	118,695142	123,557781	125,385289	119,298282	101,1660623	113,06612	116,4483357	123,169317	108,2790249	107,512492	113,4088539	104,349004
Corrente_p1	20	20	20	20	20	20	20	20	20	20	20	20	20
Fluxo_p1	2,34E-04	2,22E-04	2,32E-04	2,35E-04	2,23E-04	1,89E-04	2,12E-04	2,18E-04	2,31E-04	2,03E-04	2,01E-04	2,12E-04	1,95E-04
Tensão_p2	119,0078246	119,501381	111,2204555	111,651988	127,737282	129,7818039	129,54156	127,8929921	135,4417768	107,7948719	112,026112	103,5579385	110,6480555
Corrente_p2	20	20	20	20	20	20	20	20	20	20	20	20	20
Fluxo_p2	2,23E-04	2,24E-04	2,08E-04	2,09E-04	2,39E-04	2,43E-04	2,43E-04	2,39E-04	2,54E-04	2,02E-04	2,10E-04	1,94E-04	2,07E-04
Tensão_p3	103,2946091	98,3290675	97,9432571	109,8345556	107,9488871	119,5528797	105,55709	93,2187494	115,8477931	121,3913339	121,2658977	113,9165995	125,12937
Corrente_p3	20	20	20	20	20	20	20	20	20	20	20	20	20
Fluxo_p3	1,93E-04	1,84E-04	1,83E-04	2,06E-04	2,02E-04	2,24E-04	1,98E-04	1,75E-04	2,17E-04	2,27E-04	2,27E-04	2,13E-04	2,34E-04
Tensão_B1	93,63661408	85,1091257	105,347925	102,683131	109,762796	97,8341121	106,87495	90,1261499	109,701071	88,34003098	89,94789663	89,78285653	84,812322
Corrente_B1	20	20	20	20	20	20	20	20	20	20	20	20	20
Fluxo_B1	1,75E-04	1,59E-04	1,97E-04	1,92E-04	2,05E-04	1,83E-04	2,00E-04	1,69E-04	2,05E-04	1,65E-04	1,68E-04	1,68E-04	1,59E-04
Tensão_B2	92,4334167	88,0076226	80,3915594	100,48545	92,4218583	93,52555562	96,235304	97,9488151	107,196977	99,32828888	100,225383	77,58166115	84,5504723
Corrente_B2	20	20	20	20	20	20	20	20	20	20	20	20	20
Fluxo_B2	1,73E-04	1,65E-04	1,50E-04	1,88E-04	1,73E-04	1,75E-04	1,80E-04	1,83E-04	2,01E-04	1,86E-04	1,88E-04	1,45E-04	1,58E-04
Tensão_s	6,855639324	247,703809	415,482911	31,6222328	385,655679	35,07424285	403,643821	15,58784412	364,719746	40,37170712	401,216892	250,4188953	69,7812773
Corrente_s	6,86E-07	2,48E-05	4,15E-05	3,16E-06	3,86E-05	3,51E-06	4,04E-05	1,56E-06	3,65E-05	4,04E-06	4,01E-05	2,50E-05	6,98E-06
Fluxo_s	1,28E-05	4,64E-04	7,78E-04	5,92E-05	7,22E-04	6,57E-05	7,56E-04	2,92E-05	6,83E-04	7,56E-05	7,51E-04	4,69E-04	1,31E-04
Q	-10660,5939	-10190,843	-10375,251	-10998,979	-11141,565	-10835,3334	-11023,67	-10510,764	-11825,435	-10500,7453	-10617,652	-9962,90664	-10187,775
L	4,99025E-05	4,7704E-05	4,8567E-05	5,1487E-05	5,2154E-05	5,07205E-05	5,16E-05	4,9201E-05	5,5355E-05	4,91543E-05	4,97025E-05	4,66366E-05	4,7689E-05
$M_{p,p}$	6,41829E-07	2,319E-05	3,8898E-05	2,9605E-06	3,6105E-05	3,28367E-06	3,7796E-05	1,4593E-06	3,4145E-05	3,77962E-06	3,7562E-05	2,3444E-05	6,533E-06

(e) Open circuit on secondary (BP-R).

Desalinhamento X (mm)	-1200	-1000	-800	-600	-400	-200	0	200	400	600	800	1000	1200
Tensão_p1	8,170833541	196,39904	392,462171	196,893833	1,606013	28,47916225	12,060894	6,554620631	3,89687895	0,494700168	1,212020304	1,262562429	1,05918765
Corrente_p1	6,80E-07	2,46E-05	4,14E-05	3,17E-06	3,86E-05	3,51E-06	4,04E-05	1,55E-06	3,65E-05	4,04E-06	4,01E-05	2,50E-05	6,98E-06
Fluxo_p1	1,53E-05	3,68E-04	7,35E-04	3,69E-04	3,01E-06	5,33E-05	2,26E-05	1,23E-05	7,30E-06	9,26E-07	2,27E-06	2,36E-06	1,98E-06
Tensão_p2	5,137422058	6,46233198	11,5554461	32,5568772	4,07381135	207,176514	374,50757	203,660353	3,08758272	35,74584447	9,556153343	10,11244157	5,73888943
Corrente_p2	6,80E-07	2,46E-05	4,14E-05	3,17E-06	3,86E-05	3,51E-06	4,04E-05	1,55E-06	3,65E-05	4,04E-06	4,01E-05	2,50E-05	6,98E-06
Fluxo_p2	9,62E-06	1,21E-05	2,16E-05	6,10E-05	7,63E-06	3,88E-04	7,01E-04	3,81E-04	5,78E-06	6,69E-05	1,79E-05	1,89E-05	1,07E-05
Tensão_p3	1,170885932	1,559692342	0,82347595	1,432744495	5,18640143	6,743312944	8,83770775	33,5599218	5,88442715	190,0672579	391,0739993	205,5745933	44,2486457
Corrente_p3	6,80E-07	2,46E-05	4,14E-05	3,17E-06	3,86E-05	3,51E-06	4,04E-05	1,55E-06	3,65E-05	4,04E-06	4,01E-05	2,50E-05	6,98E-06
Fluxo_p3	2,19E-06	2,92E-06	1,54E-06	2,68E-06	9,71E-06	1,26E-05	1,65E-05	6,28E-05	1,10E-05	3,56E-04	7,32E-04	3,85E-04	8,29E-05
Tensão_B1	18,75505108	52,7071896	31,8495415	200,095255	387,327744	195,9128089	28,683142	52,44565973	18,3671151	1,802014945	2,946185991	1,877949653	3,23839423
Corrente_B1	6,80E-07	2,46E-05	4,14E-05	3,17E-06	3,86E-05	3,51E-06	4,04E-05	1,55E-06	3,65E-05	4,04E-06	4,01E-05	2,50E-05	6,98E-06
Fluxo_B1	3,51E-05	9,87E-05	5,96E-05	3,75E-04	7,25E-04	3,67E-04	5,37E-05	9,82E-05	3,44E-05	3,37E-06	5,52E-06	3,52E-06	6,06E-06
Tensão_B2	2,521408546	5,00157414	2,3443084	5,48615497	12,44542006	59,03128098	21,3265343	200,487263	376,360521	195,9933318	17,7901111	54,3218172	29,0683951
Corrente_B2	6,80E-07	2,46E-05	4,14E-05	3,17E-06	3,86E-05	3,51E-06	4,04E-05	1,55E-06	3,65E-05	4,04E-06	4,01E-05	2,50E-05	6,98E-06
Fluxo_B2	4,72E-06	9,37E-06	4,39E-06	1,03E-05	2,33E-05	1,11E-04	3,39E-05	3,75E-04	7,05E-04	3,67E-04	3,33E-05	1,02E-04	5,44E-05
Tensão_s	6173,688649	6246,15717	6341,22119	6624,63229	6767,06507	6423,995895	6282,4592	6439,67556	6767,58202	6244,079839	6257,97092	6334,351812	6188,08184
Corrente_s	20	20	20	20	20	20	20	20	20	20	20	20	20
Fluxo_s	0,011559683	0,011695377	0,01187337	0,01240403	0,01267073	0,012028361	0,0117633	0,01205772	0,0126717	0,011691484	0,01171749	0,01186051	0,01158663
L_s	0,000577984	0,000584777	0,00059367	0,0006202	0,00063354	0,000601418	0,0005882	0,00060289	0,00063358	0,000584574	0,00058587	0,000593026	0,00057933
Q	-123473,767	-124923,14	-126824,42	-132492,64	-135341,3	-128479,912	-125649,2	-128793,5	-135351,635	-124881,59	-125159,41	-126687,03	-123761,63
$M_{p,p}$	5,34746E-06	2,45541E-05	4,1103E-05	4,0862E-05	3,8444E-05	4,65615E-05	4,17E-05	4,6502E-05	3,8159E-05	3,97048E-05	3,9562E-05	2,55724E-05	7,8036E-06

(f) Open circuit on primary (BP-R).

Desalinhamento X (mm)	-1200	-1000	-800	-600	-400	-200	0	200	400	600	800	1000	1200
Tensão_p1_1	32,97648493	36,121402	37,383808	36,29309	33,5861204	30,703457	26,506836	26,2584115	26,8297334	27,44352142	27,16927181	27,809584	29,7493974
Corrente_p	20	20	20	20	20	20	20	20	20	20	20	20	20
Tensão_p1_2	32,80576042	36,532519	38,105609	35,8982	34,3204004	30,6955595	28,739742	27,072

Desalinhamento X (mm)	-1200	-1000	-800	-600	-400	-200	0	200	400	600	800	1000	1200
Tensão_p1_1	33,75777911	37,015178	38,125294	36,460955	35,2989717	33,7208215	28,5623538	27,69835	28,330039	29,297458	28,547648	27,988923	28,1386218
Corrente_p	20	20	20	20	20	20	20	20	20	20	20	20	20
Fluxo_p1_1	6,31E-05	6,92E-05	7,13E-05	6,82E-05	6,60E-05	6,30E-05	5,33E-05	5,17E-05	5,29E-05	5,47E-05	5,33E-05	5,23E-05	5,26E-05
Tensão_p1_2	34,22231433	36,8642731	38,323225	37,532593	35,2303597	33,99634	28,6397602	28,121764	29,131344	29,4970569	28,462425	28,7237164	29,1520135
Fluxo_p1_2	6,40E-05	6,89E-05	7,17E-05	7,02E-05	6,59E-05	6,35E-05	5,35E-05	5,25E-05	5,44E-05	5,51E-05	5,32E-05	5,37E-05	5,45E-05
Tensão_p2_1	28,61607352	28,600861	30,605352	31,386171	33,7895171	37,3595586	39,5416316	38,00573	35,5649	30,5953247	27,888109	30,3735337	29,6674162
Fluxo_p2_1	5,35E-05	5,34E-05	5,72E-05	5,86E-05	6,32E-05	6,99E-05	7,39E-05	7,11E-05	6,65E-05	5,72E-05	5,21E-05	5,67E-05	5,54E-05
Tensão_p2_2	28,75358649	28,3066918	30,535807	31,340426	33,0607236	37,1959354	39,0044509	38,609389	34,87784	31,2284532	28,424838	30,7737242	29,374222
Fluxo_p2_2	5,37E-05	5,29E-05	5,71E-05	5,86E-05	6,18E-05	6,95E-05	7,29E-05	7,22E-05	6,52E-05	5,84E-05	5,31E-05	5,75E-05	5,49E-05
Tensão_p3_1	28,21246463	28,9684991	27,247018	28,800258	28,4231151	27,3811838	29,598048	30,69132	34,216889	36,6333012	37,615928	36,8441282	33,6333285
Fluxo_p3_1	5,27E-05	5,41E-05	5,09E-05	5,38E-05	5,31E-05	5,11E-05	5,53E-05	5,73E-05	6,40E-05	6,85E-05	7,03E-05	6,89E-05	6,29E-05
Tensão_p3_2	28,55555596	29,2734332	28,453977	29,035983	28,5947523	27,8669245	29,9574085	31,767891	34,909911	37,5918725	39,45178	37,5653615	34,4337488
Fluxo_p3_2	5,33E-05	5,47E-05	5,31E-05	5,42E-05	5,34E-05	5,20E-05	5,60E-05	5,94E-05	6,53E-05	7,03E-05	7,38E-05	7,02E-05	6,44E-05
Tensão_s1	57,38547256	94,7074676	125,01699	102,55658	105,101921	109,584295	127,528444	106,13972	109,64848	101,241249	120,43231	98,9848248	54,3274594
Corrente_s1	1,15E-05	1,92E-05	2,47E-05	2,05E-05	2,08E-05	2,14E-05	2,53E-05	2,12E-05	2,17E-05	2,06E-05	2,44E-05	1,95E-05	1,09E-05
Fluxo_s1	1,07E-04	1,77E-04	2,34E-04	1,92E-04	1,97E-04	2,05E-04	2,39E-04	1,99E-04	2,05E-04	1,90E-04	2,25E-04	1,85E-04	1,02E-04
Tensão_s2	57,24721897	97,0261603	122,20667	102,24973	103,04086	103,957437	125,742304	105,65786	107,6518	104,389736	124,15991	95,7976303	54,7993235
Corrente_s2	1,15E-05	1,92E-05	2,47E-05	2,05E-05	2,08E-05	2,14E-05	2,53E-05	2,12E-05	2,17E-05	2,06E-05	2,44E-05	1,95E-05	1,09E-05
Fluxo_s2	1,07E-04	1,82E-04	2,29E-04	1,91E-04	1,93E-04	1,95E-04	2,35E-04	1,98E-04	2,02E-04	1,95E-04	2,32E-04	1,79E-04	1,03E-04
Q	-3634,38518	-3772,8456	-3858,222	-3883,64	-3880,4727	-3943,0025	-3898,5441	-3890,3635	-3933,2396	-3889,396	-3800,0805	-3837,7907	-3680,1238
Lp	1,70127E-05	1,7661E-05	1,806E-05	1,818E-05	1,8165E-05	1,8457E-05	1,8249E-05	1,821E-05	1,841E-05	1,8206E-05	1,779E-05	1,7965E-05	1,7227E-05
M_{p_s}	1,0732E-05	1,795E-05	2,315E-05	1,917E-05	1,9486E-05	1,9992E-05	2,3711E-05	1,983E-05	2,034E-05	1,9251E-05	2,29E-05	1,8236E-05	1,0217E-05

(k) Open circuit on secondary (DD-BP).

Desalinhamento X (mm)	-1200	-1000	-800	-600	-400	-200	0	200	400	600	800	1000	1200
Tensão_p1_1	58,13089566	96,3989436	121,6805	91,219294	54,5084451	12,140865	1,27290788	0,0665478	0,0155572	0,189785	0,0412959	0,03219523	0,05601409
Corrente_p	1,15E-05	1,92E-05	2,47E-05	2,05E-05	2,08E-05	2,13E-05	2,53E-05	2,12E-05	2,17E-05	2,06E-05	2,44E-05	1,95E-05	1,09E-05
Fluxo_p1_1	1,09E-04	1,80E-04	2,28E-04	1,71E-04	1,02E-04	2,27E-05	2,38E-06	1,25E-07	2,91E-08	3,55E-07	7,73E-08	6,03E-08	1,05E-07
Tensão_p1_2	56,47937832	94,9036665	122,95884	91,594921	54,9800969	14,0093023	1,16395308	0,2981893	0,0194885	0,11489752	0,0028112	0,00382961	0,03231621
Fluxo_p1_2	1,06E-04	1,78E-04	2,30E-04	1,72E-04	1,03E-04	2,62E-05	2,18E-06	5,58E-07	3,65E-08	2,15E-07	5,26E-09	7,17E-09	6,05E-08
Tensão_p2_1	0,037281069	0,23266349	0,9199377	11,514256	49,9005942	93,8425425	123,990301	96,341243	56,599023	10,3401446	1,0568455	0,19440614	0,04484132
Fluxo_p2_1	6,98E-08	4,36E-07	1,72E-06	2,16E-05	9,34E-05	1,76E-04	2,32E-04	1,80E-04	1,06E-04	1,94E-05	1,98E-06	3,64E-07	8,40E-08
Tensão_p2_2	0,008385198	0,09875161	1,5805528	10,316479	48,8148635	93,029806	124,193341	94,607314	52,924025	10,8357832	0,8017388	0,30089691	0,1436309
Fluxo_p2_2	1,57E-08	1,85E-07	2,96E-06	1,93E-05	9,14E-05	1,74E-04	2,33E-04	1,77E-04	9,91E-05	2,03E-05	1,50E-06	5,63E-07	2,69E-07
Tensão_p3_1	0,019471531	0,05209855	0,0184946	0,0636839	0,03434209	0,13622506	1,46927986	10,555457	53,252189	91,8806164	119,22016	96,8438866	52,3588702
Fluxo_p3_1	3,65E-08	9,76E-08	3,46E-08	1,19E-07	6,43E-08	2,55E-07	2,75E-06	1,98E-05	9,97E-05	1,72E-04	2,23E-04	1,81E-04	9,80E-05
Tensão_p3_2	0,002914554	0,01235666	0,0188623	0,0332248	0,15928332	0,31087338	1,10967794	10,594575	54,494978	92,2061534	123,2907	97,3423228	56,8502922
Fluxo_p3_2	5,46E-09	2,31E-08	3,53E-08	6,22E-08	2,98E-07	5,82E-07	2,08E-06	1,98E-05	1,02E-04	1,73E-04	2,31E-04	1,82E-04	1,06E-04
Tensão_s1	1730,518808	1823,67987	1906,352	1870,123	1823,38842	1892,04338	1895,24914	1843,7379	1881,4759	1837,46513	1879,9833	1852,6316	1775,20511
Corrente_s1	20	20	20	20	20	20	20	20	20	20	20	20	20
Fluxo_s1	0,00324024	0,00341468	0,0035695	0,0035016	0,00341413	0,00354268	0,00354868	0,0034522	0,0035229	0,00344049	0,0035201	0,00346889	0,00332391
Tensão_s2	1541,547715	1634,78203	1666,0562	1617,8821	1626,81784	1642,02503	1665,41893	1629,4034	1658,1762	1631,42048	1684,0385	1622,01909	1536,25875
Corrente_s2	20	20	20	20	20	20	20	20	20	20	20	20	20
Fluxo_s2	0,002886409	0,00306098	0,0031195	0,0030293	0,00304607	0,00307454	0,00311835	0,0030509	0,0031048	0,00305469	0,0031532	0,00303708	0,00287651
Q	-65441,2814	-69169,191	-71448,12	-69760,056	-69004,078	-70681,323	-71213,316	-69462,779	-70792,997	-69377,666	-71280,39	-69492,967	-66229,229
Ls	3,06E-04	3,24E-04	3,34E-04	3,27E-04	3,23E-04	3,31E-04	3,33E-04	3,25E-04	3,31E-04	3,25E-04	3,34E-04	3,25E-04	3,10E-04
M_{s_p}	1,07362E-05	1,7947E-05	2,314E-05	1,917E-05	1,951E-05	1,9985E-05	2,3705E-05	1,989E-05	2,034E-05	1,9245E-05	2,288E-05	1,823E-05	1,025E-05

(l) Open circuit on primary (DD-BP).

Figure C.2: Parameters along Ox for the segmented types.

C.1.2 Oy

Desalinhamento Y (mm)	0	100	200	300	400	500
Tensão_p	431,8707313	423,9725969	418,6962053	460,8942648	436,8914288	513,2726235
Corrente_p	20	20	20	20	20	20
Fluxo_p	8,09E-04	7,94E-04	7,84E-04	8,63E-04	8,18E-04	9,61E-04
L_p	4,04E-05	3,97E-05	3,92E-05	4,31E-05	4,09E-05	4,81E-05
Tensão_s	248,5515272	179,1491516	105,7685395	26,0986076	104,7481592	122,5794937
Corrente_s	2,49E-05	1,79E-05	1,06E-05	2,61E-06	1,05E-05	1,23E-05
Fluxo_s	4,65E-04	3,35E-04	1,98E-04	4,89E-05	1,96E-04	2,30E-04
M_{p_s}	2,32695E-05	1,6772E-05	9,90211E-06	2,44337E-06	9,80658E-06	1,1476E-05

(a) Open circuit on secondary (R-R).

Desalinhamento Y (mm)	0	100	200	300	400	500
Tensão_p	248,5638615	178,481087	105,2155898	24,91649036	103,6072235	121,8901384
Corrente_p	2,49E-05	1,78E-05	1,05E-05	2,49E-06	1,04E-05	1,22E-05
Fluxo_p	4,65E-04	3,34E-04	1,97E-04	4,67E-05	1,94E-04	2,28E-04
Tensão_s	6212,221911	6234,048697	6279,562662	6400,393401	6099,554475	5458,514801
Corrente_s	20	20	20	20	20	20
Fluxo_s	0,011631833	0,011672701	0,011757922	0,011984167	0,011420873	0,010220583
L_s	5,82E-04	5,84E-04	5,88E-04	5,99E-04	5,71E-04	5,11E-04
M_{s_p}	2,33E-05	1,67E-05	9,85E-06	2,33E-06	9,70E-06	1,14E-05

(b) Open circuit on primary (R-R).

Desalinhamento Y (mm)	0	100	200	300	400	500
Tensão_p1	128,6168791	146,4056123	125,6108034	134,7849963	132,359752	129,1389664
Corrente_p1	20	20	20	20	20	20
Fluxo_p1	2,41E-04	2,74E-04	2,35E-04	2,52E-04	2,48E-04	2,42E-04
Tensão_p2	126,3127033	152,8451751	127,3485672	130,680582	131,001835	132,1784296
Corrente_p2	20	20	20	20	20	20
Fluxo_p2	2,36E-04	2,86E-04	2,38E-04	2,45E-04	2,45E-04	2,47E-04
Tensão_s	11,86917186	120,7308237	193,6194787	147,8948481	103,662877	38,93390715
Corrente_s	1,19E-06	1,21E-05	1,94E-05	1,48E-05	1,04E-05	3,89E-06
Fluxo_s	2,22E-05	2,26E-04	3,63E-04	2,77E-04	1,94E-04	7,29E-05
Q	-5097,963934	-5984,480789	-5058,554769	-5308,70864	-5266,6241	-5225,73552
L	2,38637E-05	2,80135E-05	2,36792E-05	2,48502E-05	2,4653E-05	2,44618E-05
M_{p_s}	1,1112E-06	1,13029E-05	1,81268E-05	1,3846E-05	9,705E-06	3,64501E-06

(c) Open circuit on secondary (DD-R).

Desalinhamento Y (mm)	0	100	200	300	400	500
Tensão_p1	45,43267435	104,5813085	121,7803687	81,21480827	45,2486934	2,561466683
Corrente_p1	1,19E-06	1,21E-05	1,93E-05	1,47E-05	1,02E-05	3,88E-06
Fluxo_p1	8,51E-05	1,96E-04	2,28E-04	1,52E-04	8,47E-05	4,80E-06
Tensão_p2	57,29934931	16,12952946	71,71239798	66,00582835	57,0103214	41,34103928
Corrente_p2	1,19E-06	1,21E-05	1,93E-05	1,47E-05	1,02E-05	3,88E-06
Fluxo_p2	1,07E-04	3,02E-05	1,34E-04	1,24E-04	1,07E-04	7,74E-05
Tensão_s	6298,034554	6255,366961	6264,790757	6236,30996	6287,817	5830,143406
Corrente_s	20	20	20	20	20	20
Fluxo_s	0,011792509	0,011712618	0,011730263	0,011676935	0,01177338	0,010916425
L_s	5,90E-04	5,86E-04	5,87E-04	5,84E-04	5,89E-04	5,46E-04
Q	-125960,6847	-125107,3328	-125295,8088	-124726,193	-125756,33	-116602,861
M_{s_p}	9,62E-06	1,13E-05	1,81E-05	1,38E-05	9,57E-06	4,11E-06

(d) Open circuit on primary (DD-R).

Desalinhamento Y (mm)	0	100	200	300	400	500
Tensão_p1	407,679522	403,568208	418,720886	416,025961	430,427918	413,885301
Corrente_p1	20	20	20	20	20	20
Fluxo_p1	7,63E-04	7,56E-04	7,84E-04	7,79E-04	8,06E-04	7,75E-04
L_p1	3,82E-05	3,78E-05	3,92E-05	3,89E-05	4,03E-05	3,87E-05
Tensão_s1	84,8208488	153,990508	187,505489	127,42444	63,0990281	17,3908389
Corrente_s1	1,44E-06	1,73E-05	2,93E-05	2,39E-05	1,62E-05	4,50E-06
Fluxo_s1	1,59E-04	2,88E-04	3,51E-04	2,39E-04	1,18E-04	3,26E-05
Tensão_s2	70,4639605	18,5809558	105,221699	111,882185	99,3111656	62,3582332
Corrente_s2	1,44E-06	1,73E-05	2,93E-05	2,39E-05	1,62E-05	4,50E-06
Fluxo_s2	1,32E-04	3,48E-05	1,97E-04	2,09E-04	1,86E-04	1,17E-04
Tensão_s	155,284809	172,571464	292,727188	239,306626	162,410194	79,7490721
Q	-8153,4923	-8071,265	-8374,3221	-8320,423	-8608,4654	-8277,6094
M_{p_s}	1,4538E-05	1,6156E-05	2,7405E-05	2,2404E-05	1,5205E-05	7,4662E-06

(e) Open circuit on secondary (R-DD).

Desalinhamento Y (mm)	0	100	200	300	400	500
Tensão_p1	14,3538589	172,477421	292,618386	239,22555	162,339583	44,9080314
Corrente_p1	1,44E-06	1,72E-05	2,93E-05	2,39E-05	1,62E-05	4,49E-06
Fluxo_p1	2,69E-05	3,23E-04	5,48E-04	4,48E-04	3,04E-04	8,41E-05
Tensão_s1	2005,89646	2165,19985	2250,90194	1991,23624	2021,65814	2011,60741
Corrente_s1	20	20	20	20	20	20
Fluxo_s1	0,00375586	0,00405414	0,00421461	0,00372841	0,00378537	0,00376655
Tensão_s2	1950,7158	2217,6408	2228,08653	1835,43472	1717,06106	1806,52846
Corrente_s2	20	20	20	20	20	20
Fluxo_s2	0,00365254	0,00415233	0,00417189	0,00343669	0,00321504	0,00338256
Tensão_s	3956,61226	4382,84065	4478,98847	3826,67095	3738,71919	3818,13587
Q	-79132,205	-87656,777	-89579,734	-76533,377	-74774,341	-76362,675
Ls (efetivo)	0,00037042	0,00041032	0,00041933	0,00035825	0,00035002	0,00035746
M_{s_p}	1,3438E-06	1,6147E-05	2,7395E-05	2,2396E-05	1,5198E-05	4,2043E-06

(f) Open circuit on primary (R-DD).

Desalinhamento Y (mm)	0	100	200	300	400	500
Tensão_p1	130,2550831	125,400503	121,811737	123,956391	127,236797	139,640318
Corrente_p1	20	20	20	20	20	20
Fluxo_p1	2,44E-04	2,35E-04	2,28E-04	2,32E-04	2,38E-04	2,61E-04
Tensão_p2	130,8293765	126,817766	123,041456	126,8282164	121,536776	141,315548
Corrente_p2	20	20	20	20	20	20
Fluxo_p2	2,45E-04	2,37E-04	2,30E-04	2,37E-04	2,28E-04	2,65E-04
Tensão_s1	147,4794872	97,203182	20,5094754	72,38675171	82,8670501	67,9306333
Corrente_s1	3,04E-05	2,29E-05	5,04E-06	5,55E-06	8,18E-06	7,59E-06
Fluxo_s1	2,76E-04	1,82E-04	3,84E-05	1,36E-04	1,55E-04	1,27E-04
Tensão_s2	156,8793095	132,129336	70,9429103	16,89255758	1,0814289	7,94765221
Corrente_s2	3,04E-05	2,29E-05	5,04E-06	5,55E-06	8,18E-06	7,59E-06
Fluxo_s2	2,94E-04	2,47E-04	1,33E-04	3,16E-05	2,02E-06	1,49E-05
Tensão_s	304,3587967	229,332518	91,4523857	89,27930929	83,948479	75,8782855
Q	-5221,07618	-5043,73087	-4896,4103	-5015,054021	-4974,8279	-5618,54778
Lp (efetivo)	2,444E-05	2,361E-05	2,292E-05	2,34756E-05	2,3287E-05	2,6301E-05
M_{p_s}	2,84942E-05	2,147E-05	8,5618E-06	8,35838E-06	7,8593E-06	7,1038E-06

(g) Open circuit on secondary (DD-DD).

Desalinhamento Y (mm)	0	100	200	300	400	500
Tensão_p1	150,701995	139,588524	67,3307683	26,41815202	3,81930544	4,94206762
Corrente_p1	3,04E-05	2,29E-05	5,04E-06	5,55E-06	8,18E-06	7,59E-06
Fluxo_p1	2,82E-04	2,61E-04	1,26E-04	4,95E-05	7,15E-06	9,25E-06
Tensão_p2	153,4817989	89,6011508	16,9504603	81,92024613	85,5950897	70,9110575
Corrente_p2	3,04E-05	2,29E-05	5,04E-06	5,55E-06	8,18E-06	7,59E-06
Fluxo_p2	2,87E-04	1,68E-04	3,17E-05	1,53E-04	1,60E-04	1,33E-04
Tensão_s1	2238,614774	2213,94426	2100,83451	1933,096876	1837,44686	2126,81668
Corrente_s1	20	20	20	20	20	20
Fluxo_s1	0,004191605	0,00414541	0,00393362	0,00361955	0,00344045	0,00398227
Tensão_s2	2220,620611	2174,53681	2070,60951	1794,94348	1824,60096	1903,12662
Corrente_s2	20	20	20	20	20	20
Fluxo_s2	0,004157913	0,00407163	0,00387703	0,00336087	0,0034164	0,00356343
Tensão_s	4459,235385	4388,48107	4171,44402	3728,040356	3662,04781	4029,9433
Q	-89184,6718	-87769,585	-83428,842	-74560,76414	-73240,913	-80598,8261
Ls (efetivo)	0,000417476	0,00041085	0,00039053	0,000349021	0,00034284	0,00037729
M_{s_p}	2,84779E-05	2,1457E-05	7,8905E-06	1,01427E-05	8,371E-06	7,1014E-06

(h) Open circuit on primary (DD-DD).

Figure C.3: Parameters along Oy for the long types.

Desalinhamento Y (mm)	0	100	200	300	400	500
Tensão_p1	99,2944522	98,8536776	99,3035628	92,8163472	93,7069199	93,273018
Corrente_p	20	20	20	20	20	20
Fluxo_p1	1,86E-04	1,85E-04	1,86E-04	1,74E-04	1,75E-04	1,75E-04
Tensão_p2	113,942988	117,089037	116,018257	114,484518	117,768388	107,15894
Fluxo_p2	2,13E-04	2,19E-04	2,17E-04	2,14E-04	2,20E-04	2,01E-04
Tensão_p3	95,5792781	90,2482263	92,5120551	91,2892761	93,3450181	95,001146
Fluxo_p3	1,79E-04	1,69E-04	1,73E-04	1,71E-04	1,75E-04	1,78E-04
Tensão_s	406,972307	335,706361	214,219106	101,32686	9,14600562	43,940359
Corrente_s	4,07E-05	3,36E-05	2,14E-05	1,01E-05	9,15E-07	4,39E-06
Fluxo_s	7,62E-04	6,29E-04	4,01E-04	1,90E-04	1,71E-05	8,23E-05
Q	-6175,1616	-6122,62903	-6155,4973	-5970,5842	-6095,2114	-5907,4387
Lp	2,8906E-05	2,866E-05	2,8814E-05	2,7948E-05	2,8532E-05	2,765E-05
M_{p_s}	3,8101E-05	3,1429E-05	2,0055E-05	9,4863E-06	8,5625E-07	4,114E-06

(a) Open circuit on secondary (R-R).

Desalinhamento Y (mm)	0	100	200	300	400	500
Tensão_p1	12,0375624	10,1935963	10,9282059	9,9099661	9,03075898	5,8280733
Corrente_p1	4,07E-05	3,36E-05	2,14E-05	1,01E-05	9,15E-07	4,39E-06
Fluxo_p1	2,25E-05	1,91E-05	2,05E-05	1,86E-05	1,69E-05	1,09E-05
Tensão_p2	384,53033	316,58707	191,712875	81,3674123	6,99021228	55,333822
Corrente_p2	4,07E-05	3,36E-05	2,14E-05	1,01E-05	9,15E-07	4,39E-06
Fluxo_p2	7,20E-04	5,93E-04	3,59E-04	1,52E-04	1,31E-05	1,04E-04
Tensão_p3	10,3811424	8,9035455	11,5653203	10,0482029	7,11265293	5,5719626
Corrente_p3	4,07E-05	3,36E-05	2,14E-05	1,01E-05	9,15E-07	4,39E-06
Fluxo_p3	1,94E-05	1,67E-05	2,17E-05	1,88E-05	1,33E-05	1,04E-05
Tensão_s	6303,28953	6389,32452	6409,9883	6339,15669	6195,50528	5836,4434
Corrente_s	20	20	20	20	20	20
Fluxo_s	0,01180235	0,01196344	0,01200213	0,01186951	0,01160053	0,0109282
L_s	5,90E-04	5,98E-04	6,00E-04	5,93E-04	5,80E-04	5,46E-04
Q	-126065,78	-127786,484	-128199,76	-126783,13	-123910,1	-116728,86
M_{s_p}	3,8099E-05	3,1427E-05	2,0054E-05	9,4862E-06	2,1658E-06	6,248E-06

(b) Open circuit on primary (R-R).

Desalinhamento Y (mm)	0	100	200	300	400	500
Tensão_p1	93,80179704	101,9848353	101,4056719	99,38357071	93,2445961	98,1180704
Corrente_p	20	20	20	20	20	20
Fluxo_p1	1,76E-04	1,91E-04	1,90E-04	1,86E-04	1,75E-04	1,84E-04
Tensão_p2	119,9626728	118,1313671	122,4042679	120,5032044	116,117206	106,46887
Fluxo_p2	2,25E-04	2,21E-04	2,29E-04	2,26E-04	2,17E-04	1,99E-04
Tensão_p3	99,69247291	91,60003426	93,29588432	93,58690828	94,5112089	93,9811511
Fluxo_p3	1,87E-04	1,71E-04	1,75E-04	1,75E-04	1,77E-04	1,76E-04
Tensão_s	425,3408744	343,4847445	227,1225688	104,6205555	1,17239627	47,6164135
Corrente_s	4,25E-05	3,43E-05	2,27E-05	1,05E-05	1,17E-07	4,76E-06
Fluxo_s	7,96E-04	6,43E-04	4,25E-04	1,96E-04	2,20E-06	8,92E-05
Q	-6267,97733	-6233,156911	-6340,9663	-6268,311703	-6076,2634	-5970,15272
Lp	2,93406E-05	2,91776E-05	2,96822E-05	2,93421E-05	2,8443E-05	2,7946E-05
M_{p_s}	3,98206E-05	3,21572E-05	2,12633E-05	9,79463E-06	1,0976E-07	4,4579E-06

(c) Open circuit on secondary (R-R_+).

Desalinhamento Y (mm)	0	100	200	300	400	500
Tensão_p1	27,31942637	28,05597256	33,4731156	28,27503271	26,0164993	18,6916556
Corrente_p1	4,25E-05	3,43E-05	2,27E-05	1,04E-05	1,05E-07	4,87E-06
Fluxo_p1	5,12E-05	5,25E-05	6,27E-05	5,29E-05	4,87E-05	3,50E-05
Tensão_p2	369,2639371	289,0873547	163,0486539	47,68992491	48,331132	84,6008503
Corrente_p2	4,25E-05	3,43E-05	2,27E-05	1,04E-05	1,05E-07	4,87E-06
Fluxo_p2	6,91E-04	5,41E-04	3,05E-04	8,93E-05	9,05E-05	1,58E-04
Tensão_p3	28,69205494	26,28685024	30,57402959	27,96068493	23,365774	17,2264934
Corrente_p3	4,25E-05	3,43E-05	2,27E-05	1,04E-05	1,05E-07	4,87E-06
Fluxo_p3	5,37E-05	4,92E-05	5,72E-05	5,24E-05	4,38E-05	3,23E-05
Tensão_s	8468,065517	8410,301561	8373,06803	8867,613878	8828,10724	8210,98832
Corrente_s	20	20	20	20	20	20
Fluxo_s	0,015855699	0,015747542	0,015677825	0,016603818	0,01652985	0,01537435
L_s	7,93E-04	7,87E-04	7,84E-04	8,30E-04	8,26E-04	7,69E-04
Q	-169361,306	-168206,0265	-167461,356	-177352,273	-176562,14	-164219,762
M_{s_p}	3,98145E-05	3,21521E-05	2,12608E-05	9,72958E-06	9,148E-06	1,1283E-05

(d) Open circuit on primary (R-R_+).

Desalinhamento Y (mm)	0	100	200	300	400	500
Tensão_p1	113,0661237	102,8236594	103,7558508	104,8574279	101,0884889	111,6052596
Corrente_p	20	20	20	20	20	20
Fluxo_p1	2,12E-04	1,92E-04	1,94E-04	1,96E-04	1,89E-04	2,09E-04
Tensão_p2	129,5415588	131,6794579	132,9393361	130,4048015	122,5672153	123,7609668
Fluxo_p2	2,43E-04	2,47E-04	2,49E-04	2,44E-04	2,29E-04	2,32E-04
Tensão_p3	105,5570861	98,07041429	98,966144	101,7898815	106,379035	102,3082064
Fluxo_p3	1,98E-04	1,84E-04	1,85E-04	1,91E-04	1,99E-04	1,92E-04
Tensão_B1	106,8749508	95,0645531	96,88724169	97,54254033	89,15307624	98,14582978
Fluxo_B1	2,00E-04	1,78E-04	1,81E-04	1,83E-04	1,67E-04	1,84E-04
Tensão_B2	96,23530433	94,41828471	96,08112302	99,10059814	95,97287076	87,30629772
Fluxo_B2	1,80E-04	1,77E-04	1,80E-04	1,86E-04	1,80E-04	1,63E-04
Tensão_s	403,6438162	374,9562486	290,5957366	182,4059488	78,88928013	14,3580159
Corrente_s	4,04E-05	3,75E-05	2,91E-05	1,82E-05	7,89E-06	1,44E-06
Fluxo_s	7,56E-04	7,02E-04	5,44E-04	3,42E-04	1,48E-04	2,69E-05
Q	-11023,66864	-10439,18191	-10570,67383	-10672,00987	-10301,25	-10460,5927
Lp	5,16021E-05	4,88661E-05	4,94816E-05	4,9956E-05	4,82204E-05	4,89663E-05
M_{p_s}	3,77894E-05	3,51036E-05	2,72057E-05	1,70769E-05	7,38566E-06	1,34421E-06

(e) Open circuit on secondary (BP-R).

Desalinhamento Y (mm)	0	100	200	300	400	500
Tensão_p1	12,06089363	11,23731865	7,790488459	9,495164158	7,746107711	7,039796161
Corrente_p	4,04E-05	3,75E-05	2,91E-05	1,82E-05	7,89E-06	1,43E-06
Fluxo_p1	2,26E-05	2,10E-05	1,46E-05	1,78E-05	1,45E-05	1,32E-05
Tensão_p2	374,507569	325,1708911	208,1032467	95,19624101	4,685006896	50,06017513
Fluxo_p2	7,01E-04	6,09E-04	3,90E-04	1,78E-04	8,77E-06	9,37E-05
Tensão_p3	8,83770755	11,53446252	8,64506407	9,046817752	9,001075992	7,586123893
Fluxo_p3	1,65E-05	2,16E-05	1,62E-05	1,69E-05	1,69E-05	1,42E-05
Tensão_B1	28,68314235	36,158292	48,04008672	52,35159022	47,47973788	42,14590668
Fluxo_B1	5,37E-05	6,77E-05	9,00E-05	9,80E-05	8,89E-05	7,89E-05
Tensão_B2	21,32654254	36,36854371	50,86395817	53,35809848	52,8148017	36,86369069
Fluxo_B2	3,99E-05	6,81E-05	9,52E-05	9,99E-05	9,89E-05	6,90E-05
Tensão_s	6282,459207	6381,353152	6488,096871	6391,856449	6221,503008	5933,653158
Corrente_s	20	20	20	20	20	20
Fluxo_s	0,011763346	0,011948516	0,012148384	0,011968182	0,011649211	0,011110237
L_s	5,88E-04	5,97E-04	6,07E-04	5,98E-04	5,82E-04	5,56E-04
Q	-125649,1778	-127627,0568	-129761,9312	-127837,1227	-124430,0537	-118673,056
M_{s_p}	4,17001E-05	3,93646E-05	3,02809E-05	2,05448E-05	1,13961E-05	1,34529E-05

(f) Open circuit on primary (BP-R).

Desalinhamento Y (mm)	0	100	200	300	400	500
Tensão_p1_1	26,506836	28,16979333	28,1995046	27,4972947	28,295003	28,354796
Corrente	20	20	20	20	20	20
Tensão_p1_2	28,739742	28,31201542	28,3147933	28,4937412	28,614911	29,277159
Tensão_p2_1	37,812071	38,0355099	36,2328455	32,318651	28,773968	27,881893
Tensão_p2_2	38,022247	37,22130737	35,792544	33,4495785	32,074406	32,306161
Tensão_p3_1	29,135348	26,48383053	29,0956678	27,5412148	28,961971	27,406987
Tensão_p3_2	30,286772	27,87026095	29,2588645	28,4449237	29,285606	29,890275
Tensão_s1	4,2137001	124,685904	193,111389	165,700248	91,960385	18,728985
Q	-3802,348	-3713,94052	-3730,0811	-3546,74772	-3511,9118	-3494,0882
Lp	1,78E-05	1,73851E-05	1,7461E-05	1,6602E-05	1,644E-05	1,636E-05
M_{p_s}	3,945E-07	1,16732E-05	1,8079E-05	1,5513E-05	8,609E-06	1,753E-06

(g) Open circuit on secondary (DD-R).

Desalinhamento Y (mm)	0	100	200	300	400	500
Tensão_p1_1	5,1474896	3,047936946	3,38108292	2,71367313	1,3433965	0,0492165
Tensão_p1_2	4,8859427	5,504461624	4,65038358	3,72991128	4,9558337	4,8887416
Tensão_p2_1	76,266128	3,149367778	54,518825	57,6009281	41,664605	23,586334
Tensão_p2_2	79,651477	130,3789617	142,857901	112,434331	58,027382	4,2362067
Tensão_p3_1	5,0073487	3,828317975	2,94574259	2,51660099	1,7038327	0,0109663
Tensão_p3_2	4,4409214	3,931186113	5,97162401	5,86124889	5,8483336	4,4898029
Tensão_s1	6803,1983	6626,417949	6635,05337	6409,30669	6365,3335	5953,4659
Corrente_s1	20	20	20	20	20	20
Fluxo_s1	0,0127384	0,012407378	0,01242355	0,01200086	0,0119185	0,0111473
L_s1	0,0006369	0,000620369	0,00062118	0,00060004	0,0005959	0,0005574
Q	-136064	-132528,353	-132701,06	-128186,128	-127306,66	-119069,31
M_{s_p}	1,642E-05	1,40281E-05	2,0065E-05	1,7306E-05	1,063E-05	3,488E-06

(h) Open circuit on primary (DD-R).

Desalinhamento Y (mm)	0	100	200	300	400	500
Tensão_p1_1	27,8569638	29,2174165	27,1360308	28,82347709	27,90759547	27,09790041
Corrente_p	20	20	20	20	20	20
Fluxo_p1_1	5,20E-05	5,46E-05	5,07E-05	5,38E-05	5,21E-05	5,06E-05
Tensão_p1_2	28,74070721	29,47919247	27,1432772	29,13093878	28,71135614	28,35793911
Fluxo_p1_2	5,37E-05	5,51E-05	5,07E-05	5,44E-05	5,36E-05	5,30E-05
Tensão_p2_1	37,77048881	39,4893702	37,4641694	31,05810713	29,18933942	28,96587878
Fluxo_p2_1	7,06E-05	7,38E-05	7,00E-05	5,80E-05	5,45E-05	5,41E-05
Tensão_p2_2	37,44801624	38,84571335	37,2159512	33,29825132	32,36041807	32,34396642
Fluxo_p2_2	7,00E-05	7,26E-05	6,96E-05	6,22E-05	6,05E-05	6,04E-05
Tensão_p3_1	28,0227005	27,9007467	28,2268368	29,04665173	29,16845154	28,80939045
Fluxo_p3_1	5,23E-05	5,21E-05	5,27E-05	5,43E-05	5,45E-05	5,38E-05
Tensão_p3_2	28,38827264	28,33101996	28,6768475	30,00299173	29,30177569	29,28171768
Fluxo_p3_2	5,30E-05	5,29E-05	5,36E-05	5,61E-05	5,47E-05	5,47E-05
Tensão_s1	143,502716	86,60062769	11,8876516	95,13491654	96,71382114	54,8439362
Corrente_s1	2,88E-05	2,13E-05	5,51E-06	9,03E-06	1,08E-05	7,12E-06
Fluxo_s1	2,69E-04	1,62E-04	2,23E-05	1,78E-04	1,81E-04	1,03E-04
Tensão_s2	144,1377675	126,315489	67,0005022	4,79116323	11,08613456	16,37107975
Corrente_s2	2,88E-05	2,13E-05	5,51E-06	9,03E-06	1,08E-05	7,12E-06
Fluxo_s2	2,70E-04	2,37E-04	1,25E-04	8,97E-06	2,08E-05	3,07E-05
Q	-3756,742631	-3857,646719	-3709,35105	-3619,23913	-3524,599741	-3488,867156
Lp	1,75854E-05	1,80578E-05	1,7364E-05	1,69418E-05	1,64987E-05	1,63315E-05
M_{p_s}	2,69291E-05	1,99333E-05	7,3856E-06	9,35514E-06	1,00923E-05	6,66719E-06

(i) Open circuit on secondary (DD-DD).

Desalinhamento Y (mm)	0	100	200	300	400	500
Tensão_p1_1	1,9154171	2,53966123	1,83674297	0,491595994	0,109074717	0,691946702
Corrente_p	2,88E-05	2,13E-05	5,51E-06	9,03E-06	1,08E-05	7,12E-06
Fluxo_p1_1	3,59E-06	4,76E-06	3,44E-06	9,20E-07	2,04E-07	1,30E-06
Tensão_p1_2	1,342015477	1,602141148	0,7684285	0,594592661	0,794855337	1,235912286
Fluxo_p1_2	2,51E-06	3,00E-06	1,44E-06	1,11E-06	1,49E-06	2,31E-06
Tensão_p2_1	139,4979421	123,9970996	67,8681978	6,44737023	11,61837438	14,4422459
Fluxo_p2_1	2,61E-04	2,32E-04	1,27E-04	1,21E-05	2,18E-05	2,70E-05
Tensão_p2_2	139,6981934	81,57493971	17,4246111	98,00878979	98,01575087	58,71957379
Fluxo_p2_2	2,62E-04	1,53E-04	3,26E-05	1,84E-04	1,84E-04	1,10E-04
Tensão_p3_1	3,184620878	1,883127135	1,44196574	0,52655902	0,652828642	0,433926826
Fluxo_p3_1	5,96E-06	3,53E-06	2,70E-06	9,86E-07	1,22E-06	8,12E-07
Tensão_p3_2	1,871005892	1,218874544	0,58652693	0,358530813	0,286004013	0,402377174
Fluxo_p3_2	3,50E-06	2,28E-06	1,10E-06	6,71E-07	5,36E-07	7,53E-07
Tensão_s1	2365,273699	2484,059817	2390,68768	2151,53877	2081,590616	2037,167077
Corrente_s1	20	20	20	20	20	20
Fluxo_s1	0,004428763	0,00465118	0,00447635	0,004028563	0,003897592	0,003814412
Tensão_s2	2373,623295	2435,529836	2390,23674	1966,591942	1849,150974	1746,383921
Corrente_s2	20	20	20	20	20	20
Fluxo_s2	0,004444397	0,004560312	0,0044755	0,003682267	0,003462369	0,003269946
Q	-94777,9061	-98391,76053	-95618,4549	-82362,5753	-78614,79095	-75670,97741
Ls	4,44E-04	4,61E-04	4,48E-04	3,86E-04	3,68E-04	3,54E-04
M_{s_p}	2,69168E-05	1,99239E-05	8,419E-06	9,9638E-06	1,04365E-05	7,10823E-06

(j) Open circuit on primary (DD-DD).

Desalinhamento Y (mm)	0	100	200	300	400	500
Tensão_p1_1	28,56235375	28,72878365	28,30907363	30,06894685	26,9417874	29,19071258
Corrente_p	20	20	20	20	20	20
Fluxo_p1_1	5,33E-05	5,37E-05	5,29E-05	5,62E-05	5,03E-05	5,45E-05
Tensão_p1_2	28,63976017	29,40007749	28,8140012	30,38189988	27,6779422	30,45691144
Fluxo_p1_2	5,35E-05	5,49E-05	5,38E-05	5,68E-05	5,17E-05	5,69E-05
Tensão_p2_1	39,54163163	38,29477777	36,85517769	32,15525231	28,4998073	29,81605444
Fluxo_p2_1	7,39E-05	7,16E-05	6,89E-05	6,01E-05	5,32E-05	5,57E-05
Tensão_p2_2	39,00445089	36,87105494	36,68417708	33,48389985	31,1319462	31,97574027
Fluxo_p2_2	7,29E-05	6,89E-05	6,86E-05	6,26E-05	5,82E-05	5,98E-05
Tensão_p3_1	29,59804802	27,83681596	28,82396614	28,3097879	27,8677566	29,66471835
Fluxo_p3_1	5,53E-05	5,20E-05	5,38E-05	5,29E-05	5,20E-05	5,54E-05
Tensão_p3_2	29,95740852	28,30472304	29,95907337	28,94747702	29,292027	29,90392116
Fluxo_p3_2	5,60E-05	5,29E-05	5,60E-05	5,41E-05	5,47E-05	5,59E-05
Tensão_s1	127,5284438	42,93984347	47,35414448	102,19658	86,7128067	53,46897252
Corrente_s1	2,53E-05	1,77E-05	4,79E-06	6,89E-06	9,54E-06	6,89E-06
Fluxo_s1	2,39E-04	8,04E-05	8,87E-05	1,91E-04	1,62E-04	1,00E-04
Tensão_s2	125,7423038	134,2825432	95,2900295	33,2965993	8,64364863	15,47412657
Corrente_s2	2,53E-05	1,77E-05	4,79E-06	6,89E-06	9,54E-06	6,89E-06
Fluxo_s2	2,35E-04	2,51E-04	1,78E-04	6,23E-05	1,62E-05	2,90E-05
Q	-3898,54405	-3780,98368	-3781,20135	-3659,05648	-3419,79567	-3612,19017
Lp	1,82492E-05	1,76989E-05	1,76999E-05	1,71281E-05	1,6008E-05	1,69088E-05
M_{p_s}	2,37113E-05	1,65917E-05	1,33544E-05	1,26849E-05	8,9273E-06	6,45449E-06

(k) Open circuit on secondary (DD-BP).

Desalinhamento Y (mm)	0	100	200	300	400	500
Tensão_p1_1	1,272907882	0,843329552	0,996975725	0,828699386	0,64562187	0,928613744
Corrente_p	2,53E-05	1,77E-05	4,79E-06	6,89E-06	9,53E-06	6,89E-06
Fluxo_p1_1	2,38E-06	1,58E-06	1,87E-06	1,55E-06	1,21E-06	1,74E-06
Tensão_p1_2	1,163953083	1,338033916	0,808427744	0,998453074	0,75512457	1,600406952
Fluxo_p1_2	2,18E-06	2,51E-06	1,51E-06	1,87E-06	1,41E-06	3,00E-06
Tensão_p2_1	123,9903006	108,6229053	59,08135849	8,754106391	8,48746172	15,20783826
Fluxo_p2_1	2,32E-04	2,03E-04	1,11E-04	1,64E-05	1,59E-05	2,85E-05
Tensão_p2_2	124,1933414	65,09475272	14,88470393	80,40355255	90,9245406	57,9242792
Fluxo_p2_2	2,33E-04	1,22E-04	2,79E-05	1,51E-04	1,70E-04	1,08E-04
Tensão_p3_1	1,469279859	0,641485175	0,834573075	0,478651044	0,85545487	0,876868102
Fluxo_p3_1	2,75E-06	1,20E-06	1,56E-06	8,96E-07	1,60E-06	1,64E-06
Tensão_p3_2	1,109677937	0,634025615	1,081115093	0,44366489	1,80638929	0,78938324
Fluxo_p3_2	2,08E-06	1,19E-06	2,02E-06	8,31E-07	3,38E-06	1,48E-06
Tensão_s1	1895,249137	1881,430544	1818,39454	1625,942209	1751,39453	1804,430508
Corrente_s1	20	20	20	20	20	20
Fluxo_s1	0,003548684	0,003522809	0,00340478	0,00304443	0,00327933	0,003378634
Tensão_s2	1665,418929	1596,30867	1593,910996	1456,621972	1252,88192	1194,139878
Corrente_s2	20	20	20	20	20	20
Fluxo_s2	0,003118347	0,002988944	0,002984454	0,002727393	0,00234591	0,002235918
Q	-71213,3162	-69554,738	-68246,0636	-61651,2316	-60085,4742	-59971,3521
Ls	3,33E-04	3,26E-04	3,19E-04	2,89E-04	2,81E-04	2,81E-04
M_{s_p}	2,37047E-05	1,65872E-05	7,27311E-06	8,6044E-06	9,6873E-06	7,23943E-06

(l) Open circuit on primary (DD-BP).

Figure C.4: Parameters along Oy for the segmented types.

C.1.3 Oz

Airgap (mm)	100	125	150	175	200
Tensão_p	431,87073	416,055648	387,316858	392,516697	403,799635
Corrente_p	20	20	20	20	20
Fluxo_p	8,09E-04	7,79E-04	7,25E-04	7,35E-04	7,56E-04
L_p	4,04E-05	3,90E-05	3,63E-05	3,6747E-05	3,7803E-05
Tensão_s	248,55153	226,542002	157,502054	141,051886	127,115417
Corrente_s	2,49E-05	2,27E-05	1,58E-05	1,41E-05	1,27E-05
Fluxo_s	4,65E-04	4,24E-04	2,95E-04	2,64E-04	2,38E-04
M_{p_s}	2,327E-05	2,1209E-05	1,4745E-05	1,3205E-05	1,1901E-05

(a) Open circuit on secondary (R-R).

Airgap (mm)	100	125	150	175	200
Tensão_p	248,56386	224,965686	157,49537	139,854405	127,09443
Corrente_p	2,49E-05	2,25E-05	1,57E-05	1,40E-05	1,27E-05
Fluxo_p	4,65E-04	4,21E-04	2,95E-04	2,62E-04	2,38E-04
Tensão_s	6212,2219	5777,30726	5017,70696	5259,39371	5374,70703
Corrente_s	20	20	20	20	20
Fluxo_s	0,0116318	0,01081749	0,00939521	0,00984775	0,01006366
L_s	5,82E-04	5,41E-04	4,70E-04	4,92E-04	5,03E-04
M_{s_p}	2,33E-05	2,11E-05	1,47E-05	1,31E-05	1,19E-05

(b) Open circuit on primary (R-R).

Entreferro (mm)	100	125	150	175	200
Tensão_p1	128,6168791	128,75792	121,9765938	113,96681	119,4245
Corrente_p1	20	20	20	20	20
Fluxo_p1	2,41E-04	2,41E-04	2,28E-04	2,13E-04	2,24E-04
Tensão_p2	126,3127033	126,43437	117,6481213	109,0304	117,3865
Corrente_p2	20	20	20	20	20
Fluxo_p2	2,36E-04	2,37E-04	2,20E-04	2,04E-04	2,20E-04
Tensão_s	11,86917186	15,825006	3,435510702	3,8185672	6,186336
Corrente_s	1,19E-06	1,58E-06	3,44E-07	3,82E-07	6,19E-07
Fluxo_s	2,22E-05	2,96E-05	6,43E-06	7,15E-06	1,16E-05
Q	-5097,963934	-5103,219	-4791,82633	-4459,226	-4735,546
L	2,38637E-05	2,389E-05	2,24307E-05	2,087E-05	2,22E-05
M_{p_s}	1,1112E-06	1,482E-06	3,21634E-07	3,575E-07	5,79E-07

(c) Open circuit on secondary (DD-R).

Entreferro(mm)	100	125	150	175	200
Tensão_p1	45,43267435	36,713219	35,534614	36,18532	37,21725
Corrente_p1	1,19E-06	1,58E-06	3,43E-07	3,82E-07	6,19E-07
Fluxo_p1	8,51E-05	6,87E-05	6,65E-05	6,78E-05	6,97E-05
Tensão_p2	57,29934931	52,534507	38,96605022	32,368002	31,03051
Corrente_p2	1,19E-06	1,58E-06	3,43E-07	3,82E-07	6,19E-07
Fluxo_p2	1,07E-04	9,84E-05	7,30E-05	6,06E-05	5,81E-05
Tensão_s	6298,034554	5901,1309	5776,785887	5758,3062	6076,16
Corrente_s	20	20	20	20	20
Fluxo_s	0,011792509	0,0110493	0,010816517	0,0107819	0,011377
L_s	5,90E-04	5,52E-04	5,41E-04	5,39E-04	5,69E-04
Q	-125960,6847	-118022,6	-115535,711	-115166,1	-121523,2
M_{p_s}	9,61783E-06	8,355E-06	6,97479E-06	6,418E-06	6,39E-06

(d) Open circuit on primary (DD-R).

Entreferro (mm)	100	125	150	175	200
Tensão_p1	407,6795222	407,70339	381,20065	372,20437	423,9372178
Corrente_p1	20	20	20	20	20
Fluxo_p1	7,63E-04	7,63E-04	7,14E-04	6,97E-04	7,94E-04
L_p1	3,82E-05	3,82E-05	3,57E-05	3,48E-05	3,97E-05
Tensão_s1	84,82084881	68,323949	52,53848	48,569598	49,64400864
Corrente_s1	1,44E-06	8,21E-07	7,60E-07	2,36E-07	8,94E-07
Fluxo_s1	1,59E-04	1,28E-04	9,84E-05	9,09E-05	9,30E-05
Tensão_s2	70,46396045	60,114018	60,142363	46,213699	40,70184377
Corrente_s2	1,44E-06	8,21E-07	7,60E-07	2,36E-07	8,94E-07
Fluxo_s2	1,32E-04	1,13E-04	1,13E-04	8,65E-05	7,62E-05
Q	-8153,492327	-8153,9697	-7623,908	-7443,9799	-8478,65
M_{p_s}	1,45378E-05	1,202E-05	1,055E-05	8,87E-06	8,45823E-06

(e) Open circuit on secondary (R-DD).

Entreferro (mm)	100	125	150	175	200
Tensão_p1	14,35385894	8,1928935	7,6018854	2,3529359	8,929694243
Corrente_p1	1,44E-06	8,19E-07	7,60E-07	2,35E-07	8,93E-07
Fluxo_p1	2,69E-05	1,53E-05	1,42E-05	4,41E-06	1,67E-05
Tensão_s1	2005,896456	2172,0518	1922,8866	1916,4209	1843,99739
Corrente_s1	20	20	20	20	20
Fluxo_s1	0,003755861	0,004067	0,0036004	0,0035883	0,003452719
Tensão_s2	1950,715801	2156,1336	1839,4196	1951,8304	1875,145901
Corrente_s2	20	20	20	20	20
Fluxo_s2	0,00365254	0,0040372	0,0034441	0,0036546	0,003511042
L_s	1,83E-04	2,02E-04	1,72E-04	1,83E-04	1,76E-04
Q	-79132,20471	-86563,672	-75246,08	-77364,984	-74382,8228
M_{s_p}	1,34E-06	7,67E-07	7,12E-07	2,20E-07	8,36E-07

(f) Open circuit on primary (R-DD).

Entreferro (mm)	100	125	150	175	200
Tensão_p1	130,2550831	129,8877573	130,1746149	120,2802515	124,7748964
Corrente_p1	20	20	20	20	20
Fluxo_p1	2,44E-04	2,43E-04	2,44E-04	2,25E-04	2,34E-04
Tensão_p2	130,8293765	131,0292758	127,8300367	121,0205461	124,8764372
Corrente_p2	20	20	20	20	20
Fluxo_p2	2,45E-04	2,45E-04	2,39E-04	2,27E-04	2,34E-04
Tensão_s1	147,4794872	124,2097986	89,92109942	95,22996102	72,36658305
Corrente_s1	3,04E-05	2,42E-05	1,76E-05	1,94E-05	1,51E-05
Fluxo_s1	2,76E-04	2,33E-04	1,68E-04	1,78E-04	1,35E-04
Tensão_s2	156,8793095	117,4966216	86,1766797	98,49347809	78,71846508
Corrente_s2	3,04E-05	2,42E-05	1,76E-05	1,94E-05	1,51E-05
Fluxo_s2	2,94E-04	2,20E-04	1,61E-04	1,84E-04	1,47E-04
Tensão_s	304,3587967	241,7064202	176,0977791	193,7234391	151,0850481
Q	-5221,076184	-5217,727301	-5159,472752	-4825,352767	-4992,3857
Lp (efetivo)	2,444E-05	2,44243E-05	2,41516E-05	2,25876E-05	2,33695E-05
M_{p_s}	2,84942E-05	2,26287E-05	1,64864E-05	1,81365E-05	1,41447E-05

(g) Open circuit on secondary (DD-DD).

Entreferro (mm)	100	125	150	175	200
Tensão_p1	150,701995	119,7957082	88,67665934	95,78433966	73,7886123
Corrente_p1	3,04E-05	2,42E-05	1,76E-05	1,94E-05	1,51E-05
Fluxo_p1	2,82E-04	2,24E-04	1,66E-04	1,79E-04	1,38E-04
Tensão_p2	153,4817989	121,8125754	87,34169745	97,82457688	77,24530211
Corrente_p2	3,04E-05	2,42E-05	1,76E-05	1,94E-05	1,51E-05
Fluxo_p2	2,87E-04	2,28E-04	1,64E-04	1,83E-04	1,45E-04
Tensão_s1	2238,614774	2054,584629	1949,19409	2069,159708	2030,555849
Corrente_s1	20	20	20	20	20
Fluxo_s1	0,004191605	0,003847025	0,003649691	0,003874316	0,003802033
Tensão_s2	2220,620611	2061,469067	1872,757366	55.6855371517	1998,928625
Corrente_s2	20	20	20	20	20
Fluxo_s2	0,004157913	0,003859916	0,00350657	0,004036328	0,003742814
Q	-89184,67181	-82321,03504	-76438,98722	-84496,86701	-80589,64976
Ls (efetivo)	0,000417476	0,000385347	0,000357813	0,000395532	0,000377242
M_{s_p}	2,85E-05	2,26E-05	1,65E-05	1,81E-05	1,41E-05

(h) Open circuit on primary (DD-DD).

Figure C.5: Parameters along Oz for the long types.

Entreferro (mm)	100	125	150	175	200
Tensão_p1	99,2944522	99,7010829	94,1916296	94,1941359	92,51057819
Corrente_p	20	20	20	20	20
Fluxo_p1	1,86E-04	1,87E-04	1,76E-04	1,76E-04	1,73E-04
Tensão_p2	113,942988	106,681797	102,191731	99,79407952	98,7484236
Fluxo_p2	2,13E-04	2,00E-04	1,91E-04	1,87E-04	1,85E-04
Tensão_p3	95,5792781	88,3280791	93,9899858	97,89701329	95,04145628
Fluxo_p3	1,79E-04	1,65E-04	1,76E-04	1,83E-04	1,78E-04
Tensão_s	406,972307	316,091079	238,942785	206,237314	179,0633196
Corrente_s	4,07E-05	3,16E-05	2,39E-05	2,06E-05	1,79E-05
Fluxo_s	7,62E-04	5,92E-04	4,47E-04	3,86E-04	3,35E-04
Q	-6175,16156	-5892,98986	-5806,22502	-5836,47028	-5724,75064
Lp	2,8906E-05	2,7585E-05	2,7179E-05	2,73207E-05	2,67977E-05
M_{p_s}	3,8101E-05	2,9593E-05	2,237E-05	1,93081E-05	1,6764E-05

(a) Open circuit on secondary (R-R).

Entreferro (mm)	100	125	150	175	200
Tensão_p1	12,0375624	10,6394425	9,25538365	8,921387236	8,707894748
Corrente_p	4,07E-05	3,16E-05	2,39E-05	2,06E-05	1,79E-05
Fluxo_p1	2,25E-05	1,99E-05	1,73E-05	1,67E-05	1,63E-05
Tensão_p2	384,53033	294,873326	221,065554	187,6897074	162,6707044
Fluxo_p2	7,20E-04	5,52E-04	4,14E-04	3,51E-04	3,05E-04
Tensão_p3	10,3811424	10,5664489	8,61274605	9,618526238	7,67840818
Fluxo_p3	1,94E-05	1,98E-05	1,61E-05	1,80E-05	1,44E-05
Tensão_s	6303,28953	5913,24554	5572,06053	5480,097285	5631,107754
Corrente_s	20	20	20	20	20
Fluxo_s	0,01180235	0,01107203	0,01043319	0,010260994	0,010543748
L_s	5,90E-04	5,54E-04	5,22E-04	5,13E-04	5,27E-04
Q	-126065,784	-118264,904	-111441,203	-109601,938	-112622,148
M_{s_p}	3,8099E-05	2,9592E-05	2,2369E-05	1,93073E-05	1,67634E-05

(b) Open circuit on primary (R-R).

Entreferro (mm)	100	125	150	175	200
Tensão_p1	93,80179704	98,2306686	98,87836455	97,17210083	98,07103318
Corrente_p	20	20	20	20	20
Fluxo_p1	1,76E-04	1,84E-04	1,85E-04	1,82E-04	1,84E-04
Tensão_p2	119,9626728	113,831055	112,3419289	107,3780615	108,5531264
Fluxo_p2	2,25E-04	2,13E-04	2,10E-04	2,01E-04	2,03E-04
Tensão_p3	99,69247291	91,8785682	96,37459249	95,02696525	94,66037423
Fluxo_p3	1,87E-04	1,72E-04	1,80E-04	1,78E-04	1,77E-04
Tensão_s	425,3408744	363,536575	295,4096694	256,4440153	238,8203068
Corrente_s	4,25E-05	3,64E-05	2,95E-05	2,56E-05	2,39E-05
Fluxo_s	7,96E-04	6,81E-04	5,53E-04	4,80E-04	4,47E-04
Q	-6267,97733	-6077,61152	-6150,7218	-5990,33722	-6024,49153
Lp	2,93406E-05	2,8449E-05	2,87917E-05	2,80409E-05	2,82008E-05
M_{p_s}	3,98206E-05	3,4034E-05	2,76564E-05	2,40084E-05	2,23585E-05

(c) Open circuit on secondary (R-R_+).

Entreferro (mm)	100	125	150	175	200
Tensão_p1	27,31942637	28,8233601	27,12543563	18,86810989	21,99707794
Corrente_p	4,25E-05	3,64E-05	2,95E-05	2,56E-05	2,39E-05
Fluxo_p1	5,12E-05	5,40E-05	5,08E-05	3,53E-05	4,12E-05
Tensão_p2	369,2639371	307,734132	247,367379	214,3568951	197,546804
Fluxo_p2	6,91E-04	5,76E-04	4,63E-04	4,01E-04	3,70E-04
Tensão_p3	28,69205494	26,9569226	20,90096177	23,19122396	19,26421341
Fluxo_p3	5,37E-05	5,05E-05	3,91E-05	4,34E-05	3,61E-05
Tensão_s	8468,065517	8143,96722	7734,514601	7559,057569	7552,230801
Corrente_s	20	20	20	20	20
Fluxo_s	0,015855699	0,01524885	0,01448219	0,014153663	0,01414088
L_s	7,93E-04	7,62E-04	7,24E-04	7,08E-04	7,07E-04
Q	-169361,306	-162879,339	-154690,287	-151181,146	-151044,611
M_{s_p}	3,98145E-05	3,4032E-05	2,76549E-05	2,40058E-05	2,23573E-05

(d) Open circuit on primary (R-R_+).

Entreferro (mm)	100	125	150	175	200
Tensão_p1	113,0661237	101,3123905	106,0844001	106,7326883	109,742174
Corrente_p	20	20	20	20	20
Fluxo_p1	2,12E-04	1,90E-04	1,99E-04	2,00E-04	2,05E-04
Tensão_p2	129,5415588	125,3599139	121,3352932	119,3536866	120,0218978
Fluxo_p2	2,43E-04	2,35E-04	2,27E-04	2,23E-04	2,25E-04
Tensão_p3	105,5570861	102,6676302	104,5045202	108,2110095	104,9489606
Fluxo_p3	1,98E-04	1,92E-04	1,96E-04	2,03E-04	1,96E-04
Tensão_B1	106,8749508	93,31221327	95,10255014	89,7947333	93,5174346
Fluxo_B1	2,00E-04	1,75E-04	1,78E-04	1,68E-04	1,75E-04
Tensão_B2	96,23530433	92,39175234	91,62647786	97,39709842	92,18056549
Fluxo_B2	1,80E-04	1,73E-04	1,72E-04	1,82E-04	1,73E-04
Tensão_s	403,6438162	307,4232024	235,6635576	174,4468046	147,5573809
Corrente_s	4,04E-05	3,07E-05	2,36E-05	1,74E-05	1,48E-05
Fluxo_s	7,56E-04	5,76E-04	4,41E-04	3,27E-04	2,76E-04
Q	-11023,66864	-10298,91254	-10371,11791	-10427,84838	-10406,27987
Lp	5,16021E-05	4,82095E-05	4,85475E-05	4,8813E-05	4,87121E-05
M_{p_s}	3,77894E-05	2,87811E-05	2,2063E-05	1,63318E-05	1,38144E-05

(e) Open circuit on secondary (BP-R).

Entreferro (mm)	100	125	150	175	200
Tensão_p1	12,06089363	11,7106181	9,361469657	10,251563	7,136308361
Corrente_p	4,04E-05	3,07E-05	2,36E-05	1,74E-05	1,48E-05
Fluxo_p1	2,26E-05	2,19E-05	1,75E-05	1,92E-05	1,34E-05
Tensão_p2	374,507569	301,479733	241,4634965	193,6763926	165,7888058
Fluxo_p2	7,01E-04	5,64E-04	4,52E-04	3,63E-04	3,10E-04
Tensão_p3	8,83770755	8,543260769	8,523609495	10,2083071	9,683190876
Fluxo_p3	1,65E-05	1,60E-05	1,60E-05	1,91E-05	1,81E-05
Tensão_B1	28,68314235	13,1262843	3,925102068	3,151443383	0,708503195
Fluxo_B1	5,37E-05	2,46E-05	7,35E-06	5,90E-06	1,33E-06
Tensão_B2	21,32654254	13,05172352	8,14989129	1,928902687	0,71156988
Fluxo_B2	3,99E-05	2,44E-05	1,53E-05	3,61E-06	1,33E-06
Tensão_s	6282,459207	6023,406627	5793,99525	5631,972392	5463,50636
Corrente_s	20	20	20	20	20
Fluxo_s	0,011763346	0,011278293	0,01084874	0,010545367	0,010229929
L_s	5,88E-04	5,64E-04	5,42E-04	5,27E-04	5,11E-04
Q	-125649,1778	-120468,1259	-115879,8981	-112639,4407	-109270,1199
M_{s_p}	4,17001E-05	3,25717E-05	2,54108E-05	2,05232E-05	1,72288E-05

(f) Open circuit on primary (BP-R).

Entreferro (mm)	100	125	150	175	200
Tensão_p1_1	26,50683571	28,3808183	29,0158796	28,785964	27,57089
Corrente	20	20	20	20	20
Tensão_p1_2	28,73974227	29,0074173	30,821331	29,983006	27,72247
Tensão_p2_1	37,81207133	34,7898858	33,7049129	32,123246	32,57204
Tensão_p2_2	38,02224733	34,5988395	33,2165756	32,388683	32,85639
Tensão_p3_1	29,13534771	26,8104979	28,5934688	27,787936	27,41156
Tensão_p3_2	30,28677187	27,6461883	30,0255563	28,205036	28,94582
Tensão_s1	4,213700057	4,22041016	2,85619967	1,1759581	1,884737
Q	-3802,34761	-3616,6306	-3699,74767	-3577,407	-3533,393
Lp	1,77989E-05	1,693E-05	1,7319E-05	1,675E-05	1,65E-05
M_{p_s}	3,94489E-07	3,9512E-07	2,674E-07	1,101E-07	1,76E-07

(g) Open circuit on secondary (DD-R).

Entreferro(mm)	100	125	150	175	200
Tensão_p1_1	5,147489604	4,25280535	2,5745988	2,7294141	3,031316
Tensão_p1_2	4,885942712	4,58357397	3,95406553	3,4052087	3,495356
Tensão_p2_1	76,26612795	64,369751	52,7522001	44,834363	38,43563
Tensão_p2_2	79,65147688	61,1212464	51,365889	47,098891	41,13527
Tensão_p3_1	5,007348651	3,91051805	3,62269414	3,0551251	2,710118
Tensão_p3_2	4,440921375	4,55179947	3,71295526	3,4653886	3,060842
Tensão_s1	6803,198267	6621,99687	6094,01756	6190,1823	5984,287
Corrente_s1	20	20	20	20	20
Fluxo_s1	0,012738383	0,0123991	0,01141051	0,0115906	0,011205
L_s1	6,37E-04	6,20E-04	5,71E-04	5,80E-04	5,60E-04
Q	-136063,959	-132439,93	-121880,345	-123803,6	-119685,7
M_{s_p}	1,6421E-05	1,3368E-05	1,1046E-05	9,792E-06	8,6E-06

(h) Open circuit on primary (DD-R).

Entreferro (mm)	100	125	150	175	200
Tensão_p1_1	27,8569638	28,5667328	31,34732399	29,0464455	28,5943004
Corrente_p	20	20	20	20	20
Fluxo_p1_1	5,20E-05	5,34E-05	5,86E-05	5,43E-05	5,34E-05
Tensão_p1_2	28,74070721	29,12074117	30,88625076	29,3592557	29,02519935
Fluxo_p1_2	5,37E-05	5,44E-05	5,77E-05	5,48E-05	5,42E-05
Tensão_p2_1	37,77048881	36,16106258	33,71664239	31,5517481	31,51074014
Fluxo_p2_1	7,06E-05	6,76E-05	6,30E-05	5,90E-05	5,89E-05
Tensão_p2_2	37,44801624	36,03290969	33,23948842	31,7244719	31,30406658
Fluxo_p2_2	7,00E-05	6,74E-05	6,21E-05	5,93E-05	5,85E-05
Tensão_p3_1	28,0227005	28,00386043	29,39246162	28,8222891	28,3385179
Fluxo_p3_1	5,23E-05	5,23E-05	5,49E-05	5,38E-05	5,29E-05
Tensão_p3_2	28,38827264	28,26736684	29,01259571	30,6268033	28,49260781
Fluxo_p3_2	5,30E-05	5,28E-05	5,42E-05	5,72E-05	5,32E-05
Tensão_s1	143,502716	124,5289455	95,21113728	75,5340612	62,3064411
Corrente_s1	2,88E-05	2,48E-05	1,90E-05	1,51E-05	1,24E-05
Fluxo_s1	2,69E-04	2,33E-04	1,78E-04	1,41E-04	1,17E-04
Tensão_s2	144,1377675	123,1506367	94,84749457	75,7264921	61,78295268
Corrente_s2	2,88E-05	2,48E-05	1,90E-05	1,51E-05	1,24E-05
Fluxo_s2	2,70E-04	2,31E-04	1,78E-04	1,42E-04	1,16E-04
Q	-3756,742631	-3715,210963	-3744,18657	-3614,64929	-3537,159537
Lp	1,75854E-05	1,7391E-05	1,75266E-05	1,692E-05	1,65575E-05
M_{p_s}	2,69291E-05	2,31879E-05	1,77934E-05	1,4161E-05	1,16173E-05

(i) Open circuit on secondary (DD-DD).

Entreferro(mm)	100	125	150	175	200
Tensão_p1_1	1,9154171	2,221556881	2,648829345	2,92444436	1,899051656
Corrente_p	2,88E-05	2,48E-05	1,90E-05	1,51E-05	1,24E-05
Fluxo_p1_1	3,59E-06	4,16E-06	4,96E-06	5,48E-06	3,56E-06
Tensão_p1_2	1,342015477	2,707697073	2,214067297	2,87164981	2,037381815
Fluxo_p1_2	2,51E-06	5,07E-06	4,15E-06	5,38E-06	3,81E-06
Tensão_p2_1	139,4979421	118,0347063	89,86796429	70,8858296	57,13320655
Fluxo_p2_1	2,61E-04	2,21E-04	1,68E-04	1,33E-04	1,07E-04
Tensão_p2_2	139,6981934	119,0761866	89,47422466	69,9017451	57,87700445
Fluxo_p2_2	2,62E-04	2,23E-04	1,68E-04	1,31E-04	1,08E-04
Tensão_p3_1	3,184620878	2,84380136	2,834849013	2,28412759	2,357979013
Fluxo_p3_1	5,96E-06	5,32E-06	5,31E-06	4,28E-06	4,42E-06
Tensão_p3_2	1,871005892	2,712472974	2,971494564	2,35887438	2,760588017
Fluxo_p3_2	3,50E-06	5,08E-06	5,56E-06	4,42E-06	5,17E-06
Tensão_s1	2365,273699	2327,899596	2132,541007	2059,47493	1973,284392
Corrente_s1	20	20	20	20	20
Fluxo_s1	0,004428763	0,004358783	0,003992992	0,00385618	0,003694798
Tensão_s2	2373,623295	2305,603566	2155,603571	2037,80647	1967,323991
Corrente_s2	20	20	20	20	20
Fluxo_s2	0,004444397	0,004317036	0,004036174	0,00381561	0,003683637
Q	-94777,9061	-92670,02869	-85762,8542	-81945,5889	-78812,12707
Ls	4,44E-04	4,34E-04	4,01E-04	3,84E-04	3,69E-04
M_{s_p}	2,69168E-05	2,31801E-05	1,7789E-05	1,4158E-05	1,16151E-05

(j) Open circuit on primary (DD-DD).

Entreferro(mm)	100	125	150	175	200
Tensão_p1_1	28,5623538	27,39949967	27,61101368	26,88226286	28,57674642
Corrente_p	20	20	20	20	20
Fluxo_p1_1	5,33E-05	5,12E-05	5,16E-05	5,02E-05	5,34E-05
Tensão_p1_2	28,6397602	28,57931265	28,11899302	27,18569988	30,51838875
Fluxo_p1_2	5,35E-05	5,34E-05	5,25E-05	5,08E-05	5,70E-05
Tensão_p2_1	39,5416316	35,72986283	33,76314604	32,07241391	31,99057495
Fluxo_p2_1	7,39E-05	6,68E-05	6,31E-05	5,99E-05	5,98E-05
Tensão_p2_2	39,0044509	36,10058706	33,97961807	32,3210522	32,12787484
Fluxo_p2_2	7,29E-05	6,75E-05	6,35E-05	6,04E-05	6,00E-05
Tensão_p3_1	29,598048	28,70031202	27,91518775	31,49374953	27,73964717
Fluxo_p3_1	5,53E-05	5,36E-05	5,21E-05	5,89E-05	5,18E-05
Tensão_p3_2	29,9574085	29,11640776	28,34521873	30,29018528	28,88902785
Fluxo_p3_2	5,60E-05	5,44E-05	5,29E-05	5,66E-05	5,40E-05
Tensão_s1	127,528444	96,55628118	75,40100536	59,79649393	54,85258262
Corrente_s1	2,53E-05	1,91E-05	1,51E-05	1,22E-05	1,04E-05
Fluxo_s1	2,39E-04	1,81E-04	1,41E-04	1,12E-04	1,03E-04
Tensão_s2	125,742304	94,63577407	75,88475826	62,56581046	49,40382759
Corrente_s2	2,53E-05	1,91E-05	1,51E-05	1,22E-05	1,04E-05
Fluxo_s2	2,35E-04	1,77E-04	1,42E-04	1,17E-04	9,25E-05
Q	-3898,54405	-3704,65619	-3586,576826	-3596,86324	-3588,803622
Lp	1,8249E-05	1,73416E-05	1,67889E-05	1,6837E-05	1,67993E-05
M_{p_s}	2,3711E-05	1,78995E-05	1,41635E-05	1,14556E-05	9,76054E-06

(k) Open circuit on secondary (DD-BP).

Entreferro (mm)	100	125	150	175	200
Tensão_p1_1	1,27290788	0,798871364	0,90271202	1,884364483	1,284480818
Corrente_p	2,53E-05	1,91E-05	1,51E-05	1,22E-05	1,04E-05
Fluxo_p1_1	2,38E-06	1,50E-06	1,69E-06	3,53E-06	2,41E-06
Tensão_p1_2	1,16395308	1,120251751	1,007068875	2,151651258	1,373035397
Fluxo_p1_2	2,18E-06	2,10E-06	1,89E-06	4,03E-06	2,57E-06
Tensão_p2_1	123,990301	94,64957869	73,69575111	59,07172606	49,69718803
Fluxo_p2_1	2,32E-04	1,77E-04	1,38E-04	1,11E-04	9,31E-05
Tensão_p2_2	124,193341	92,72467855	72,7745089	56,45815953	48,38843571
Fluxo_p2_2	2,33E-04	1,74E-04	1,36E-04	1,06E-04	9,06E-05
Tensão_p3_1	1,46927986	1,018363932	1,221269248	1,633703842	1,780677996
Fluxo_p3_1	2,75E-06	1,91E-06	2,29E-06	3,06E-06	3,33E-06
Tensão_p3_2	1,10967794	0,842632266	1,661514269	1,143253518	1,718695651
Fluxo_p3_2	2,08E-06	1,58E-06	3,11E-06	2,14E-06	3,22E-06
Tensão_s1	1895,24914	1772,763203	1697,285777	1699,673177	1692,737023
Corrente_s1	20	20	20	20	20
Fluxo_s1	0,00354868	0,003319339	0,003178015	0,003182485	0,003169497
Tensão_s2	1665,41893	1522,136387	1430,670681	1379,760586	1349,38044
Corrente_s2	20	20	20	20	20
Fluxo_s2	0,00311835	0,002850063	0,002678801	0,002583476	0,002526592
Q	-71213,3162	-65897,943	-62559,07763	-61588,6227	-60842,29598
Ls	3,33E-04	3,08E-04	2,93E-04	2,88E-04	2,85E-04
M_{s_p}	2,3705E-05	1,7896E-05	1,41613E-05	1,14538E-05	9,75924E-06

(l) Open circuit on primary (DD-BP).

Figure C.6: Parameters along Oz for the segmented types.

Appendix D

Speed of the vehicle

D.1 Simulation for 120 km/h

In section 5.2.1 an explanation regarding speed vs energy transfer is made for the R-R geometry. However, it is done with extreme speed levels that are not reasonable in a real situation. Because of that, an additional simulation was done where the simulation time was left untouched but the speed was changed. At 10000 m/s, the vehicle passes through the simulated length of 1600 mm (two segments) in 160 μs. So, it goes through a single segment in 80 μs.

The speed was then changed to 33.33(3) m/s which is approximately 120 km/h and the position of the secondary was moved to a perfectively aligned position with one primary segment. Knowing that $33.33(3) \ll 10000$, the distance covered will be much lower at $d = 33.33 \cdot 80 \times 10^{-6}$ which is approximately 2.67 mm. The secondary at $T_s = 0$ will be aligned with a segment and at $T_s = 80$ μs will be only 2.67 mm misaligned in the x direction, which means that it is essentially aligned throughout the simulation. As Fig. D.1a illustrates this results in a greater average power and as a consequence greater energy transfer. Even though T_s is the same, P_{avg} is not. Table D.1 shows P_{avg} and the subsequent energy values transfered in both speeds. The energy value was calculated from equation 5.2 and effectively

Table D.1: Average power and energy values.

Speed (m/s)	P_{avg} (W)	E (mJ)
33.33	132.7	10.62
10000	50.97	4.08

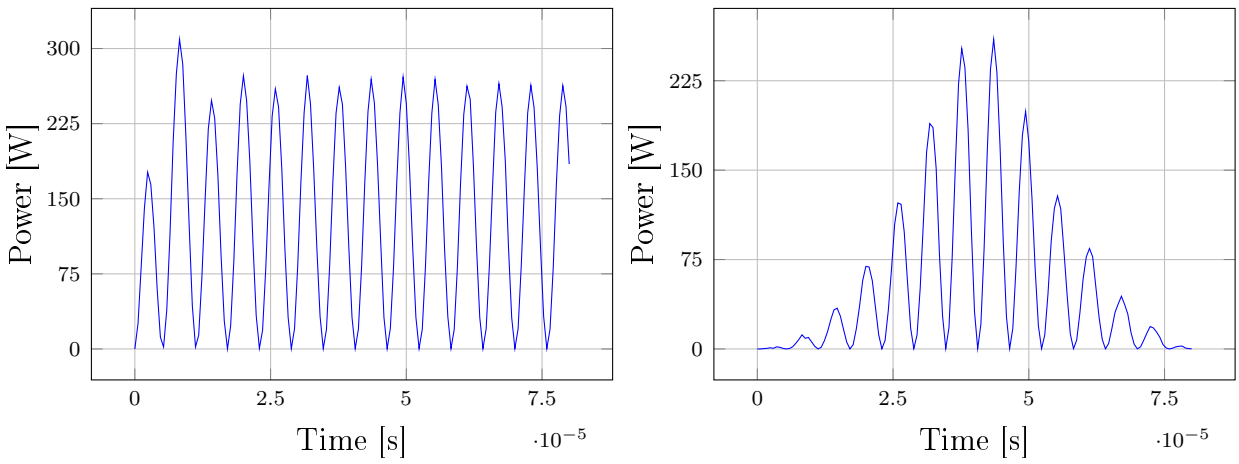

(a) 33.33 m/s (b) 10000 m/s

Figure D.1: Load power comparison.

shows that for the same time-span an higher energy transfer is evident with the lower speed.

Moreover, the fact that the secondary is basically on the same aligned position on this additional test, guarantees that P_{avg} is equivalent to the maximum values obtained in steady state at aligned positions (see Fig. 5.23).